Spring 2010

Advanced control of large scale wind turbines

Jacob Aho
University of New Hampshire, Durham

NOTE TO USERS

This reproduction is the best copy available.

ADVANCED CONTROL OF LARGE SCALE WIND TURBINES

JACOB AHO
B.S., University of New Hampshire, 2008

THESIS

Submitted to the University of New Hampshire
in Partial Fulfillment of
the Requirements for the Degree of

Master of Science
in
Electrical Engineering

May, 2010

This thesis has been examined and approved.

Thesis Director, Dr. L. Gordon Kraft, Professor of Electrical and Computer Engineering

Dr. Allen Drake, Associate Professor of Marine Sciences and Electrical and Computer Engineering and Ocean Engineering

Dr. Richard Messner, Associate Professor of Electrical and Computer Engineering

Dr. Barry Fussell, Professor of Mechanical Engineering

Dr. May-Win Thein, Associate Professor of Mechanical Engineering

5/7/10

Date

ACKNOWLEDGEMENTS

This thesis is dedicated to the hundreds of individuals who have supported me throughout the years. I have been very blessed to be in the position to perform this research and write this document. A special thanks to the faculty and staff of the UNH ECE Department for their support over the past six years.

I especially want to thank my parents for all the hard work they have devoted to my development. Their support and guidance has been critical to where I am today.

Last but certainly not least, thanks to Dr. L. G. Kraft for always taking the time to share his wisdom with me; inspiring me and giving me advice for academia and life. He has always provided useful analogies to relate complicated control topics to baseball, hunting and other life situations. He has been my advisor, mentor and also a great friend.

A special thanks to the financial and educational sponsors of this research:

UNH Electrical and Computer Engineering Department

UNH ECE Department Graduate Student Fellowship Award

UNH Energy Laboratory

National Renewable Energy Laboratory

Magnomatics Ltd.

FORWARD

My father once told me how important energy would be in our future. I was young and didn't understand how true his words were until I learned more about the world around me. I became interested in wind energy throughout my undergraduate experience at the University of New Hampshire (UNH). This interest was bolstered by a renewable energy course that I took during my senior year. I also found a new interest while taking the senior level control systems class at UNH. My advisor, Dr. L. G. Kraft, had opened my eyes to a field of research which combined these two topics: wind turbine control systems.

A summer energy conference at UNH inspired me to be more involved and start the UNH Energy Club. My involvement paid off in many ways. The following summer, the UNH Electrical and Computer Engineering Department and UNH Energy Laboratory provided funds for the Energy Club vice president and me to embark on an energy road trip. We attended the International Student Energy Summit in Calgary, Canada where we learned about global energy issues. We stopped at many wind farms along our journey. I was taken aback by the size of the turbines and the vastness of the wind farms. In addition, we visited the National Renewable Energy Laboratory's National Wind Technology Center in Golden, Colorado. A senior controls engineer, Dr. Alan Wright, gave us extensive tours of the campus. He also explained current wind turbine control system research and pointed me in a direction to learn more about this subject matter. This thesis is a result of the knowledge gained since taking this trip.

There are many engineers working on wind turbine control systems around the world. It was difficult to decide on a specific research topic relating wind turbine control systems. Dr. Kraft and I decided to tackle the most common cause of wind turbine failure, the gearboxes. This was my first significant research project, so the hardest part for me was to define a starting point and begin work. Dr. Kraft helped me jump this hurdle, providing guidance and a vision for this thesis. Once I had a good feel for the work that needed to be done, I was off and running. I learned a lot during the course of this thesis. Though I lost a bit of sleep and neglected some of my friends for a month or two during the final push to meet the thesis deadlines, I am nonetheless very happy to have had the experience.

I will continue my research in wind turbine control systems at the University of Colorado at Boulder in efforts to earn my Ph.D. in the Electrical Computer and Energy Engineering Department under the guidance of Dr. Lucy Pao. This research will focus on feed-forward control using light detection and ranging (LIDAR) sensors to measure the incoming wind flow before it reaches the rotor plane.

I am excited to continue my work in the area of wind turbine control systems. To me, wind turbines are beautiful works of art and engineering. My future goal is to produce research that is practical and implementable in wind turbines so that I will make a difference to the industry and help provide our country with clean, renewable energy.

TABLE OF CONTENTS

LIST OF FIGURES

LIST OF TABLES

NOMENCLATURE

NREL- National Renewable Energy Laboratory

FAST- Fatigue Aerodynamic Structures and Turbulence software

HSS- High Speed Shaft

LSS- Low Speed Shaft

CVT- Continuously Variable Transmission

DLIN- Derived Linear Wind Turbine Model

DCVT- Derived Wind Turbine Model with magnetic CVT

PI- Proportional-Integral (control)

PI MF- Proportional-Integral Controller with Measurement Filter

Kp- Proportional Gain

Ki- Integral Gain

LQR- Linear Quadratic Regulator

Q- State Penalty Matrix

R- Input Penalty Matrix

SI LQR- Single-Input LQR Controller

MI LQR- Multi-Input LQR Controller

$\boldsymbol{x}$- State Vector

$\boldsymbol{u}$- Input Vector

$\boldsymbol{A}$- State Matrix

$\boldsymbol{B}$- Input Matrix

RMS- Root Mean Square

STD- Standard Deviation

VARIABLES AND UNITS

Variable Name	Symbol	Alternate	Units
Blade actuator time constant	τ_b	TauB	seconds
Blade damping coefficient	D_b		Nm/(rad/s)
Blade drag	B_b		Nm/(rad/s)
Blade flex	$(\theta_b - \theta_r)$	Pb-Pr	rad
Blade inertia (all 3)	J_b		Kg-m^2
Blade mass (all 3)	M_b		Kg
Blade pitch angle	β		degrees
Blade pitch angle	β	B	deg
Blade pitch command rate	$\dot{\beta}_u$	Budot	deg/s
Blade pitch command signal	β_u	Bu	deg
Blade pitch rate	$\dot{\beta}$	Bdot	deg/s
Blade spring coefficient	K_b		Nm/rad
Blade tip rotational acceleration	$\ddot{\theta}_b$	Ab	rad/s^2
Blade tip rotational jerk	$\dddot{\theta}_b$	Jb	rad/s^3
Blade tip rotational position	θ_b	Pb	rad
Blade tip rotational velocity	$\dot{\theta}_b$	Wb	rad/s
Change in torque from the wind due to change in blade pitch angle	$\frac{\partial T_w}{\partial \beta}$	dTw/dB	Nm/degree
Change in torque from the wind due to change in rotor speed	$\frac{\partial T_w}{\partial \dot{\theta}_r}$	dTw/dWr	Nm/(rad/s)
Change in torque from the wind due to change in wind speed	$\frac{\partial T_w}{\partial W_s}$	dTw/dWs	Nm/(m/s)
CVT actuator time constant	τ_n	TauN	seconds
Electrical load equivalent friction	B_L		Nm/(rad/s)
Electrical Power	Epower		watts
Gear ratio	N		-
Gear ratio command	N_u	Nu	-
Gear ratio command rate of change	$\dot{N}_u$	Nudot	s^{-1}
Gear ratio rate of change	$\dot{N}$	Ndot	s^{-1}
Gearbox LSS jerk	$\dddot{\theta}_{gb}$	Jgb	rad/s^3
Gearbox LSS rotational acceleration	$\ddot{\theta}_{gb}$	Agb	rad/s^2

Variable Name	Symbol	Alternate	Units
Gearbox LSS rotational position	θ_{gb}	Pgb	rad
Gearbox LSS rotational velocity	$\dot{\theta}_{gb}$	Wgb	rad/s
Generator friction	B_g		Nm/(rad/s)
Generator inertia	J_g		Kg-m^2
Generator Load Torque	T_L		Nm
Generator rotational acceleration	$\ddot{\theta}_{gen}$	Agen	rad/s^2
Generator shaft jerk	$\dddot{\theta}_{gen}$	Jgen	rad/s^3
Generator shaft rotational position	θ_{gen}	Pgen	rad
Generator shaft rotational velocity	$\dot{\theta}_{gen}$	Wgen	rad/s
Low speed shaft flex	$(\theta_r - \theta_{gb})$	Pr-Pgb	rad
Rated generator speed	$\dot{\theta}_{gen_0}$	Wgo	rad/s
Rated mechanical power	P_0		Watts
Rotor friction	B_r		Nm/(rad/s)
Rotor inertia	J_r		Kg-m^2
Rotor shaft (LSS) damping coefficient	D_r		Nm/(rad/s)
Rotor shaft (LSS) spring coefficient	K_r		Nm/rad
Rotor shaft rotational acceleration	$\ddot{\theta}_r$	Ar	rad/s^2
Rotor shaft rotational jerk	$\dddot{\theta}_r$	Jr	rad/s^3
Rotor shaft rotational position	θ_r	Pr	rad
Rotor shaft rotational velocity	$\dot{\theta}_r$	Wb	rad/s
Torque applied to generator	T_{gen}	GenTq	N-m
Torque from wind	T_w		Nm
Wind Speed	W_s	Wspd	m/s

ABSTRACT

ADVANCED CONTROL OF LARGE SCALE WIND TURBINES

by

Jacob Aho

University of New Hampshire, May, 2010

Wind turbines have experienced an economy of scale that caused them to become larger, more expensive and provided the challenge to protect the components, particularly the failure-prone gearboxes. This thesis focused on new control systems for wind turbines in above-rated, or Region 3, wind regimes. The control goals were to regulate the generator speed and protect the gearbox by mitigating drivetrain torque variations.

This thesis included the development of a linear wind turbine model based on the National Renewable Energy Laboratory's FAST 5MW model. A magnetic continuously variable transmission (CVT) was included in the model. A multi-input linear quadratic regulator (LQR) controller was developed and simulated. The multi-input controller provided large improvements in speed regulation and torque variation reduction when compared to blade-pitch industry standard proportional-integral and single-input LQR controllers. Results indicated that use of a magnetic CVT and multi-input LQR controller could reduce fatigue on wind turbine gearboxes.

INTRODUCTION

Wind energy is an alternative energy technology that is growing at an increasing rate. Each year, more wind turbines are installed and connected to the utility grid. Wind power is beginning to make significant contributions to the United States energy profile. Wind energy technology experiences an economy of scale. Manufacturers of these wind turbines are producing larger wind turbines every year, with recent production of machines rated over 10 megawatts. Engineers have significantly improved wind turbine technology over the past 40 years. The machines are now quieter, more reliable and produce more power with better regulation of output power. Despite all of these improvements, there are still significant challenges facing wind turbines that must be overcome. One of the primary areas of research in wind technology is the preservation of the turbine's gearbox. This thesis addresses the issue of premature gearbox failure. By developing new smarter control systems, gearboxes can be protected from large torque variations caused by the wind. If gearbox lifetimes are extended, wind energy will be a more cost competitive alternative to other energy sources.

Chapter 1 of this thesis contains information about the past, present and future of wind energy. This chapter includes the historical development of wind turbines, several present day challenges facing wind turbines, and some research topics that may be implemented to change the future of wind energy.

The nature of producing energy from wind involves converting a stochastically turbulent wind source into precisely regulated power via the wind turbine. As wind

turbines become larger, they produce more power and become more expensive. Higher power turbines experience larger torques and stresses due to wind turbulence and variation.

Chapter 2 of this thesis provides an overview of wind turbines and industry standard control. It is important for the reader to become familiar with the terminology of wind turbine components in order to understand the research presented in this thesis. Knowledge of turbine operating regions and industry standard control methodology is also fundamental to understanding the developed control systems described in this document.

Conventional large scale wind turbines use a mechanical gearbox to transform the low speed rotation of the rotor to the high speed rotation of the generator. The generator spins at much faster speeds than the blades and rotor. Typically the gear ratios in large scale wind turbines are approximately 100:1. Large scale wind turbine gearboxes translate megawatts of mechanical power. The torque on these gearboxes is constantly varying with the turbulent and stochastic nature of the wind. Wind variations deliver extreme stresses on wind turbine components and can lead to premature gearbox failure. These failures increase the cost of wind energy. Failed bearings have been the primary cause of gearbox malfunction due in part to large torque variations. One way to mitigate the torque variations is to implement more advanced control systems.

When typical large scale wind turbines operate in above-rated wind speeds, control systems actuate the turbine blades to shed excess power so that the generator is not over-torqued. Conventional large scale wind turbines use simple control techniques

that are based on the generator shaft speed. Controlling the turbine solely on measurements at the load can make it difficult to minimize torque variations.

The research presented in this thesis focuses on new control systems for wind turbines in above-rated wind speeds to reduce the torque variations through the drivetrain. To be able to simulate these control systems, a new linear model of a wind turbine is developed. The developed model is representative of a 5MW wind turbine in above-rated wind speeds. The procedure of developing this model can be found in Chapter 3.

A new blade-pitch single-input linear quadratic regulator (SI LQR) is also developed in this thesis. The goals of the SI LQR controller are to regulate the generator speed and reduce the torque variations in the drivetrain better than the industry standard controllers without large increases in blade pitch rate. The SI LQR control system incorporated knowledge of the wind turbine model and utilized sensor feedback from turbine components, such as rotational velocities, bending of the blades and flexing of the drivetrain. This controller was simulated with the linear model and compared to simulations of the industry standard control methodology with the same model. The development of the SI LQR controller is explained in Chapter 4. Simulation results can be found in Chapter 5.

Another approach to reducing unwanted torque variations in the gearbox is also studied in this thesis. This method focuses on the addition of a magnetic continuously variable transmission (CVT) into the turbine drivetrain as an additional control input. Magnetic CVTs are claimed to be fast, efficient, and contactless. Equations representing a variable gear ratio were derived and properties of a magnetic CVT were added in series

with the conventional gearbox. The CVT equations and properties were added to the linear model to produce a new, non-linear two input model. The CVT and model development are described in Chapter 3.

A new multi-input linear quadratic regulator (MI LQR) controller was designed for the two input non-linear model. The controller's goal was to pitch the blades to limit the aerodynamic torque and control the CVT to regulate the generator speed and intercept torque variations propagating along the drivetrain. The development of the MI LQR controller is documented in Chapter 4. The results of simulating the MI LQR controller on the derived model with a CVT can be found in Chapter 5.

The results of this study indicate that implementation of additional sensors and advanced control systems on wind turbines has potential to provide moderate damping to torque variations in the gearboxes when information about the wind turbine is known and modeled. Results of this study also indicate that implementation of magnetic CVTs with advanced control systems may show significant reductions in torque variations and improvement of speed regulation. The conclusions of the thesis and recommendations for future study can be found in Chapter 6.

Appendix A contains the FAST user input file. Appendix B contains the TurbSim user input file that was used to generate the wind file for simulations. Appendix C shows the MATLAB® code used to design the controller and set up the simulation environment. The full Simulink® models can be found in Appendix D. The models, controllers and simulations were primarily based upon these files. The appendices were included for reference if the reader wishes to gain further understanding of the subject matter, duplicate the results found in this document or expand the research of this thesis.

CHAPTER 1:

PAST, PRESENT AND FUTURE OF WIND ENERGY

Historical Developments

The wind had been blowing long before humans made their appearance on Earth. Wind is created from the coreolis effect of Earth spinning and pressure differences caused by spatial thermal gradients due to the sun's rays heating the atmosphere and the surface of Earth. These pressure differences force the movement of air particles from high pressure regions to low pressure regions. [1] The air is composed of many different gasses, all of which have mass. Whenever a mass of material is moving, it has kinetic energy. This energy has been transporting moisture for life to thrive and transforming our landscape for millions of years. [2]

Humans have been utilizing the energy from the wind for thousands of years. Long before Nikola Tesla had invented the AC motor, wind energy was being used to sail boats around the world, to grind grain, to pump water for irrigation and to mechanically power machinery in factories. Though these applications are widely diverse in nature, they all use the same principle. They all convert the kinetic energy of the wind to translational or rotational energy which is used for a specific purpose. [3]

The first wind turbine that produced electrical energy was developed in Denmark by Paul la Cour in 1891. The electricity that was produced was not used in its direct form or distributed on a utility grid, a common call name for a collection of electric power

transmission and distribution networks. The electricity was used to electrolyze water, producing hydrogen which was used for lighting the local schoolhouse via gas lamps. Some feel that he was ahead of his time, as using wind energy to produce hydrogen is still an active area of research. [2]

Electricity generating wind turbines started appearing in America in the late 1890's and became more abundant through the 1930's and 40's. By this time estimates show there were hundreds of thousands of these wind turbines in operation, most producing electricity for rural areas where there was no utility grid. The largest of these early turbines was installed in 1941 at Grandpa's Knob in Vermont. This turbine was rated at 1,250 kW and operated for 4 years before launching one of its 8 ton, 85 foot blades a distance of 750 feet. Wind turbine development had shown great progress, but reliability of mechanical and electrical components needed improvement. [2]

Development and implementation of wind turbines dwindled as the United States continued to expand its utility grid. As the grid stretched out to electrify rural areas with reliable and inexpensive power, there was less demand for electricity producing wind turbines. A short lived boom in wind energy occurred in the 1970's into the 1980's. An oil crisis in the 1970's brought energy to the forefront of many American minds. There were also significant financial and regulatory incentives for manufacturing and installing renewable energy systems during this time period, which pushed forward a revival for the wind industry in America. When the oil prices dropped and the incentives ran dry in the 1980's the American wind economy slowed to a crawl. [2]

After the decline in wind energy in America, several European countries continued research and development of wind turbines, most notably Denmark, Germany

and Spain. These countries reaped the rewards when wind technology sales began to increase in the mid-1990's. One such company is Vestas, a Danish company that started making wind turbines in 1979 and is now one of the world's leading wind turbine suppliers. The United States was left behind and was not ready to compete with these countries when demand increased. [2]

There were some lasting effects of the energy conscious period of the 1970's. The focus on energy brought some changes to the US national government. In 1977 the Department of Energy (DOE) was activated and the Solar Energy Research Institute was developed. The Solar Energy Research institute was part of DOE as a national laboratory. In 1991 this laboratory was renamed the National Renewable Energy Laboratory (NREL). The purpose of NREL is to advance the nation's energy goals and "support critical market objectives to accelerate research from scientific innovations to market-viable alternative energy solutions." [4]

Continued research and development combined with more favorable regulations has allowed wind energy to be installed at a steadily increasing rate. In 2008 8,500 MW of new generating capacity was installed in the U.S., doubling the countries total generating capacity from wind in a single year. These installations injected $17 billion into the wind energy economy in that year alone. [5] In 2009 the United States was the global leader in wind power, installing over 10,000 MW of wind power. Wind energy provided 39% of all new generating capacity in 2009, putting current US wind power capacity over 35,000 MW. [5] In 2009 NREL received a record high $521.1 million in funding. [4] The recent investment in wind energy has driven down the cost of wind

energy even further by improving manufacturing and investing in more research and development.

Wind turbines are not only becoming more prevalent, but are also becoming much larger. The economy of scale that comes with wind power is pushing manufacturers to produce larger turbines every year. The average wind turbine size installed in 2008 was 1.67 MW. Typical installed turbine sizes in the US reached 3MW in the last quarter of 2009. [5] REpower set the bar in 2005 with a 5MW wind turbine, the turbine which this thesis and the NREL 5MW model is based on. [6] The record for the largest wind turbine is frequently broken, as the largest present day turbines are passing the 10 megawatt mark. Larger turbines extract power from the wind more economically, but also face many challenges.

Challenges Facing Wind Turbines

Though much progress has been made in converting wind energy to electricity efficiently and reliably, there are still obstacles to be overcome by these modern day wind turbines. These challenges are multidisciplinary, relating to policies, societal perceptions, engineering and the sciences. This document will primarily focus on the technical problems facing wind turbine control systems.

There are many factors that determine the economic viability of wind turbines. A wind turbine cannot be installed at a location only because the site's wind profile, or temporal distribution of wind speeds, indicates that there could be significant energy harvests. There must be a way to connect the source to the load to transport the electricity to the consumer. The U.S. utility grid is traditionally installed at locations

where there is demand for power in residential or industrial areas. Some of the best wind resource locations in America are in hilly, remote regions of the country. There are often few people living in these areas, and the utility grid in these areas is not rated for such high power, if it exists in these areas at all. The need to improve or install power lines in these locations greatly increases the capital costs of installing wind turbines at these sites. [2]

Often wind turbines are installed in groups, called wind farms. These wind farms contain wind turbines that are positioned in offset arrays to minimize turbulence. The current control systems installed in these wind turbines are designed to optimize the power extraction for each individual turbine. Studies show that individual control of wind turbines does not provide the optimal power output of the entire wind farm. Coordinated intelligent control of farms that would slightly limit the power of the upwind turbines can allow the downwind turbines to produce more power and the net wind farm power output would increase. [7]

Another issue facing wind turbines is that there is often not sufficient energy storage capacity to store the wind energy that is produced. Pumped hydro storage can be utilized at some sites that have elevated water reservoirs nearby. Other sites have salt mines near them which can be sealed and used for compressed air storage. Most sites do not have these assets nearby, so the energy must go directly onto the utility grid which brings it to the consumers. The wind is a variable resource and there must be a balance of supply and load on the utility grid. The variable output power of wind turbines forces conventional power plants to increase production when the wind stops blowing and scale back production during windy periods. These conventional energy sources cannot

change their power output instantaneously. When there is an excess of power, conventional generators sometimes go through an emergency shut down or excess power needs to be dissipated as heat through resistors if such technology is in place. [8]

Scientists and engineers are still trying to completely understand the stochastic turbulent nature of the wind and the interactions of the wind on the blades. It is difficult to perform tests of very large wind turbine blades in a controlled environment, as the largest wind tunnel is 120 feet wide located at the NASA Ames Research Center (the 5MW model used in this study has 197 foot blades). [9] Since direct experimentation is difficult, the wind to blade interactions are typically calculated using finite element analysis. The more degrees of freedom the blades are assumed to have, the higher order the calculations become. It is not a trivial task to design controllers for systems of such high order of magnitude, especially when the equations are non-linear. [10]

The wind energy industry has suffered high gearbox failure rates ever since the technology was developed. Gearboxes are one of the most expensive components in a wind turbine. Wind turbine manufacturers often include significant overhead costs to cover the gearbox warranties due to their high failure rate. These overhead costs have increased the price of wind energy. Gearbox failures have been the leading cause of turbine downtime. The price of wind energy has been additionally inflated as wind turbines were taken offline until a new gearbox can be delivered and a crane can be brought to the site for installation. The National Renewable Energy Laboratory has formed a Gearbox Reliability Collaborative to assess this problem. [11]

Wind turbines have become larger and taller due to the economy of scale with wind energy. As wind turbines have become larger, the significance of gearbox failures

has been amplified. Conventional large scale wind turbines need gearboxes to convert low speed rotation of the rotor shaft to high speed rotation of the generator shaft. These gearboxes ride on bearings to reduce friction as they rotate. The gearboxes have become heavier and more expensive as they are manufactured to handle more mechanical power. As the wind turbine blades experience wind gusts and turbulence, high power torque variations can be delivered to the drivetrain. The increased stress on the gearboxes as they transfer the torque along the drivetrain can cause the bearings to fail, often destroying the gearbox. The bearings are the most common point of failure in wind turbine gearboxes. Rapid large torque variations are one of the main measures of fatigue in gearbox bearings. [11]

Wind turbines are getting larger each year. The power available from a steadily blowing wind stream is a function of the wind speed cubed and the rotor radius squared. Larger blades means that more power can be captured from a given wind stream, and taller towers also allow for more power production. The wind is typically moving at a faster velocity at increased height. As turbines are manufactured larger, they are also becoming more expensive and flexible. Both of these factors indicate that controlling the turbines to minimize fatigue on the components becomes much more important. [10] The primary goal of this thesis is to develop control systems that mitigate the torque variations in the turbine drivetrain and thereby extend gearbox lifetimes. By reducing maintenance costs, wind energy systems will be more competitive with other energy sources.

Wind Energy Future Potential

Wind energy has the potential to become a significant contribution to our energy generation profile if the installed capacity continues to grow at the current rate. The recent increase of investments in wind energy has provided funding for research on topics that could greatly improve the reliability and efficiency of wind turbines. Many agree that the implementation of wind turbines cannot continue to succeed without future policies and regulations that are in favor of the technology. These topics will not be the focus of this thesis. The focus of this section of the document is on future research in controlling wind turbines to regulate speed and energy with a higher reliability.

There have been recent improvements in localized short term wind forecasting for wind farm sites. Approximate predictions of a wind farm's power production can be estimated for the upcoming day, hour and sometimes 15 minute intervals. The predictions allow the scheduling of increasing or decreasing energy production from fossil fuel power plants. This coordination of sources is important because supply must always match demand. As the localized forecasting and communication improves so will the coordination between wind and conventional energy sources to match power production and consumption. [8]

The integration of more sensors on the wind turbine can also provide more intelligent control. For instance, if stress/strain gauges are built into the blades, the controller could have an earlier indication of an increase in wind speed in comparison to measuring the generator shaft rotational speed. If a more advanced controller was used to utilize this information then the controllers could react earlier, which could help in regulate power and reduce torque variations. This is particularly important as wind

turbines become larger due to the aforementioned economy of scale. The cost of additional sensors might be offset by the overall savings of a more reliable wind turbine. This could be particularly important as turbines become larger and their components more expensive.

The use of Light Detection and Ranging (LIDAR) sensors to measure the incoming wind flow shows potential for improved energy capture and minimizing unwanted torque variations along the drive train and in the gearbox. These LIDAR units could measure wind variations even earlier than the blade-flex sensors. Preliminary studies show that wind turbine control systems that utilize LIDAR measurements can react to these wind variations before the wind energy reaches the blades. The earlier actuation of the turbine components has potential to better regulate the turbine and improve reliability. Feed-forward control with LIDAR sensors is a research topic that is still being pursued. [12] [13]

Studies have also showed that installing a mechanical continuously variable transmission (CVT) in the drive train of the wind turbine can allow for greater energy capture when operating below-rated wind speeds while also eliminating the need for power electronics. The adjustable gear ratio allows for the generator to run at a relatively constant speed, which produces constant power. [14] A Canadian wind turbine manufacturer, AAER, has claimed to have recently developed a 2MW wind turbine with a mechanical CVT, or superpostition gear. AAER has claimed that their turbines can capture more energy and control the dynamic loads in the drivetrain while using a synchronous generator to produce electricity directly on to the grid. [15]

Described in this chapter are examples of several active research areas relating to wind energy. There are many other research topics besides those mentioned here. Many different avenues of research are being pursued to provide solutions to the present day challenges of the wind energy industry.

This thesis will focus on the potential benefit of adding sensors to the wind turbine and the implementation of a magnetic CVT in above-rated wind speeds. The additional sensors can be used to actuate the blades earlier than standard control. Implementation of the CVT introduces another control variable which could allow the controller to regulate power output and minimize torque variations on the gearbox.

CHAPTER 2:

WIND TURBINE COMPONENTS AND INDUSTRY STANDARD CONTROL

Overview of Wind Turbine Components

Though there are many different configurations of wind turbines that exist today, the most common is a horizontal axis wind turbine (HAWT). A typical HAWT sits atop a tower so that the turbine is elevated above the surrounding terrain where the wind typically blows at higher speeds with less turbulence. Most large scale HAWTs are 'upwind' turbines, meaning that they have an active control system to point the turbine so that the blades are upwind of the tower. As the wind blows across the blades, it creates a rotational torque on the rotor. In large scale wind turbines, the rotor typically turns at relatively low speeds (12.1 rpm). The rotor is connected to a gearbox via a drive shaft. The gearbox of a typical large scale HAWT has a fixed gear ratio of approximately 1/100 (driving shaft speed/generator shaft speed). The load side of the gearbox spins a generator, which is either connected to power electronics or directly connected to the utility grid, depending on the generator technology. The drive shafts, gearbox and generator are typically housed in a casing atop the tower which is called the nacelle. The drive shafts rotate on an axis that is horizontal to the ground, hence the name HAWT. A diagram of a typical HAWT can be seen in Figure 2.1. [2]

Figure 2.1- Basic wind turbine diagram

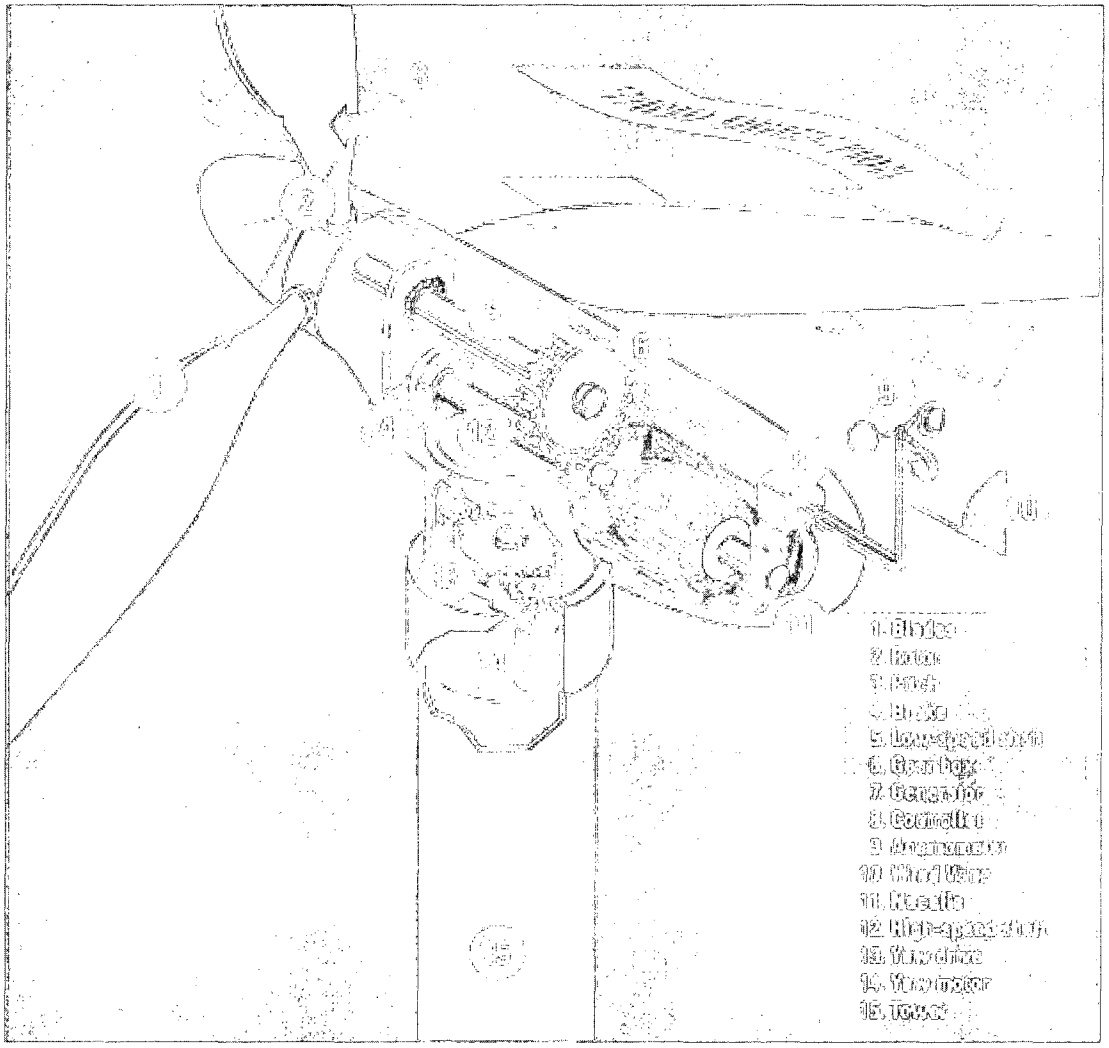

Image Source: (http://www.alliantenergy.com/Newsroom/MediaKitsPhotoGalleries/015077)

The energy from the wind is captured via the blades. Typically, large scale HAWTs have three blades. Two bladed turbines often suffer from unwanted dynamics from tower interference and differences in wind velocity at different heights. As the air flows over a wind turbine blade it creates a drag force and a lift force. The drag force flexes the wind turbine blades out of the plane of rotation and the lift force flexes the wind turbine blades in the plane of rotation as they transfer the torque to the rotor. The

lift force that provides rotational energy to the turbine is similar in principal to the lift force of airplane wings. [2]

The drive train of a typical large scale wind turbine connects the rotor to the generator. The torque that is applied to the rotor is transferred to the low speed side of the gearbox via the low speed shaft (LSS). The gearbox transforms the low speeds and high torques of the LSS to higher speeds and lower torques which drives the high speed shaft (HSS). The HSS connects the high speed side of the gearbox to the generator. [16]

Several different types of generators can be implemented in modern day wind turbines. Synchronous generators are the most common for producing electric power in the world. The drawback to these generators is that they are directly connected to the utility grid so they have to spin at a constant rotational speed to regulate the frequency of the output. [2] The constant speed requirement makes these generators a poor choice for a wind turbine that is driven by a variable source. Studies have been done on implementing CVTs in wind turbines with synchronous generators. [14] Another drawback to synchronous generators is that they must have their field windings excited by a DC source and transferred to the rotor via slip-rings which implies a maintenance issue. [2]

The most common generators for wind turbines are asynchronous induction generators. One advantage of asynchronous generators in wind turbines is that they do not require brushes, exciters or slip rings as synchronous generators do. This means that they are less complicated and require less maintenance. Induction generators can also spin at variable speeds which has several advantages. Variable speed operation allows the wind turbine to extract more power from below-rated wind speeds. It also allows the

wind turbine to handle more stresses on their mechanical components during turbulent winds. If a dramatic increase in wind speed were to occur, the wind turbine could speed up, rather than absorbing the forces directly into the components. Operating the generator at variable speeds does have a downside. The generator does not spin at a constant speed so it does not produce a constant frequency voltage signal and cannot be directly connected to the grid. Such generators must be connected to an inverter, which converts the wild AC voltage to DC and then back to AC. Some power is lost during this process, but it is necessary to produce a regulated frequency voltage that is compatible with the utility grid. [2]

Industry Standard Wind Turbine Operation and Control

There are several different regions of operations for wind turbines. When the turbine is at rest and starts to spin it is considered to be in Region 1. Once the wind turbine is spinning, but experiencing below-rated wind speeds, the wind turbine is said to be in Region 2. When the wind turbine is experiencing above-rated wind speeds it is in Region 3. The transition between Region 2 and Region 3 is considered to be operating in Region 2 ½. When the wind blows hard enough, the wind turbine must shut down to prevent damage. This is typically done through the use of a mechanical brake on the high speed shaft and this operation is considered to be Region 4. [17] Figure 2.2 shows the wind turbine operating regions.

Figure 2.2- Wind turbine operating regions

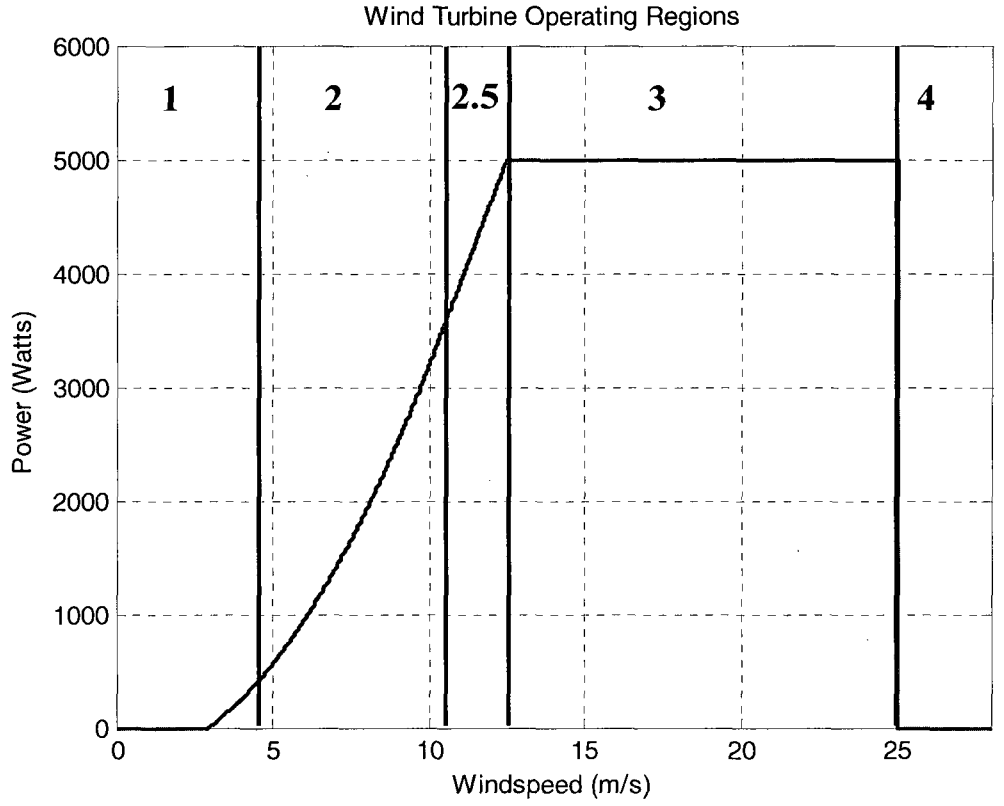

When operating in Region 2, industry standard wind turbine control systems have the goal of extracting the maximum amount of energy from the wind stream. The controller maintains the blades at a constant pitch angle and controls the rotor speed by changing the back torque of the generator, referred to as generator torque control. The torque is controlled by changing the firing angle of the converter. This has the effect of inducing a variable load torque to the high speed shaft. Varying this torque allows for control of the rotational speed of the wind turbine. [17]

The ideal operational speed of the wind turbine in Region 2 is dependent upon the wind speed. The blades are set to a constant pitch angle in Region 2. For the constant blade pitch angle, there is a fixed tip speed ratio (TSR) for maximum power extraction from the wind stream. This tip speed ratio is the ratio of the linear speed of the blade tips

divided by the wind speed. The wind turbine must rotate faster as the wind speed increases for maximum power extraction. This is the problem with installing synchronous, constant speed generators in conventional large scale HAWTs. A tachometer measures generator shaft speed and the generator torque is commanded to track the optimal TSR of the turbine. More details about generator torque control can be found in NREL technical papers. [10] [16] [17]

Control in Region 2 ½ is designed to allow the generator torque to increase so that operation in Region 3 occurs at rated speed and rated torque. If this intermediate region were not built into the control system and the turbine continued along the Region 2 trajectory, then the turbine would over-speed before it reached rated torque. [17]

The industry standard control systems have a different goal when operating in Region 3. In this region the wind speed is above the rated wind speed of the turbine. This means that more power can be extracted from the wind stream than the generator and components are rated for. To ensure that the turbine does not over-speed or over-torque the generator, the control system pitches the blades to shed some of the aerodynamic torque. The goal of the industry standard controllers in Region 3 is to produce constant regulated power at the rated level. [17]

When the turbine is operating in Region 3, the generator torque controller is typically exerting a constant drag torque through the generator on the load end of the HSS. This adds drive train torsional damping. [10] The blade pitch is actuated to achieve constant rotational speed. Since there is constant torque applied at the rated level, operating the wind turbine at constant rated speed will produce constant power at the rated output. Typical large scale HAWTs control blade pitch angle based on

proportional-integral-derivative (PID) feedback control applied to the generator rotational speed error (actual speed minus desired speed). The speed is measured by a tachometer or encoder on the HSS. [17]

This thesis will focus on Region 3 turbine operation and control. Constant generator torque will be commanded via the power electronics, as is consistent with standard operation and control in Region 3. The industry standard PI control performance will be used as a baseline to compare the performance of advanced controllers developed in Chapter 4.

CHAPTER 3:

MODEL DEVELOPMENT AND TESTING

Modeling Overview

Principal equations of motion for a wind turbine are derived and a model is developed. The purpose of developing the model is to gain understanding of how a wind turbine works and to test the control systems documented in Chapter 4. A linearized model of a large scale horizontal axis wind turbine (HAWT) in Region 3 is developed first. This model will be referred to as the derived linear model or DLIN model. Non-linear equations representing a magnetic continuously variable transmission (CVT) is then derived and substituted into the linear model. This model will be referred to as the derived non-linear model with a CVT, or DCVT model. Many of the parameters for the derived models come from a non-linear wind turbine model developed by the National Renewable Energy Laboratory (NREL) in their modeling software called Fatigue Aerodynamics Structures and Turbulence (FAST). Output responses of the DLIN and FAST model simulations are compared.

Model Derivation

The wind turbine lumped parameter model developed in this study was derived by approximating a HAWT with rotational inertias, torsion springs and dampers. This simplified wind turbine model is shown in Figure 3.1.

Figure 3.1- Simplified wind turbine model

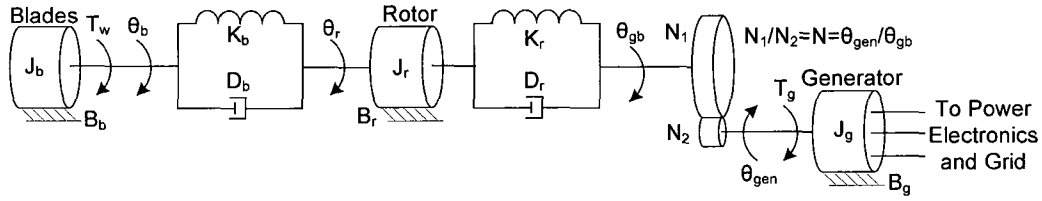

The blades are combined together into a single rotational inertia, J_b. The blades are combined into a single torsion spring and damper, K_b and D_b. The rotor and low speed shaft (LSS) were combined into a single rotational inertia, J_r. The equivalent spring and damping coefficient of the high speed shaft (HSS) were translated to the LSS and added to those of the LSS as a single drivetrain spring and damper, K_r and D_r. The rotational inertia of the gearbox is coupled with that of the generator, denoted as J_g.

This model simplifies many of the higher order complexities of a real wind turbine. All of the blades are assumed to flex the same amount. This model does not include the higher order blade bending dynamics and the effect of gravity on the blades. The torque due to the wind is calculated from a single wind speed. This means that the wind input to the model is assumed to be uniform over the entire rotor plane.

A series of equations were derived from the model in Figure 3.1. Equation (3.1) was written as the sum of the torques on the blades.

$$T_w = J_b\ddot{\theta}_b + B_b\dot{\theta}_b + D_b(\dot{\theta}_b - \dot{\theta}_r) + K_b(\theta_b - \theta_r). \tag{3.1}$$

The left hand side of equation (3.1) is the driving torque from the wind, T_w. The right hand side of the equation contains the load torque at the blades. The rotational inertia of the blades is denoted as J_b, B_b is the blade drag coefficient, D_b is the torsion damping coefficient of the blades, K_b is the torsion spring coefficient of the blades, $\ddot{\theta}_b$,

$\dot{\theta_b}$, θ_b are the respective rotational acceleration, velocity and position of the blade tips and $\dot{\theta_r}$, θ_r are the respective rotational velocity and position of the rotor. Solving equation (3.1) for $\ddot{\theta_b}$ results in:

$$\ddot{\theta}_b = \frac{T_w}{J_b} - \frac{B_b}{J_b}\dot{\theta}_b - \frac{D_b}{J_b}(\dot{\theta}_b - \dot{\theta}_r) - \frac{K_b}{J_b}(\theta_b - \theta_r). \tag{3.2}$$

Summing the torques at the rotor leads to the following equation:

$$D_b(\dot{\theta}_b - \dot{\theta}_r) + K_b(\theta_b - \theta_r) = J_r\ddot{\theta}_r + B_r\dot{\theta}_r + D_r(\dot{\theta}_r - \dot{\theta}_{gb}) + K_r(\theta_r - \theta_{gb}). \tag{3.3}$$

The rotational inertia of the rotor is J_r, B_r is the rotor friction coefficient, D_r is the torsion damping coefficient of the LSS, K_r is the torsion spring coefficient of the LSS, $\ddot{\theta}_r$, $\dot{\theta}_r$, θ_r are the respective rotational acceleration, velocity and position of the rotor respectively and $\dot{\theta}_{gb}$, θ_{gb} are the respective rotational velocity and position of the LSS side of the gearbox. Solving this equation for $\ddot{\theta_r}$:

$$\ddot{\theta}_r = \frac{D_b}{J_r}(\dot{\theta}_b - \dot{\theta}_r) + \frac{K_b}{J_r}(\theta_b - \theta_r) - \frac{B_r}{J_r}\dot{\theta}_r - \frac{D_r}{J_r}(\dot{\theta}_r - \dot{\theta}_{gb}) - \frac{K_r}{J_r}(\theta_r - \theta_{gb}). \tag{3.4}$$

The gear ratio N is defined as the speed of the driving shaft, or low speed shaft (LSS) divided by the speed of the load shaft, or high speed shaft (HSS).

$$N = \frac{\dot{\theta}_{LSS}}{\dot{\theta}_{HSS}}. \tag{3.5}$$

$$\dot{\theta}_{HSS}N = \dot{\theta}_{LSS}. \tag{3.6}$$

If a lossless gearbox is assumed there is conservation of energy ($E_{HSS} = E_{LSS}$). The mechanical energy of the shaft in watts is the rotational speed ($\dot{\theta}_x$) in radians per second multiplied by the torque (T_x) in Newton-meters.

$$E_{HSS} = \dot{\theta}_{HSS} * T_{HSS}. \tag{3.7}$$

$$E_{LSS} = \dot{\theta}_{LSS} * T_{LSS}. \tag{3.8}$$

$$\dot{\theta}_{HSS} * T_{HSS} = \dot{\theta}_{LSS} * T_{LSS}. \tag{3.9}$$

Substituting equation (3.6) into equation (3.9) and dividing by $\dot{\theta}_{HSS}$ results in the relation of torque through a gearbox:

$$NT_{LSS} = T_{HSS}. \tag{3.10}$$

Based on this relation, the equation for the sum of the torques at the high speed shaft side of the gearbox is:

$$N\left[D_r\left(\dot{\theta}_r - \dot{\theta}_{gb}\right) + K_r\left(\theta_r - \theta_{gb}\right)\right] = J_g\ddot{\theta}_{gen} + B_g\dot{\theta}_{gen} + T_L. \tag{3.11}$$

The rotational inertia of the generator is J_g, T_L is the load torque of the generator on the HSS, B_g is the rotor friction coefficient, and $\ddot{\theta}_{gen}$, $\dot{\theta}_{gen}$ are the rotational acceleration and velocity of the generator respectively. Solving this equation for $\ddot{\theta}_{gen}$:

$$\ddot{\theta}_{gen} = \frac{ND_r}{J_g}\left(\dot{\theta}_r - \dot{\theta}_{gb}\right) + \frac{NK_r}{J_g}\left(\theta_r - \theta_{gb}\right) - \frac{B_g}{J_g}\dot{\theta}_{gen} - \frac{T_L}{J_g}. \tag{3.12}$$

To put equation (3.12) in terms of the rotor and LSS side of the gearbox, the generator speed and acceleration must be transformed through the gearbox. The relation in equation (3.13) of the generator and gearbox speed is from equation (3.6).

$$\dot{\theta}_{gen} = \frac{\dot{\theta}_{gb}}{N}. \tag{3.13}$$

A relation between the LSS side of the gearbox and generator accelerations can be found by differentiating both sides of equation (3.13). The resulting relation can be seen below:

$$\ddot{\theta}_{gen} = \frac{\ddot{\theta}_{gb}}{N}. \tag{3.14}$$

From this point forward in the document the rotational velocity of the LSS side of the gearbox will be referred to as the 'gearbox velocity' or $\dot{\theta}_{gb}$. The same is true for the

position and acceleration. Note that a fixed gear ratio is assumed for this section of the document, so the gear ratio N is constant. The implementation of a continuously variable transmission will be analyzed in the next section of this chapter.

This wind turbine model will be studied in Region 3 operation. As stated in Chapter 2, it is common to have the generator torque controller exerting a constant back-torque on the HSS when operating in Region 3. [10] This study assumes that the generator torque control in Region 3 is ideal, providing a constant back-torque on the HSS. This model will transform the constant back torque into a frictional force proportional to the speed of the HSS. This allows the back torque to be implemented in state space representation, as seen in Chapter 4. If a control system was developed to regulate the speed of the generator, as is the goal in Region 3, then this torque will also be regulated. The equation for this transformation can be seen in equation (3.15).

$$T_L = B_L \dot{\theta}_{gen}. \tag{3.15}$$

Substituting equations (3.13), (3.14) and (3.15) into equation (3.12) results:

$$\frac{\ddot{\theta}_{gb}}{N} = \frac{ND_r}{J_g}\left(\dot{\theta}_r - \dot{\theta}_{gb}\right) + \frac{NK_r}{J_g}\left(\theta_r - \theta_{gb}\right) - \frac{B_g}{N}\dot{\theta}_{gb} - \frac{B_L}{N}\dot{\theta}_{gb}. \tag{3.16}$$

Solving this equation for $\ddot{\theta}_{gb}$:

$$\ddot{\theta}_{gb} = \frac{N^2 D_r}{J_g}\left(\dot{\theta}_r - \dot{\theta}_{gb}\right) + \frac{N^2 K_r}{J_g}\left(\theta_r - \theta_{gb}\right) - \frac{(B_g + B_L)}{J_g}\dot{\theta}_{gb}. \tag{3.17}$$

Equations (3.2), (3.4) and (3.17) were then realized as a model in Simulink®. Simulink® is a software program that is an environment for model based design and simulation for dynamic systems. The Simulink® environment allows the graphical design of these systems with drag-and-drop implementation of blocks from a library.

Simulink® interfaces with MATLAB® software, both produced by the Mathworks™. The implementation of these equations in Simulink® can be seen in Figure 3.2.

Figure 3.2- Block diagram of wind turbine model

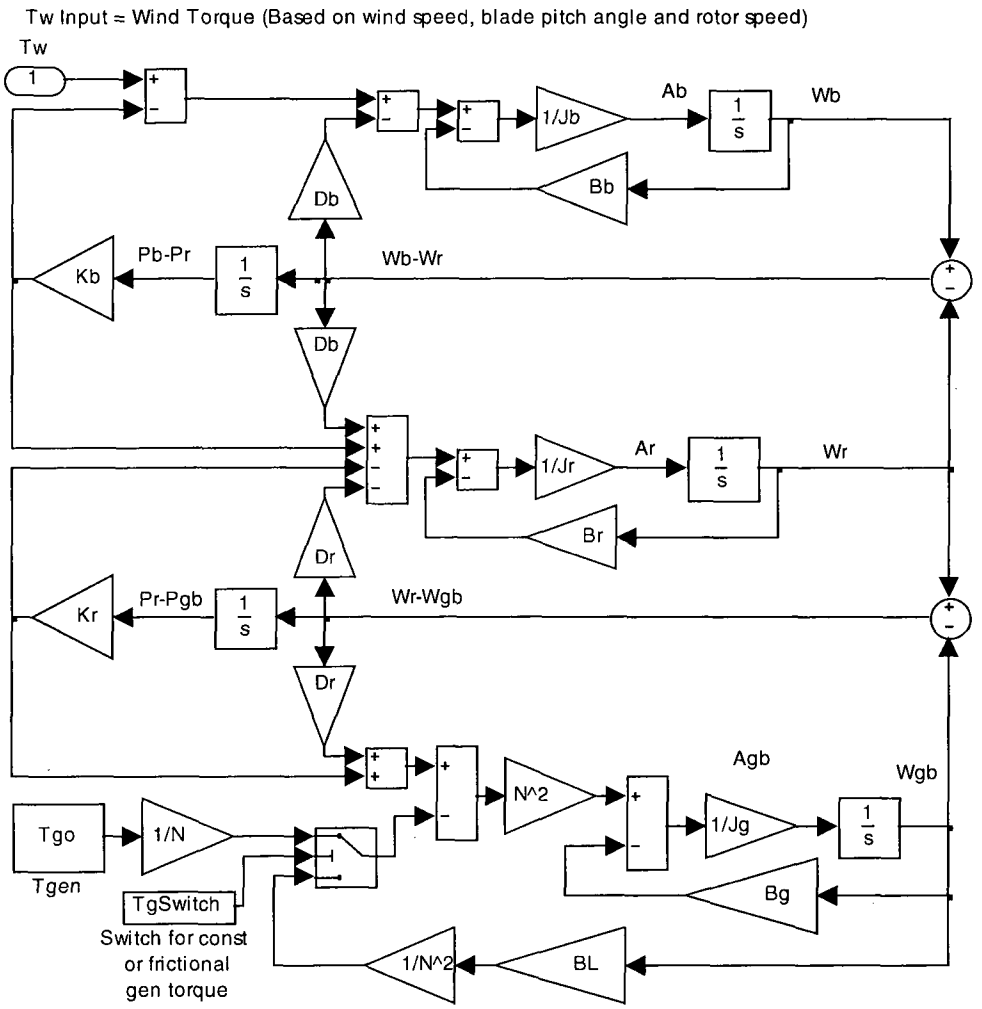

In Figure 3.2 Ab, Ar and Agb are the rotational accelerations of the blades, rotor and gearbox respectively, and Wb, Wr and Wgb are the rotational velocities of the blades, rotor and gearbox respectively. The flex of the blades is denoted as Pb-Pr and Pr-Pgb is the flex of the LSS. The model shown in Figure 3.2 includes a switch to change the model from a constant generator torque load (Tgo) to a frictional torque. The

switching variable, TgSwitch, and all other variables are initialized in a MATLAB® program that is run before the Simulink® model is run. This allows for the variables to be changed in a text-based format without having to manually enter the values into the Simulink® model.

Including a Continuously Variable Transmission

There are many types of continuously variable transmissions (CVTs) in the market. Most of these CVTs are mechanical in nature but magnetic CVTs have recently been developed by Magnomatics Ltd., a company based out of Sheffield, UK. According to their website, "Magnomatics revolutionary contactless, lubricant-free magnetic gear systems and ultra high torque electrical machines offer dramatic new engineering possibilities for a range of industries from aerospace to automotive to renewable energy and beyond." [18]

Figure 3.3- Magnetic CVT diagram

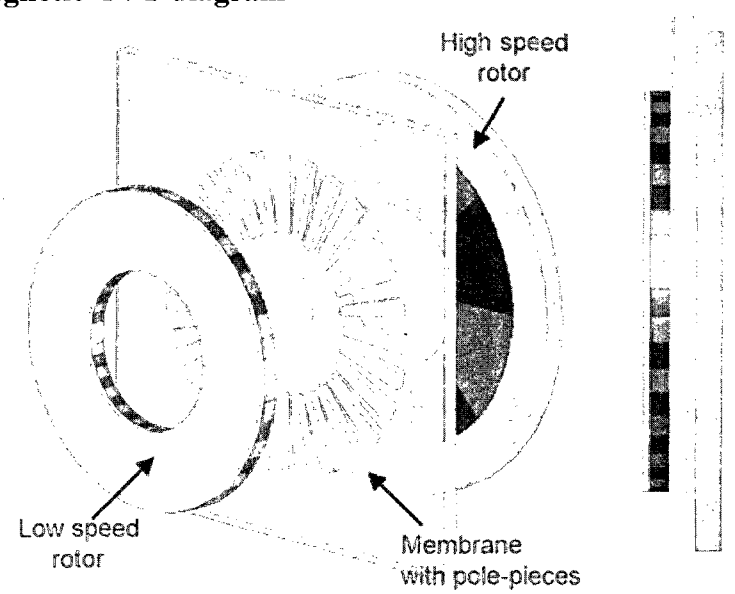

Image Source:
(http://www.engineerlive.com/Design-Engineer/Power_Transmission/Magnets_offer_advantages_as_an_alternative_to_mechanical_gears/22078/)

Communication was made with Magnomatics Ltd. to learn more about their magnetic CVT. The CVT works by coupling the high speed and low speed shaft with a magnetic field. This magnetic field is altered by rotating a membrane with pole pieces between the magnets of the high speed and low speed shafts, as seen in Figure 3.3. The rotational speed of the membrane determines the gear ratio. In Figure 3.3 the low speed and high speed rotors are depicted as flat plates for ease of viewing. For a high torque application such as the wind turbine, the rotors and pole embedded membrane would be cylinders to provide more surface area for coupling. Though Magnomatics Ltd. does not currently produce a CVT on the megawatt (MW) scale, conversations with them indicate that their CVTs are efficient and very fast with a virtually negligible time constant. The magnetic CVTs do introduce some springiness into the drivetrain. The CVT is assumed to have a gear ratio of .3-3, which is within the range of current magnetic CVTs. [19]

Studies have indicated that the implementation of a CVT in a wind turbine could allow for the elimination of power electronics. This is possible by actuating the CVT to maintain a constant generator rotational speed. [20] [21]

AAER, a Canadian wind turbine manufacturer, is implementing mechanical CVTs in their 2MW wind turbines. The CVTs are used to run a synchronous generator at constant speeds for direct grid connection. The dynamic loads in the drive train are also being controlled with the CVT. The CVT specifications and turbine performance data were not readily available from AAER. [15]

The utilization of a synchronous generator in the wind turbine was beyond the scope of this study. This thesis focused on the use of a postulated magnetic CVT to regulate power and mitigate torque variations in the drive train.

An approximation of a magnetic CVT was augmented in the DLIN model, creating a new non-linear model referred to as DCVT. The DCVT model was developed to analyze the potential benefits of implementing such a device in a wind turbine. Incorporating the CVT into the model provided an additional control input. The CVT model also added a spring (K_{CVT}) to the HSS. This spring was reflected through the gearbox to the low speed shaft by multiplying the spring constant by $\frac{1}{N^2}$. The spring constant of the CVT was unknown, so the CVT was assumed to have the equivalent spring constant of the turbine drive train, as seen in equation (3.18). The CVT spring was then combined in series with the spring of the rotor shaft, as seen in equation (3.19). When the CVT was included in the model, the resulting equivalent drivetrain spring constant (K_{eq}) is equal to the rotor shaft spring constant (K_r) divided in half. Figure 3.4 shows the inclusion of the CVT into the simplified wind turbine model.

$$\frac{K_{CVT}}{N^2} = K_r \tag{3.18}$$

$$\frac{1}{K_{eq}} = \frac{1}{K_r} + \frac{N^2}{K_{CVT}} = \frac{1}{K_r} + \frac{1}{K_r} = \frac{1}{2K_r} \tag{3.19}$$

Figure 3.4- Simplified wind turbine model with a CVT

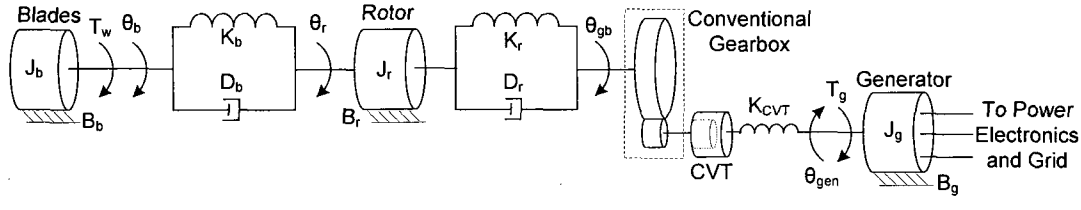

The wind turbine was designed around a fixed gear ratio of 1/97. This allows for the blades to have the proper aerodynamics while the generator is running at rated speed. The CVT is assumed to have a gear ratio of .3-3. For proper wind turbine operation, the conventional gearbox must be augmented with the CVT. The combined gear ratio of the

conventional gearbox and CVT is referred to as N. Figure 3.4 shows the wind turbine model of Figure 3.1 with a CVT added on the HSS side of the conventional gearbox.

When a CVT is incorporated into the model the acceleration of the generator is decoupled from the acceleration of the gearbox.

$$\ddot{\theta}_{gen} = \frac{d}{dt}(\dot{\theta}_{gen}) = \frac{d}{dt}(X\dot{\theta}_{gb}) = X\ddot{\theta}_{gb} + \dot{\theta}_{gb}\dot{X}, \tag{3.20}$$

where $X = \frac{1}{N}$. Using the chain rule:

$$\dot{X} = \frac{dX}{dt} = \frac{d\left(\frac{1}{N}\right)}{dt} = -\frac{1}{N^2}\frac{dN}{dt} = -\frac{1}{N^2}\dot{N}. \tag{3.21}$$

Substituting the equation above into equation (3.18) produces:

$$\ddot{\theta}_{gen} = \frac{d}{dt}(\dot{\theta}_{gen}) = \frac{d}{dt}\left(\frac{1}{N}\dot{\theta}_{gb}\right) = \frac{1}{N}\ddot{\theta}_{gb} - \frac{\dot{\theta}_{gb}}{N^2}\dot{N}. \tag{3.22}$$

Since the generator and gearbox accelerations are not directly proportional to each other, expressions are derived for both accelerations. Substituting equations (3.13), (3.15) and (3.22) into equation (3.12) produces:

$$\frac{1}{N}\ddot{\theta}_{gb} - \frac{\dot{\theta}_{gb}}{N^2}\dot{N} = \frac{ND_r}{J_g}(\dot{\theta}_r - \dot{\theta}_{gb}) + \frac{NK_r}{J_g}(\theta_r - \theta_{gb}) - \frac{(B_g + B_L)}{NJ_g}\dot{\theta}_{gb}. \tag{3.23}$$

Solving for $\ddot{\theta}_{gb}$:

$$\ddot{\theta}_{gb} = \frac{N^2D_r}{J_g}(\dot{\theta}_r - \dot{\theta}_{gb}) + \frac{N^2K_r}{J_g}(\theta_r - \theta_{gb}) - \frac{(B_g + B_L)}{J_g}\dot{\theta}_{gb} + \frac{\dot{\theta}_{gb}}{N}\dot{N}. \tag{3.24}$$

This equation was implemented in the Simulink® model as seen in Figure 3.5.

Figure 3.5- Block diagram of wind turbine model with a CVT

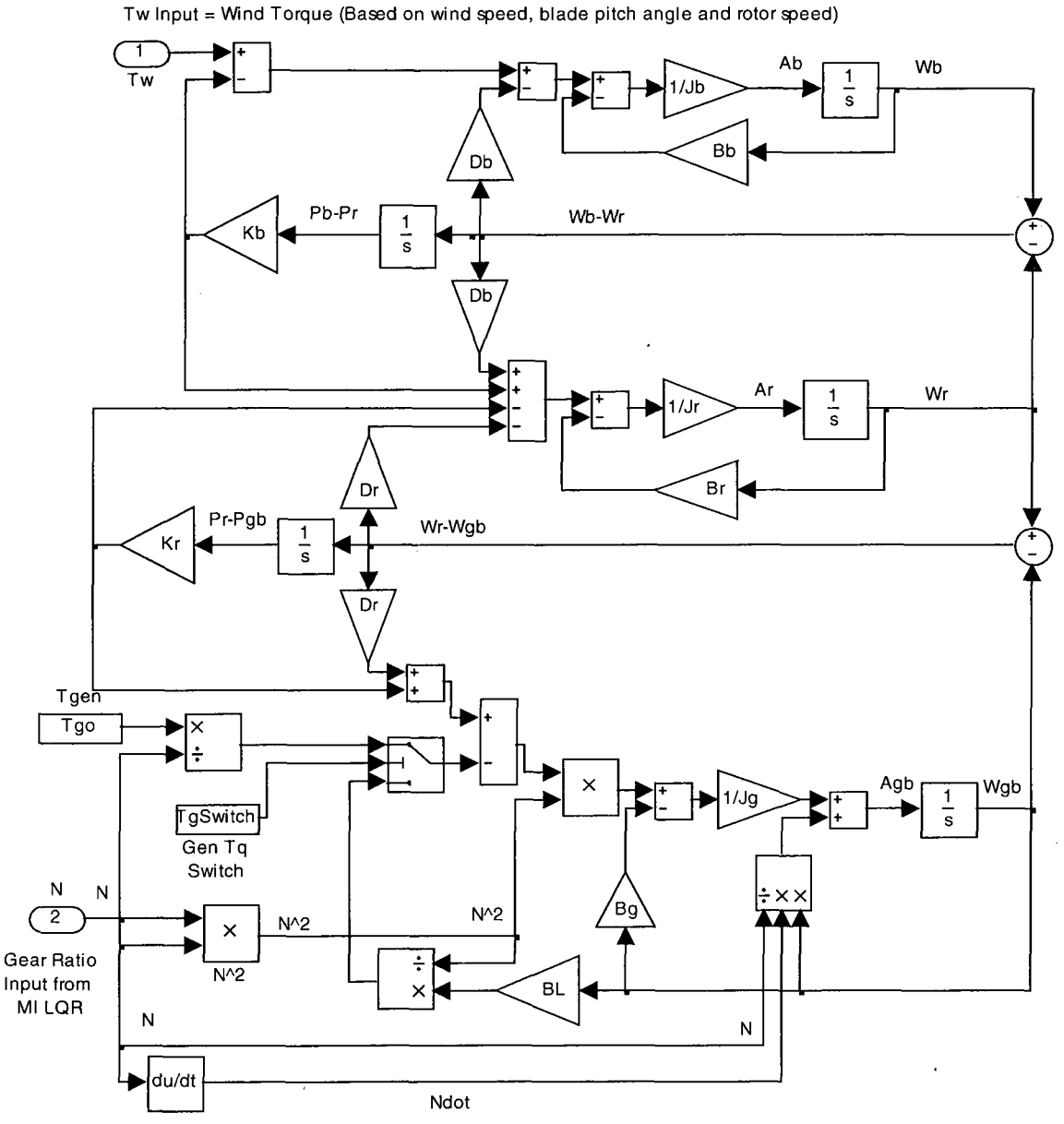

FAST Wind Turbine Model

The National Renewable Energy Laboratory (NREL) National Wind Technology Center (NWTC) has developed a wind turbine simulation code called Fatigue Aerodynamics Structures and Turbulence (FAST). FAST is documented thoroughly on its website, from which the following description is taken:

> NREL has sponsored the development, verification, and validation of various codes for prediction of wind-turbine loads and responses. A streamlined code was developed through a subcontract between NREL and Oregon State University. This code, called FAST, can be used to model both two- and three-bladed, horizontal-axis wind turbines.
>
> The FAST code models the wind turbine as a combination of rigid and flexible bodies. For example, two-bladed, teetering-hub turbines are modeled as four rigid bodies and four flexible ones. The rigid bodies are the earth, nacelle, hub, and optional tip brakes (point masses). The flexible bodies include blades, tower, and drive shaft. The model connects these bodies with several DOFs. These include tower bending, blade bending, nacelle yaw, rotor teeter, rotor speed, and drive shaft torsional flexibility. The flexible tower has two modes each in the fore-aft and side-to-side directions. The flexible blades have two flapwise modes and one edgewise mode per blade. One can turn these DOFs on or off individually in the analysis by simply setting a switch in the input data file.
>
> FAST uses Kane's method to set up equations of motion, which are solved by numerical integration. The implemented method makes direct use of the generalized coordinates, eliminating the need for separate constraint equations. FAST uses the AeroDyn subroutine package developed by Windward Engineering to generate aerodynamic forces along the blade.
>
> FAST is extensively documented in the FAST User's Guide. Please refer to it for details on the use of the program. ...
>
> FAST with AeroDyn was evaluated by Germanischer Lloyd WindEnergie and found suiTable for "the calculation of onshore wind turbine loads for design and certification. [22]

The certificate, report, FAST user's guide and the FAST archives can be found on the FAST website. FAST has gone through several revisions, so it is important to note that FAST version 6.01 was used for this study.

FAST has the ability to interface with Simulink® software. FAST can generate a Simulink® S-Function that incorporates custom FAST Fortran routines. A text document that contains turbine physical properties and operating conditions can be edited. This text document can be compiled into the Simulink S-Function. This S-Function can be

incorporated in a Simulink® model so that the user may design and test control systems in Simulink®. [16]

The Simulink® S-Function block takes 3 control inputs: yaw control, blade pitch angle and generator torque control. This study will utilize only the blade pitch control input of the FAST model. [16] The FAST Nonlinear Wind Turbine block can be seen in Figure 3.6. 'OutData' is a multi-channel bus of all output variables specified in the input text document. These outputs can be used as control inputs or for post simulation analysis.

Figure 3.6- FAST wind turbine block in Simulink

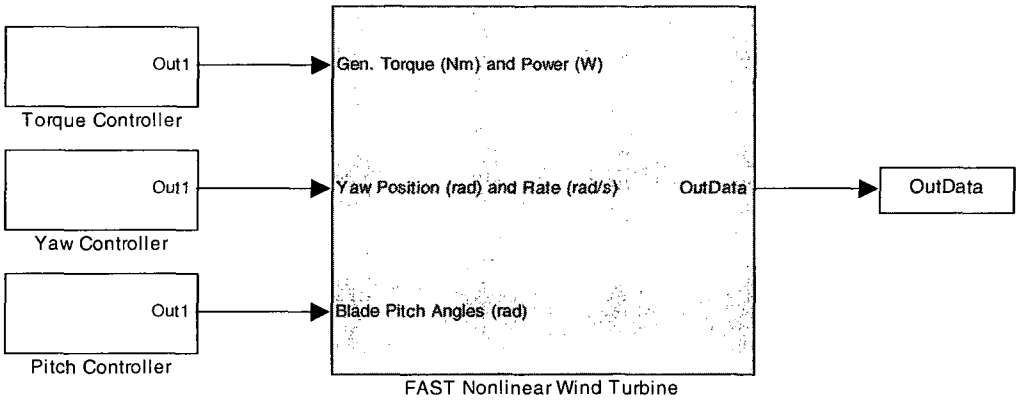

The engineers at NREL NWTC have developed FAST files for several different wind turbine models. Many of the values used in the derived model were extracted from the NREL FAST 5MW wind turbine model. This model was created based on information on large scale wind turbines from manufacturers, primarily the Repower 5M machine. More specific information can be found in the 5MW reference guide. [6] The gross properties of the 5MW FAST model are listed in Table 3.1. These values were assumed for the derived model. Specific values used in the derived model were largely taken from the 5MW model and can be found in Table 3.2.

Table 3.1- Gross properties of the NREL FAST 5MW wind turbine

Rating	5 MW
Rotor Orientation, Configuration	Upwind, 3 Blades
Control	Variable Speed, Collective Pitch
Drivetrain	High Speed, Multiple-Stage Gearbox
Rotor, Hub Diameter	126 m, 3 m
Hub height	90 m
Cut-In, Rated, Cut-Out Wind Speed	3 m/s, 11.4 m/s, 25 m/s
Cut-In, Rated Rotor Speed	6.9 rpm, 12.1 rpm
Rated Tip Speed	80 m/s

Source: [6]

Table 3.2- Wind turbine parameters and values

Variable Name	**Symbol**	**Value**	**Units**
Blade mass (all 3)	M_b	5.322e+004	Kg
Blade inertia (all 3)	J_b	3.528e+007	Kg-m^2
Blade drag	B_b	5.7117e+005	Nm/(rad/s)
Blade damping coefficient	D_b	1.7135e+006	Nm/(rad/s)
Blade spring coefficient	K_b	1.6225e+009	Nm/rad
Rotor inertia	J_r	1.15e+005	Kg-m^2
Rotor friction	B_r	1.1e+004	Nm/(rad/s)
LSS damping coefficient	D_r	6.215e+006	Nm/(rad/s)
LSS spring coefficient	K_r	8.67637e+008	Nm/rad
Generator inertia	J_g	5.34116e+002	Kg-m^2
Generator friction	B_g	0	Nm/(rad/s)
Rated generator speed	$\dot{\theta}_{gen_0}$	122.91 (1174)	rad/s (rpm)
Rated Mechanical Power	P_0	5.296610e+006	Watts
Generator Torque	T_L	4.309355+004	Nm
Electrical load equivalent friction	B_L	350.6118	Nm/(rad/s)
Generator Efficiency	GenEff	94.4	%
Blade actuator time constant	τ_b	.2	seconds
Max Generator Torque	-	4.740291e+004	Nm
Max Blade Pitch Rate	-	8	degrees/sec
Min Blade Pitch Angle	-	0	degrees
Max Blade Pitch Angle	-	90	degrees

Values for M_b, J_b, J_r, D_r, K_r, and J_g came directly from the National Renewable Energy Laboratory (NREL) National Wind Technology Center (NWTC) 5 MW FAST model and associated report. The values for the rated mechanical power, rated generator speed, generator efficiency, max blade pitch rate, max blade pitch angle and min blade pitch angle also came from this source. [6] The blade actuator time constant (τ_b) came from an NREL report that provided the time constant from the model of a real wind turbine. [10]

The generator load torque (T_L) was calculated by dividing the rated mechanical power (P_0) by the rated generator speed $\left(\dot{\theta}_{gen_0}\right)$. When the turbine is running at the rated speed, it will also be running at rated mechanical power. The electrical load equivalent friction (B_L) was calculated to produce the generator load torque (T_L) when the turbine is operating at rated speed. This value is multiplied by the speed of the generator shaft to produce a torque, so the value is calculated as T_L divided by $\left(\dot{\theta}_{gen_0}\right)$. FAST does not account for generator friction, as this friction would be negligible when compared to the generator constant torque. Therefore, the generator friction term (B_g) was set to 0. [16]

The blade spring and damping coefficients (K_b and D_b) were chosen by matching blade response characteristics provided by NREL with that of the blade equations derived earlier in this report. The NREL 5MW model had a structural damping ratio of 0.477465, and the first natural mode of the blade asymmetric edgewise pitch is at 1.0793 Hz. To implement these blade properties in the derived model equation (3.1) is analyzed with the rotor locked in position.

$$T_w = J_b\ddot{\theta}_b + (B_b + D_b)\dot{\theta}_b + K_b\theta_b. \tag{3.25}$$

Applying the Laplace transform to this equation results in:

$$T_w(s) = J_b\Theta s^2 + (B_b + D_b)\Theta s + K_b\Theta. \tag{3.26}$$

Turning this equation into a transfer function results in:

$$\frac{\Theta}{T_w(s)} = \frac{1}{J_b s^2 + (B_b + D_b)s + K_b}. \tag{3.27}$$

Normalizing the coefficient of the highest order term of the denominator:

$$\frac{\Theta}{T_w(s)} = \frac{\frac{1}{J_b}}{s^2 + \frac{(B_b + D_b)}{J_b}s + \frac{K_b}{J_b}}. \tag{3.28}$$

The standard form for a normalized second order transfer function is:

$$H(s) = \frac{\omega_n^2 K}{s^2 + 2\zeta\omega_n s + \omega_n^2}. \tag{3.29}$$

Where ζ is the damping ratio and ω_n is the undamped natural frequency. The equation for the damped natural frequency ω_d is:

$$\omega_d = \omega_n\sqrt{1 - \zeta^2}. \tag{3.30}$$

Setting each term of the denominators in equations (3.26) and (3.27) equal to each other and solving for K_b and (D_b+B_b) results in the following two equations:

$$K_b = \omega_n^2 * J_b = \frac{\omega_d * J_b}{\sqrt{1 - \zeta^2}}. \tag{3.31}$$

$$B_b + D_b = 2\zeta\omega_n * J_b = \frac{\omega_d * J_b}{\sqrt{1 - \zeta^2}}. \tag{3.32}$$

[23]

Since NREL provided values of J_b= 35,280,000 kg*m^2, ζ= .477465 and ω_d= 1.0793*(2π) rad/s, the left hand side of the two previous equations can be calculated directly. The blade spring constant, K_b was evaluated and included in Table 3.2. The blade drag coefficient (B_b) represents the air resistance force as the blades are spinning.

This value has roughly the same effect as the change in torque from the wind due to a change in rotor speed $\left(\frac{dT_w}{dW_s}\right)$ as described in the next section of the report. The ratio of D_b to B_b was chosen to be 3:1. This relationship was decided by comparing the step response of the DLIN model compared to that of FAST. The step responses of the models can be seen in Figure 3.8, found in the 'Model Validation and Testing' section of this chapter. Step response comparisons were made with different ratios of D_b and B_b. The 3:1 ratio provided the closest output response to the FAST model. The respective values of D_b and B_b can be seen in Table 3.2.

Linearization

A linearized model must be derived in order to develop a state-space model and utilize modern state-space control techniques. State-space means that states are assigned to the variables of the equations of motion. The derivative of any state (change in state divided by change in time) can be described as a time invariant linear combination of the states. To linearize the functions, Taylor series expansion is applied by evaluating a function at the operating point and taking the partial derivatives with respect to variables in the function, as seen below for a two variable equation:

$$f(x,y) = f(x_0,y_0) + \left.\frac{\partial f}{\partial x}\right|_0 \delta x + \left.\frac{\partial f}{\partial y}\right|_0 \delta y + \cdots$$
$$\cdots \frac{1}{2!}\left[\left.\frac{\partial^2 f}{\partial x^2}\right|_0 \delta x^2 + 2\left.\frac{\partial^2 f}{\partial x \partial y}\right|_0 \delta x \delta y + \left.\frac{\partial^2 f}{\partial y^2}\right|_0 \delta y^2\right] + \cdots. \quad (3.33)$$

[24]

Here $\left.\frac{\partial f}{\partial x}\right|_0$ means the partial derivative of the function with respect to x and evaluated at the operating point and δx is the change in variable x. The Taylor series

equation above continues for an infinite amount of terms. For linearization, only the first three terms are used. This report will be using Δx instead of δx. The linearization equation can be seen below.

$$f(x,y) \approx f(x_0 + \Delta x, y_0 + \Delta y) = f(x_0, y_0) + f(\Delta x, \Delta y). \tag{3.34}$$

$$f(x,y) \approx f(x_0, y_0) + \left.\frac{\partial f}{\partial x}\right|_0 \Delta x + \left.\frac{\partial f}{\partial y}\right|_0 \Delta y. \tag{3.35}$$

The torque due to the wind (T_w) is a nonlinear function that depends upon the wind speed, rotor speed and the blade pitch angle. The Taylor series expansion of this function can be seen in the following equation:

$$T_w(W_s, \beta, \dot{\theta}_r) = T_w(W_{s0}, \beta_0, \dot{\theta}_{r_0}) + \frac{\partial T_w}{\partial W_s}\Delta W_s + \frac{\partial T_w}{\partial \beta}\Delta\beta + \frac{\partial T_w}{\partial \dot{\theta}_r}\Delta\dot{\theta}_r + H.O.T. \tag{3.36}$$

Where W_s is the wind speed, β is the blade pitch angle and $\dot{\theta}_r$ is the rotational speed of the rotor and $H.O.T.$ is the higher order terms which are neglected in linearization. [10] Figure 3.7 shows the incorporation of the linearized wind torque equation in Simulink®.

The wind turbine is linearized about an operating point. The linearization operating point variables are described in Table 3.3.

Figure 3.7- Wind torque linearization block diagram

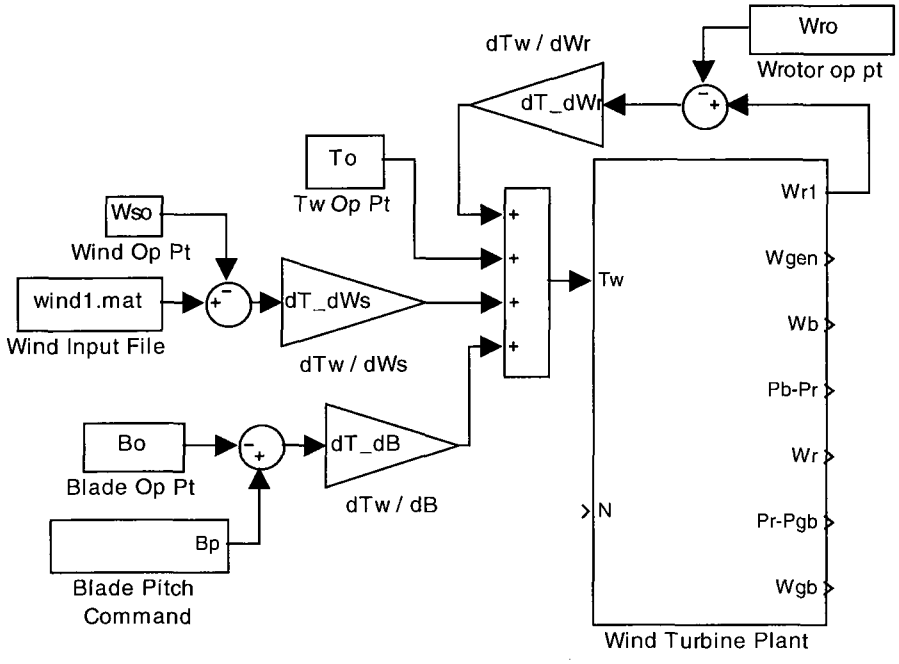

Table 3.3- Linearization point for wind turbine model

Variable Name	Symbol	Value	Units
Wind Speed	W_{s0}	18	m/s
Blade rotational speed	$\dot{\theta}_{g_0}$	1.267 (12.1)	rad/s (rpm)
Rotor rotational speed	$\dot{\theta}_{r_0}$	1.267 (12.1)	rad/s (rpm)
Gearbox (LSS side) rotational speed	$\dot{\theta}_{gb_0}$	1.267 (12.1)	rad/s (rpm)
HSS rotational speed	$\dot{\theta}_{gen_0}$	122.91 (1174)	rad/s (rpm)
Torque from wind at op pt.	T_{w_0}	4.9178e+006	Nm
Blade pitch angle	β_0	15.98	degrees
Gear ratio	N_0	1/97 (.0103)	-
Change in torque from the wind due to change in blade pitch angle	$\frac{\partial T_w}{\partial \beta}$	-9.1991e+005	Nm/degree
Change in torque from the wind due to change in rotor speed	$\frac{\partial T_w}{\partial \dot{\theta}_r}$	-1.0941e+007	Nm/(rad/s)
Change in torque from the wind due to change in wind speed	$\frac{\partial T_w}{\partial W_s}$	1.2074e+006	Nm/(m/s)
Blade flex	$(\theta_b - \theta_r)_0$	2.63e-003	radians
LSS flex	$(\theta_r - \theta_{gb})_0$	4.82e-003	radians

Region 3 operation of this wind turbine spans from wind speeds of 11.4 m/s to 25 m/s. [6] A wind speed of 18 m/s was chosen for the linearization point since it is close to the center of this operating range. Wind input files could then be generated with mean of 18 m/s without the wind speed exceeding the Region 3 range.

The blade, rotor and gearbox linearization speeds were chosen as the rated speed of the 5MW FAST wind turbine model. The gear ratio linearization point was chosen as the fixed value of the gearbox in the 5MW model. Note that the NREL engineers define N as the angular velocity of the HSS divided by the angular velocity of the LSS. This document uses the inverse notation. The linearization generator speed is calculated by simply dividing the rated rotor speed divided by the operating point gear ratio.

The wind turbine is assumed to be in steady state operation at the linearization point. All rotational accelerations at the linearization point are zero. This also means that the net torque on the wind turbine must be zero. The generator is assumed to have a constant load torque on the HSS. The torque due to the wind at the linearization point is then calculated as the generator torque divided by the gear ratio plus the sum of the friction coefficients multiplied by their respective rated speeds.

The blade pitch angle for the linearization point was realized by running the FAST model with a constant wind input. The blade pitch angle was controlled with the standard PI controller described in Chapter 4. The model arrived at a steady state condition with the rotor and generator speed at the rated speed. The steady state blade pitch angle was used as that of the linearization point.

The FAST software has the ability to linearize the wind turbine around a set point. The 5MW wind turbine model was linearized in FAST about the operating point.

The FAST linearization does not use the same blade deflection states as chosen for the DLIN model. Through manual calculations, the values for the change in torque on the blades due to changes in blade pitch angle, rotor speed and wind speed were extracted from the FAST linearization. To explore the FAST linearization procedure in detail, please refer to the FAST User's Guide. [16]

As the shafts rotate θ_b, θ_r, θ_{gb}, θ_{gen} are all periodic over the range of 0 to 2π. These variables have no independent operating point value. When the wind delivers torque is to the turbine components, the blades and LSS flex to deliver the rotational energy down the drivetrain. The steady state blade and LSS flex was measured at the operating point. The model was simulated with constant wind input and all values set to the linearization point. The steady state values of the blade and rotor shaft flex were recorded. FAST linearization validated the steady state flex of the rotor shaft, producing a value of 4.547e-003 rads.

The equations of motion for the wind turbine were then linearized about this operating point. Applying Taylor expansion to equation (3.2):

$$\ddot{\theta}_b = \frac{T_{w0}}{J_b} - \frac{B_b}{J_b}\dot{\theta}_{b0} - \frac{D_b}{J_b}(\dot{\theta}_{b0} - \dot{\theta}_{r0}) - \frac{K_b}{J_b}(\theta_b - \theta_r)_0 + \ldots$$
$$\ldots \frac{\frac{\partial T_w}{\partial W_s}\Delta W_s + \frac{\partial T_w}{\partial \beta}\Delta\beta + \frac{\partial T_w}{\partial \dot{\theta}_r}\Delta\dot{\theta}_r}{J_b} - \frac{B_b}{J_b}\Delta\dot{\theta}_b - \frac{D_b}{J_b}(\Delta\dot{\theta}_b - \Delta\dot{\theta}_r) - \frac{K_b}{J_b}(\Delta\theta_b - \Delta\theta_r). \quad (3.37)$$

The blade acceleration can be broken into the operating point plus a deviation away from the operating point:

$$\ddot{\theta}_b = \ddot{\theta}_{b0} + \Delta\ddot{\theta}_b. \quad (3.38)$$

Separating equation (3.37) into the function evaluated at the operating point and deviations away from this point can be seen in the following two equations:

$$\ddot{\theta}_{b_0} = \frac{T_{w0}}{J_b} - \frac{B_b}{J_b}\dot{\theta}_{b_0} - \frac{D_b}{J_b}(\dot{\theta}_{b_0} - \dot{\theta}_{r_0}) - \frac{K_b}{J_b}(\theta_b - \theta_r)_0. \tag{3.39}$$

$$\Delta\ddot{\theta}_b = \frac{\frac{dT_w}{dW_s}\Delta W_s + \frac{dT_w}{d\beta}\Delta\beta + \frac{dT_w}{d\dot{\theta}_r}\Delta\dot{\theta}_r}{J_b} - \frac{B_b}{J_b}\Delta\dot{\theta}_b - \frac{D_b}{J_b}(\Delta\dot{\theta}_b - \Delta\dot{\theta}_r) - \frac{K_b}{J_b}\Delta(\theta_b - \theta_r). \tag{3.40}$$

The turbine is assumed to be in steady state at the operating point, with the blade acceleration $\ddot{\theta}_{b_0} = 0$. Evaluating the right hand side of equation (3.37) results in zero. Notice in Table 3.2 that the operating points of the blade and rotor rotational speed are equal. The subtraction of these two values in the equation results in 0.

One could have derived equation (3.40) by noticing that equation (3.2) was already a linear equation. The same is true for equations (3.4) and (3.17) if a fixed gear ratio is assumed. These equations are linearized using the same method.

$$\begin{aligned}\ddot{\theta}_{r_0} = {} & \frac{D_b}{J_r}(\dot{\theta}_{b_0} - \dot{\theta}_{r_0}) + \frac{K_b}{J_r}(\theta_b - \theta_r)_0 - \frac{B_r}{J_r}\dot{\theta}_{r_0} \dots \\ & - \frac{D_r}{J_r}\left(\dot{\theta}_{r_0} - \dot{\theta}_{gb_0}\right) - \frac{K_r}{J_r}\left(\theta_r - \theta_{gb}\right)_0.\end{aligned} \tag{3.41}$$

$$\begin{aligned}\Delta\ddot{\theta}_r = {} & \frac{D_b}{J_r}(\Delta\dot{\theta}_b - \Delta\dot{\theta}_r) + \frac{K_b}{J_r}\Delta(\theta_b - \theta_r) - \frac{B_r}{J_r}\Delta\dot{\theta}_r \dots \\ & - \frac{D_r}{J_r}(\Delta\dot{\theta}_r - \Delta\dot{\theta}_{gb}) - \frac{K_r}{J_r}\Delta(\theta_r - \theta_{gb}).\end{aligned} \tag{3.42}$$

$$\ddot{\theta}_{gb_0} = \frac{N^2 D_r}{J_g}\left(\dot{\theta}_{r_0} - \dot{\theta}_{gb_0}\right) + \frac{N^2 K_r}{J_g}\left(\theta_r - \theta_{gb}\right)_0 - \frac{(B_g + B_L)}{J_g}\dot{\theta}_{gb_0}. \tag{3.43}$$

$$\Delta\ddot{\theta}_{gb} = \frac{N^2 D_r}{J_g}(\Delta\dot{\theta}_r - \Delta\dot{\theta}_{gb}) + \frac{N^2 K_r}{J_g}\Delta(\theta_r - \theta_{gb}) - \frac{(B_g + B_L)}{J_g}\Delta\dot{\theta}_{gb}. \tag{3.44}$$

Linearization with a CVT

When adding a continuously variable transmission (CVT), the equation for the acceleration of the gearbox side of the LSS will change. These changes introduce

nonlinear terms into the equation. The equation for the generator acceleration is repeated below for ease of reference:

$$\ddot{\theta}_{gen} = \frac{ND_r}{J_g}(\dot{\theta}_r - \dot{\theta}_{gb}) + \frac{NK_r}{J_g}(\theta_r - \theta_{gb}) - \frac{(B_g + B_L)}{NJ_g}\dot{\theta}_{gb}. \tag{3.45}$$

Recall from the previous section that the operating point accelerations are zero. Here the generator acceleration equation is separated as the operating point plus a deviation from that operating point for ease of viewing.

$$\ddot{\theta}_{gen} = \ddot{\theta}_{gen_0} + \Delta\ddot{\theta}_{gen}. \tag{3.46}$$

$$\ddot{\theta}_{gen_0} = \frac{N_0 D_r}{J_g}\left(\dot{\theta}_{r_0} - \dot{\theta}_{gb_0}\right) + \frac{N_0 K_r}{J_g}(\theta_r - \theta_{gb})_0 - \frac{(B_g + B_L)}{N_0 J_g}\dot{\theta}_{gb_0}. \tag{3.47}$$

The operating point rotational speeds for the rotor and gearbox end of the LSS are equal, causing the terms to subtract to zero. The other two terms on the right hand side of the above equation subtract to be zero. This result is as expected since the wind turbine is in equilibrium at the operating point.

The rest of the Taylor series linearization equation is:

$$\begin{aligned}\Delta\ddot{\theta}_{gen} = {} & \frac{N_0 D_r}{J_g}(\Delta\dot{\theta}_r - \Delta\dot{\theta}_{gb}) + \frac{D_r}{J_g}\left(\dot{\theta}_{r_0} - \dot{\theta}_{gb_0}\right)\Delta N + \frac{N_0 K_r}{J_g}\Delta(\theta_r - \theta_{gb}) \ldots \\ & \ldots + \frac{K_r}{J_g}(\theta_r - \theta_{gb})_0 \Delta N - \frac{(B_g + B_L)}{N_0 J_g}\dot{\theta}_{gb} + \frac{(B_g + B_L)}{N_0^2 J_g}\dot{\theta}_{gb_0}\Delta N.\end{aligned} \tag{3.48}$$

Again, the shaft speeds are equal at the operating point. Canceling out this term results:

$$\begin{aligned}\Delta\ddot{\theta}_{gen} = {} & \frac{N_0 D_r}{J_g}(\Delta\dot{\theta}_r - \Delta\dot{\theta}_{gb}) + \frac{N_0 K_r}{J_g}\Delta(\theta_r - \theta_{gb}) + \frac{K_r}{J_g}(\theta_r - \theta_{gb})_0 \Delta N \ldots \\ & \ldots - \frac{(B_g + B_L)}{N_0 J_g}\dot{\theta}_{gb} + \frac{(B_g + B_L)}{N_0^2 J_g}\dot{\theta}_{gb_0}\Delta N.\end{aligned} \tag{3.49}$$

The same process must be applied to the equation for gearbox acceleration. Equation (3.24) is repeated below for ease of reference. This equation is linearized and separated into the function evaluated at the operating point at zero acceleration and

deviations away from the operating point in the same method as undertaken in generator acceleration expressions above.

$$\ddot{\theta}_{gb} = \frac{N^2 D_r}{J_g}(\dot{\theta}_r - \dot{\theta}_{gb}) + \frac{N^2 K_r}{J_g}(\theta_r - \theta_{gb}) - \frac{(B_g + B_L)}{J_g}\dot{\theta}_{gb} + \frac{\dot{\theta}_{gb}}{N}\dot{N}. \tag{3.50}$$

$$\ddot{\theta}_{gb} = \ddot{\theta}_{gb_0} + \Delta\ddot{\theta}_{gb}. \tag{3.51}$$

$$\ddot{\theta}_{gb_0} = \frac{{N_0}^2 D_r}{J_g}\left(\dot{\theta}_{r_0} - \dot{\theta}_{gb_0}\right) + \frac{{N_0}^2 K_r}{J_g}(\theta_r - \theta_{gb})_0 - \frac{(B_g + B_L)}{J_g}\dot{\theta}_{gb_0} + \frac{\dot{\theta}_{gb_0}}{N_0}\dot{N}_0. \tag{3.52}$$

$$\begin{aligned}\Delta\ddot{\theta}_{gb} = {} & \frac{{N_0}^2 D_r}{J_g}(\Delta\dot{\theta}_r - \Delta\dot{\theta}_{gb}) + \frac{2N_0 D_r}{J_g}\left(\dot{\theta}_{r_0} - \dot{\theta}_{gb_0}\right)\Delta N + \frac{{N_0}^2 K_r}{J_g}\Delta(\theta_r - \theta_{gb}) \ldots \\ & \ldots + \frac{2N_0 K_r}{J_g}(\theta_r - \theta_{gb})_0 \Delta N - \frac{(B_g + B_L)}{J_g}\Delta\dot{\theta}_{gb} + \frac{\dot{\theta}_{gb_0}}{N_0}\Delta\dot{N} + \frac{\dot{N}_0}{N_0}\Delta\dot{\theta}_{gb} - \frac{\dot{\theta}_{gb_0}}{N_0^2}\dot{N}_0\Delta N.\end{aligned} \tag{3.53}$$

Again, the shaft speeds at the linearization point are equal so the second and fourth terms are zero. The gear ratio rate of change at the operating point, $\dot{N}_0$, is also zero. Canceling these terms results in:

$$\begin{aligned}\Delta\ddot{\theta}_{gb} = {} & \frac{{N_0}^2 D_r}{J_g}(\Delta\dot{\theta}_r - \Delta\dot{\theta}_{gb}) + \frac{{N_0}^2 K_r}{J_g}\Delta(\theta_r - \theta_{gb}) + \frac{2N_0 K_r}{J_g}(\theta_r - \theta_{gb})_0 \Delta N \ldots \\ & \ldots - \frac{(B_g + B_L)}{J_g}\Delta\dot{\theta}_{gb} + \frac{\dot{\theta}_{gb_0}}{N_0}\Delta\dot{N}.\end{aligned} \tag{3.54}$$

These linearized equations are utilized to represent the system in a state-space model when describing the LQR control system development in Chapter 4.

Model Testing and Validation

Tests were done comparing the simulations of the DLIN and the FAST 5MW model to ensure that the DLIN model was a reasonable representation of a wind turbine. These tests were performed by comparing the open loop turbine output responses when

using the same wind input in the DLIN model and FAST. Running the simulations open loop means that the blades are set to the operating point pitch angle and remain constant for the entire simulation. Both the DLIN model and FAST employed constant generator torque control.

First, the step response of the two models was compared to ensure that the developed model had a reasonable DC gain and time constant to the step input. The wind speed input was 18 m/s with a half meter per second step increase and decrease in the wind speed. Output plots of the DLIN and FAST model step responses can be seen in Figure 3.8.

The step responses from the DLIN model and FAST can be directly compared when plotted in the same graph. Overall the responses are remarkably similar to each other, as seen in Figure 3.8. A closer look at the rising edge of the step response can be seen in Figure 3.9. From this plot it is noticeable that the DLIN model has a slightly longer time constant than the FAST model. Variations in the response are due to flexing of the blades and LSS. When the step in wind speed first occurs, the FAST model has significantly larger fluctuations due to the higher order model of the blades. Several seconds after the step in wind input, the more extreme fluctuations of the FAST response dissipate and the variations in the two responses are of similar shape and magnitude.

Figure 3.8- Model responses to step changes in wind speed

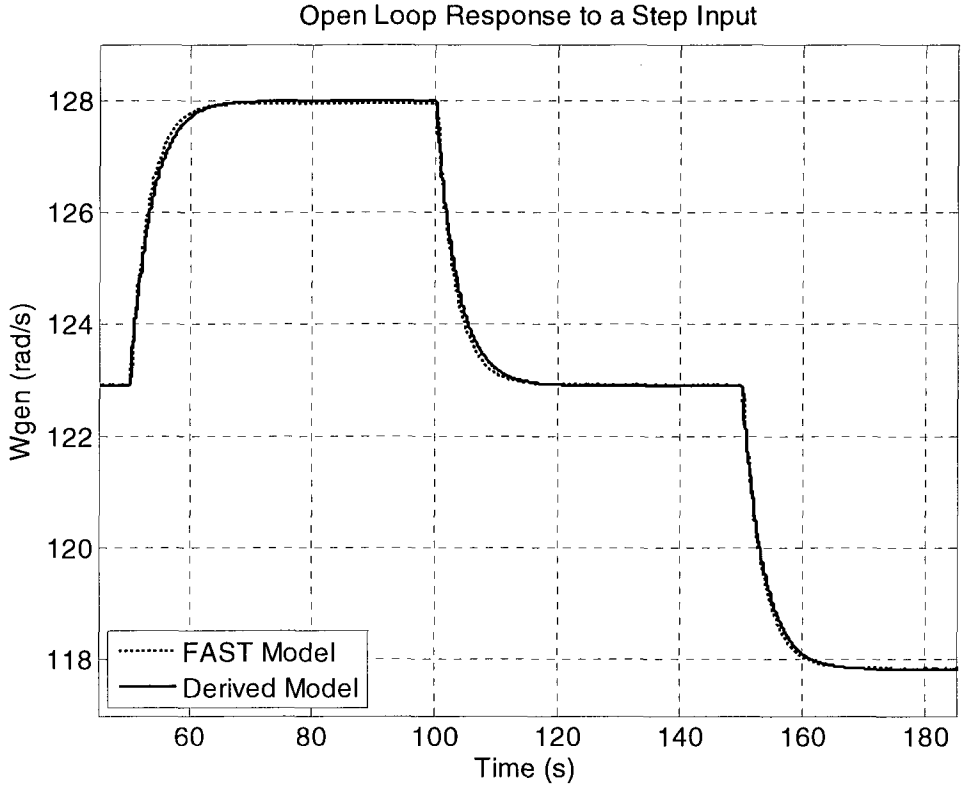

Figure 3.9- Model responses to a step increase in wind speed

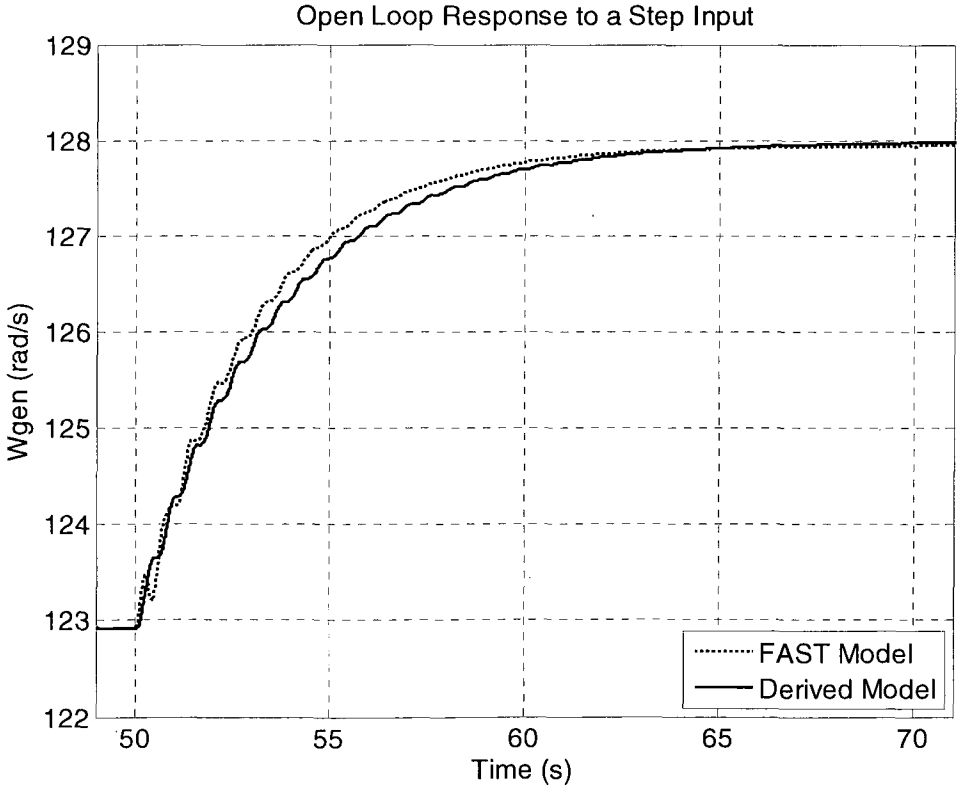

The frequency response of the models was compared by analyzing the Bode plots of the two models. The Bode plot of the DLIN model can be generated directly through Simulink® by setting input and output linearization points at the wind speed input and generator shaft speed output respectively. The Bode plot for the FAST model could not be generated in such a manner since the wind input file must be generated as a text file and compiled with the wind turbine model when the S-Function block is created. For each point on the Bode plot, a time series wind input file was generated with .5 m/s amplitude sinusoidal wind variations at the tested frequency. This sinusoidal wind was DC shifted by the linearization wind speed of 18m/s. These tests were performed open loop with the blade pitch angle set to that of the linearization point. The wind input and generator speed output were then compared to get the magnitude and phase for each tested frequency. The individual points where then plotted on the DLIN model Bode plot, as seen in Figure 3.10.

Figure 3.10- Open loop Bode diagram for FAST and DLIN models

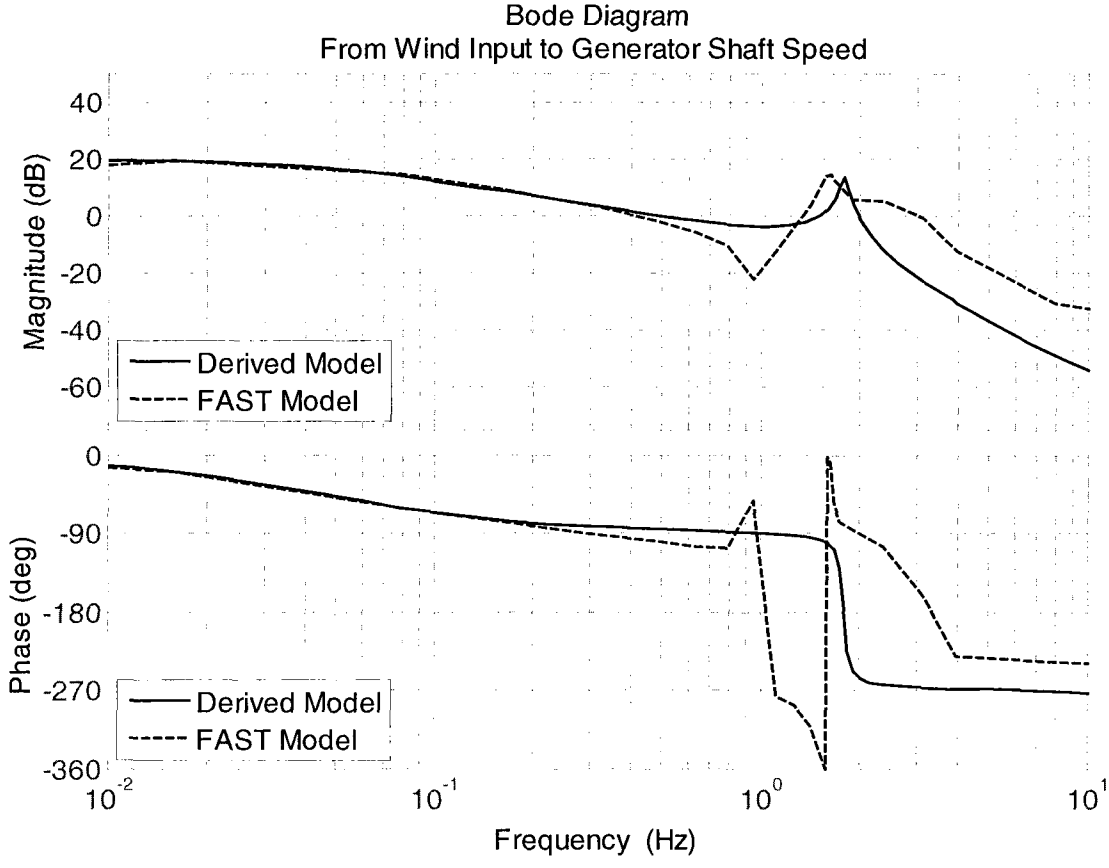

The frequency responses of the DLIN and FAST models were compared. Their magnitude Bode plots have similar DC gains and have a resonant peak near 10 rad/s. Both attenuate frequencies before the resonant peak. After the resonant peak, the non-linearities of the FAST model blades cause larger high frequency gains than those that occur in the DLIN model. It can be seen that there is a dramatic drop in gain and a spike in phase at 6 rad/s. This is caused by aerodynamic blade non-linearities, shown in a normalized plot of the wind speed and generator speed at a driving frequency of 6 rad/s, as seen in Figure 3.11. The out of phase peak of the generator speed response seen in Figure 3.11 at 33.4 seconds increases dramatically and the in phase peak at 34 seconds is

attenuated as the frequency of the wind speed increases to 7 rad/s second. This caused a sharp 180 degree shift seen in the Bode plot of Figure 3.10.

Figure 3.11- Non-linear response of FAST wind turbine

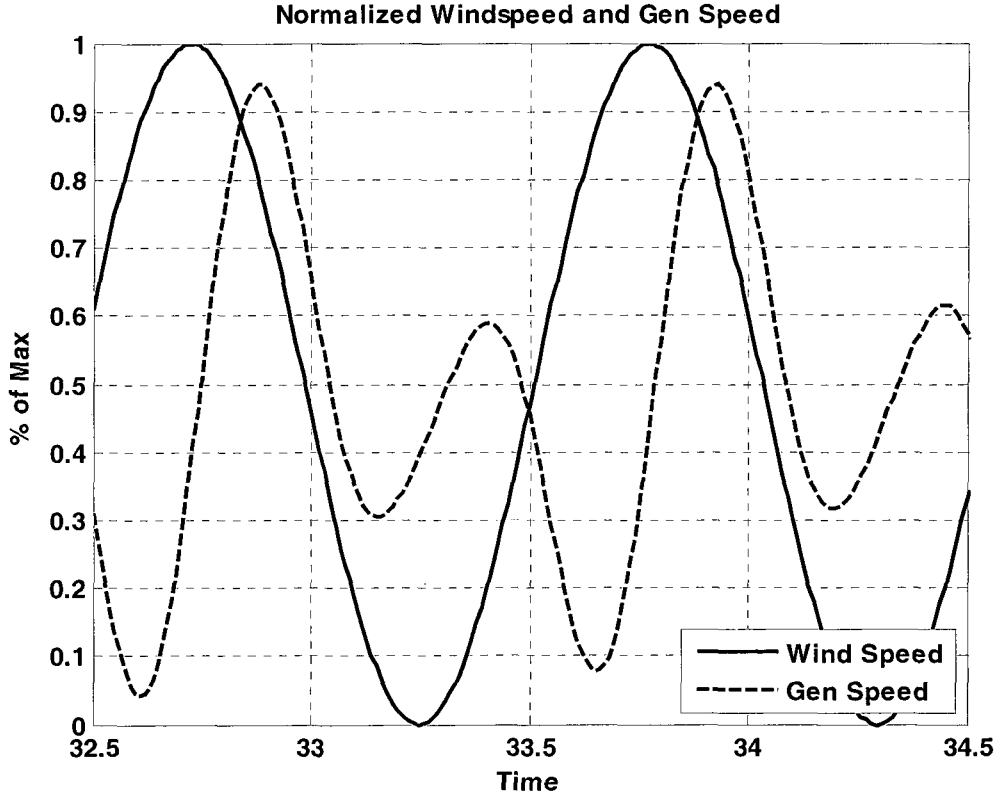

The response of the DLIN model has some similarities and some differences from the FAST model. The differences are primarily caused by the differences in blade models and the calculation of the aerodynamic forces. The DLIN model was considered to be a simplified representation of a class of large scale wind turbines.

CHAPTER 4:

CONTROL SYSTEM DEVELOPMENT

Control System Development Overview

There are three different control designs in this chapter. The first is a classical proportional-integral (PI) control system and measurement filter designed by NREL engineers. This controller is used as a baseline for the two controllers developed as part of this research and is referred to as PI and PI MF when including the measurement filter. The developed controllers are full state feedback LQR control systems. The first developed controller is a single-input LQR with blade pitch rate as the input, referred to as 'SI LQR'. The second developed controller is a multiple-input LQR control system with blade pitch rate and gear ratio slew rate as inputs, referred to as 'MI LQR'.

The goals of the developed control systems are to:

- Regulate the generator speed better than PI controller
- Mitigate torque variations in the gearbox and generator
- Keep blade pitch rates on par with that of the PI controller

The PI and SI LQR controllers are tested with the DLIN and FAST models. The MI LQR controller is tested on the DCVT model. The results of the simulations can be seen in Chapter 5.

PI Control

PI control is a widely used control methodology. A PI controller can be tuned to achieve satisfactory results based on the principal system time constraints with only a basic understanding of the process model. [24] According to Dorf and Bishop, "the popularity of PID controllers can be attributed partly to their robust performance in a wide range of operating conditions and party to their functional simplicity, which allows engineers to operate them in a simple, straightforward manner." [25]

The implementation of PI control is fairly straightforward. A sensor is needed measure the state of the system and output the data to the control system. The difference between the sensor data and a set-point, or desired sensor output, is then evaluated to get an error signal. In this case the sensor is a tachometer measuring the rotational speed of the HSS and the set-point is the rated HSS rotational speed. This error signal is integrated and multiplied by an integral gain (K_i) and added to the error signal multiplied by a proportional gain (K_p). The sum of the outputs of the two gains is called the control signal, which is typically the input to the actuator that controls the system. Sometimes the derivative of the error signal is taken and multiplied by a derivative gain (K_d) and added to this control signal. Gain K_d is not used in the control systems discussed in this document.

Another noteworthy feature of the PI controller is that the system will ideally have zero steady state error for type '0' and higher systems. This is due to the component of the control signal that is comprised of the K_i gain multiplied by the continual integration of the error signal. For example, if the system is running at a level which is below the set-point, the controller will continually integrate this error over time and

increment the control signal until the state reaches the set-point. Once the system arrives at the set-point, the error is zero and the output of the integrator remains constant with the control signal set to that value which brought the system to the desired set-point.

PI control was simulated as a baseline controller to which other controllers were compared. As stated in Chapter 2, PI control is currently the industry standard for controlling blade pitch angles in Region 3. Engineers at NREL have studied the implementation of PI control with the 5MW FAST model. The technical report documenting the 5MW model describes the calculation of K_p and K_i for a desired natural frequency response and damping ratio (ζ=0.7) of the generator shaft speed with the controller implemented in the loop. A damping ratio of 0.7 provides a fast response and a very small amount of overshoot for minimal overshoot. Adding a gain term to the derivative of the error signal (K_d) had been analyzed for this model, but did not result in any improvement in overall system response. [6]

The pitch sensitivity (change in power due to change in blade pitch angle, or $dP/d\beta$) changes as a function of pitch angle. With this in mind, the NREL engineers developed a gain correction curve to scale the PI controller gains based on the current pitch angle. The gain correction curve (GK) is defined by equation (4.1) and seen in Figure 4.1. Specific details on the calculations of the gains and the gain correction curve can be seen in the report associated with the NREL 5MW model. [6]

$$GK(\theta) = \frac{1}{1 + \frac{\theta}{\theta_k}} \tag{4.1}$$

In equation 4.1 θ is the present blade pitch angle in degrees and θ_k= 6.302336°, the blade pitch at which the pitch sensitivity doubles compared to θ=0°. When θ is zero the gain correction factor (GK) is 1. NREL has provided the recommended gains with

the blade pitch angle of zero. These values are K_{p0} = 0.01882681 sec, K_{i0} =.008068634 and K_{d0} = 0.0 sec^2. These would be the gains if converting from generator speed in rad/s and commanding blade pitch angle in radians. This study references blade pitch angle in degrees, so the above values are multiplied by 180°/π rads. The gains are therefore K_{p0} = 1.0787 deg/(rad/s) and K_{i0} = 0.4623 deg/rad.

Figure 4.1- PI gain scheduling curves

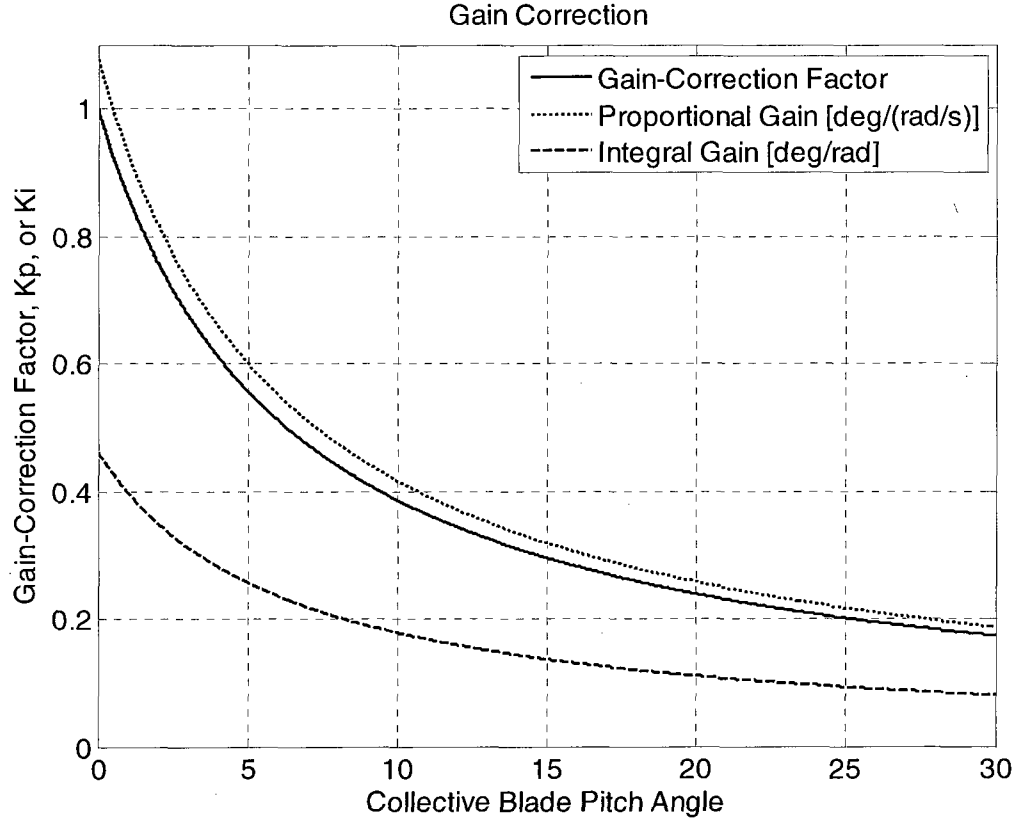

The PI controller was built in Simulink®, as seen in Figure 4.2. This controller was included in the DLIN and FAST Simulink® files. A gain scheduling switch 'GainSched' allowed for either static PI gains or the gain scheduled PI gains to be implemented into the models. All variables in Figure 4.2 have already been defined or

follow notation used previously in this report with the exception of Tk, previously referred to as θ_k.

The blade actuator was modeled as a first order low pass filter with unity gain and a time constant τ_b. A rate limiter is applied to the blade pitch angle with an absolute value of 8°/s. A saturation limit was also included, as the blades should stay within the range of 0°-90°. [6]

Figure 4.2- PI controller with gain scheduling

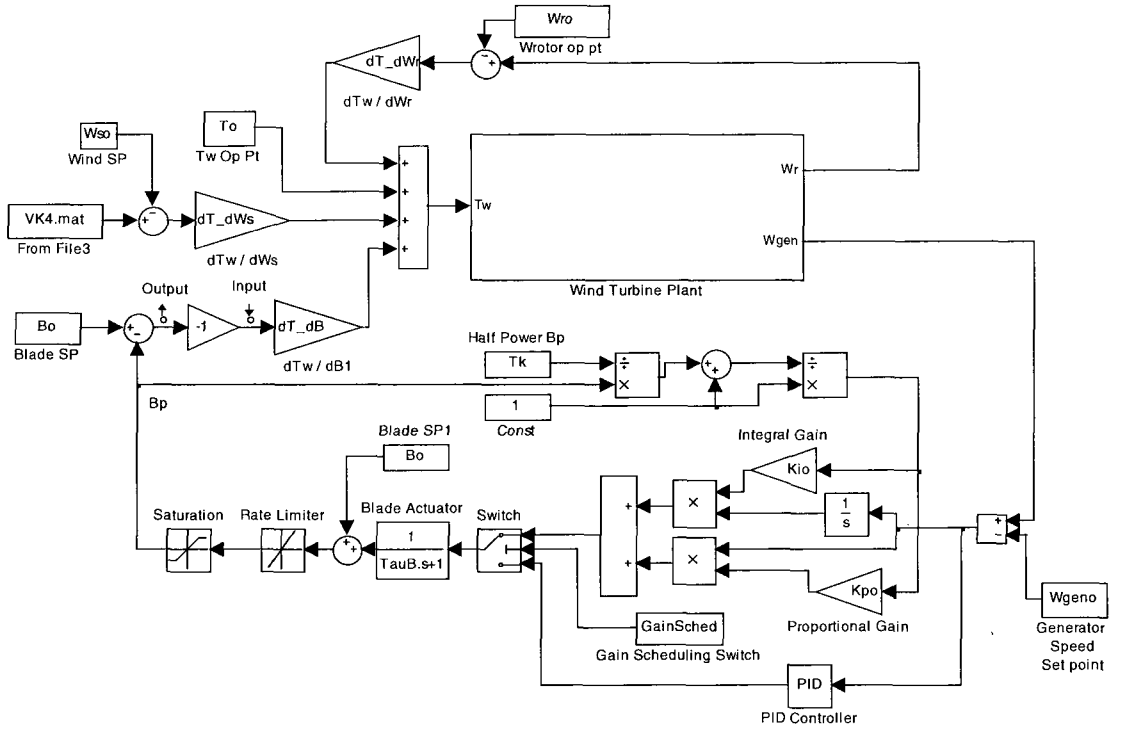

To analyze the frequency response from blade pitch input to control system output, static gains were implemented according to the gain-correction curve at the blade pitch linearization point. A linearized open loop Bode plot was generated with the input as blade pitch input to the turbine plant, and the output as the output of the PI control signal. The input and output points are denoted in Figure 4.2 by the small circles with

arrows attached to them labeled as input and output. The Bode and nyquist plots allow for the analysis of the gain and phase margin of the wind turbine with the controller, as seen in Figure 4.3 and 4.4.

Figure 4.3- Open loop Bode plot of PI controller with DLIN model

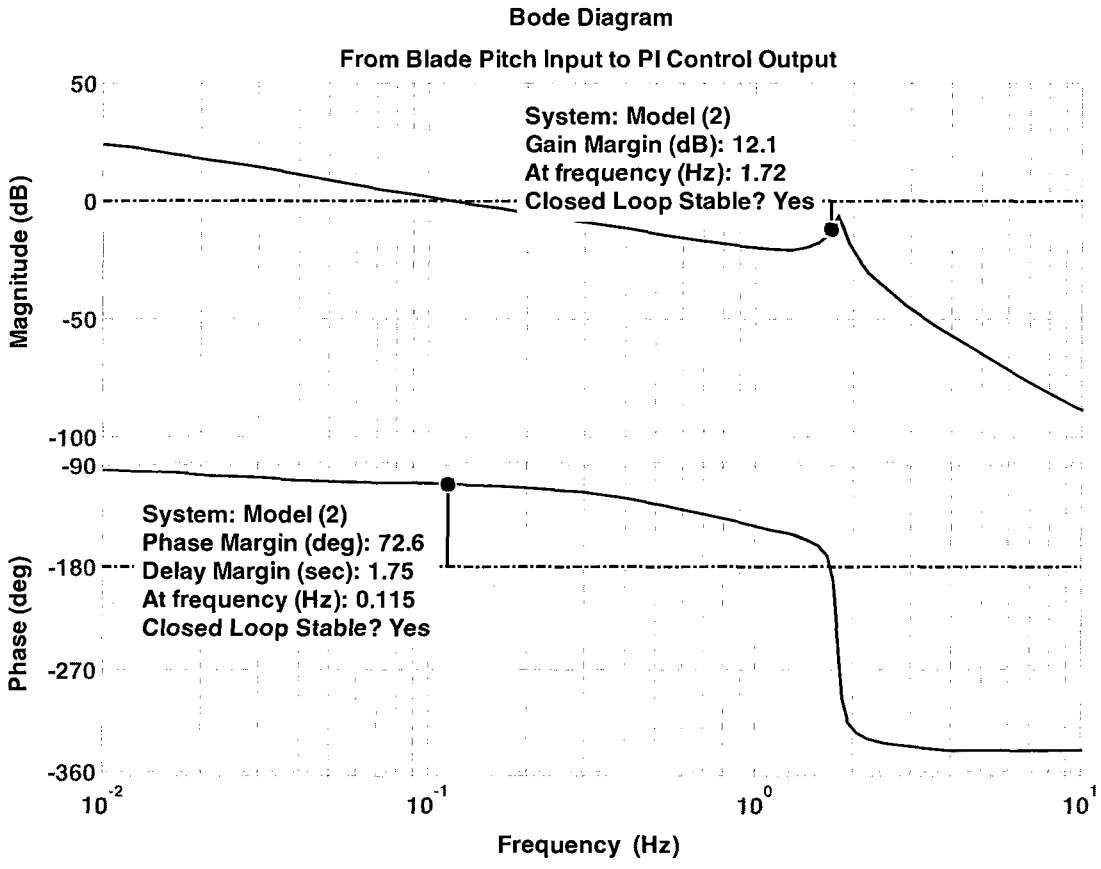

The gain margin is defined as "the increase in the system gain when the phase is equal to -180° that will result in a marginally stable system with the intersection of the -1+*j*0 point on the nyquist diagram." [25] In other words, the gain margin is the factor that the loop gain can increase before the system will go unstable. The phase margin is defined as "the amount of phase shift of the system at unity magnitude that will result in a marginally stable system with the intersection of the -1+*j*0 point on the nyquist diagram."

[25] These measures show how much room for error there is in the system in terms of the gain and phase before the system becomes unstable. The minimum desirable gain and phase margins for acceptable transient responses are roughly 6 dB and 30° respectively. [24] Note that the gain margin of the wind turbine with the PI controller in Figure 4.3 and 4.4 is 12.1 dB and phase margin is 72.6°. The PI controller's gain and phase margins are relatively large and will ensure stability even if the model is not entirely accurate.

Figure 4.4- Nyquist plot for PI controller

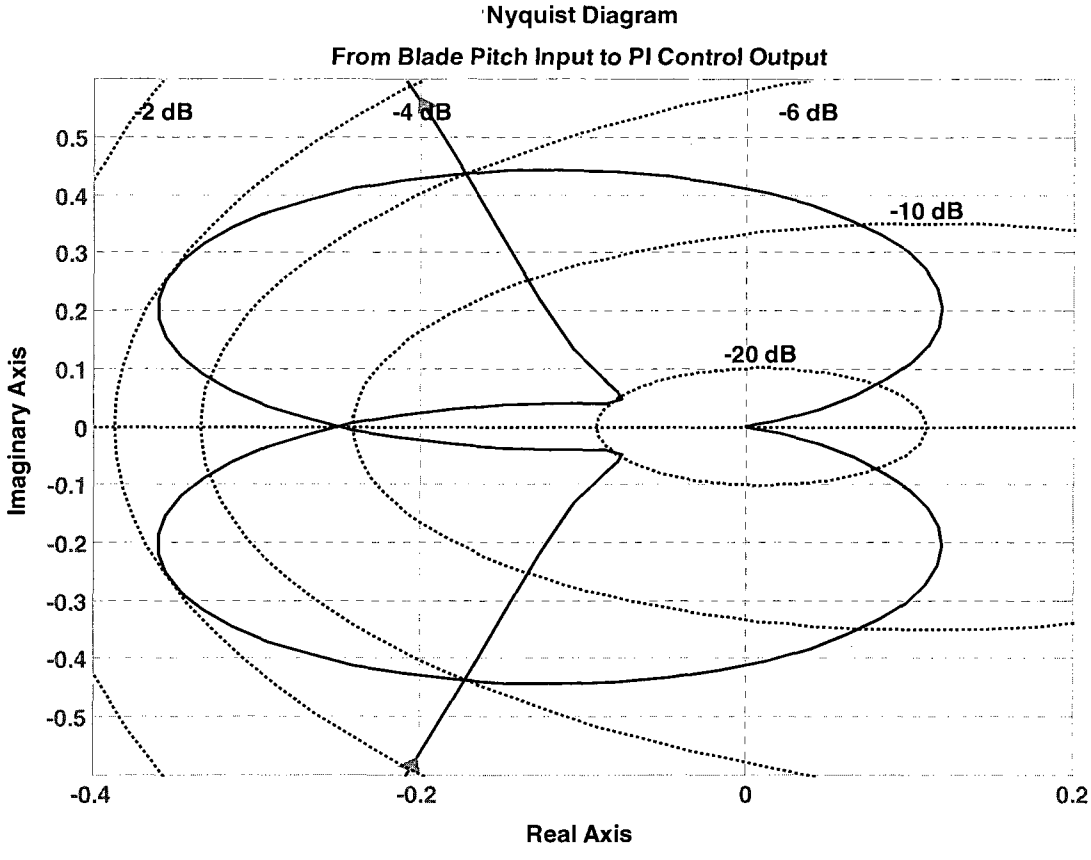

A generator speed measurement filter was developed by engineers at NREL to mitigate high-frequency excitation of the control systems. The measurement filter developed was a recursive, single-pole, low-pass filter of the form:

$$y[n] = (1 - \alpha)u[n] + \alpha y[n - 1], \tag{4.2}$$

with

$$\alpha = e^{-2\pi T_s f_c}. \tag{4.3}$$

"Where y is the filtered generator speed, u is the unfiltered generator speed, α is the low-pass filter coefficient, n is the discrete-time-step counter, T_s is the discrete time step, and f_c is the corner frequency." [6]

This measurement filter was built in the Simulink model, as seen in Figure 4.5. The corner frequency of the low pass filter was set to roughly one-quarter of the blade's first edgewise natural frequency or .25 Hz. [6] The bode plot of the filter can be seen in Figure 4.6. Other higher order filter types were considered but none provided better overall system performance. [6] Chapter 5 will show the effect of the filter in simulations.

Figure 4.5- Generator speed measurement filter

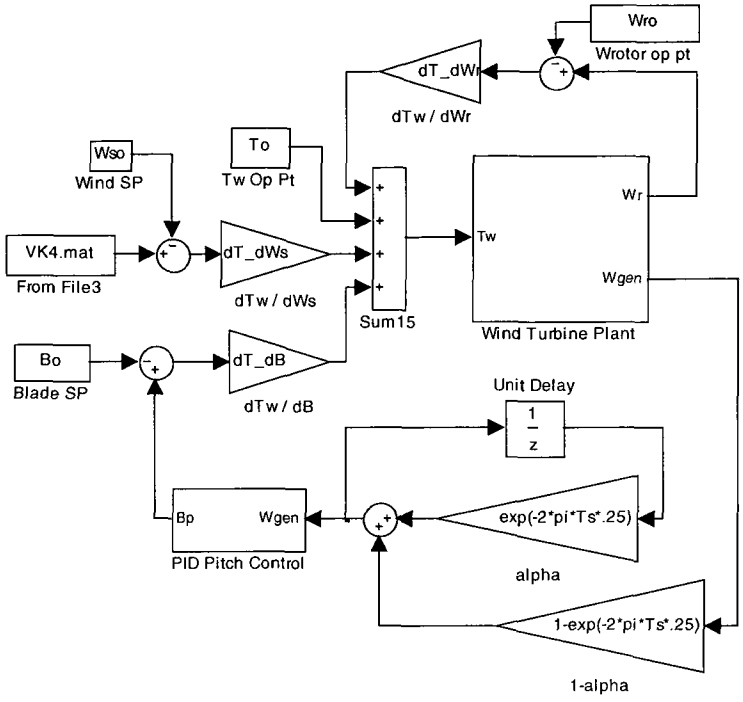

Figure 4.6- Bode plot of generator speed measurement filter

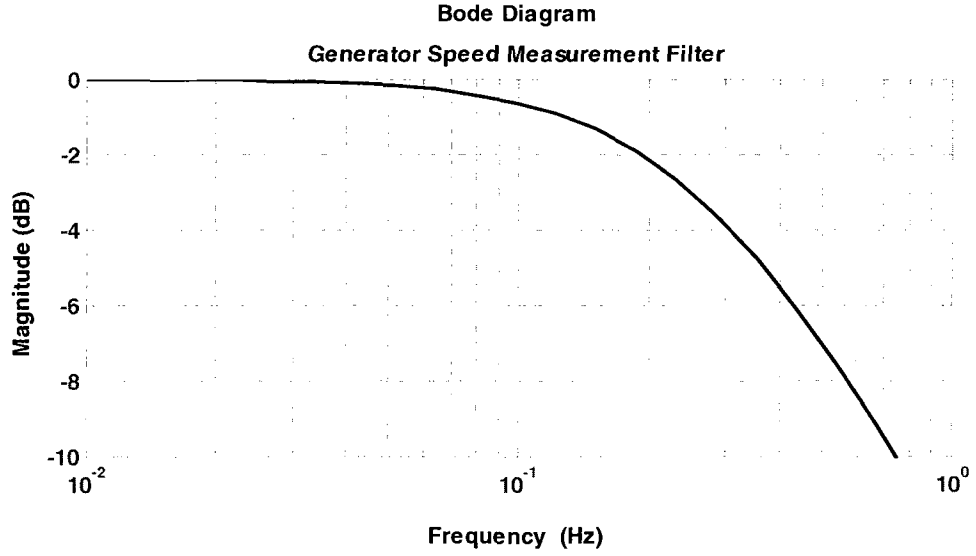

The Bode and nyquist plots of the DLIN model with the PI controller and the measurement filter can be seen in Figure 4.7 and 4.8 respectively. Introducing the filter improves the gain margin of the system from 12.1 dB to 17.6 dB but decreases the phase margin from 72.6° to 49.4°.

Figure 4.7- Open loop bode plot of DLIN model with PI MF controller

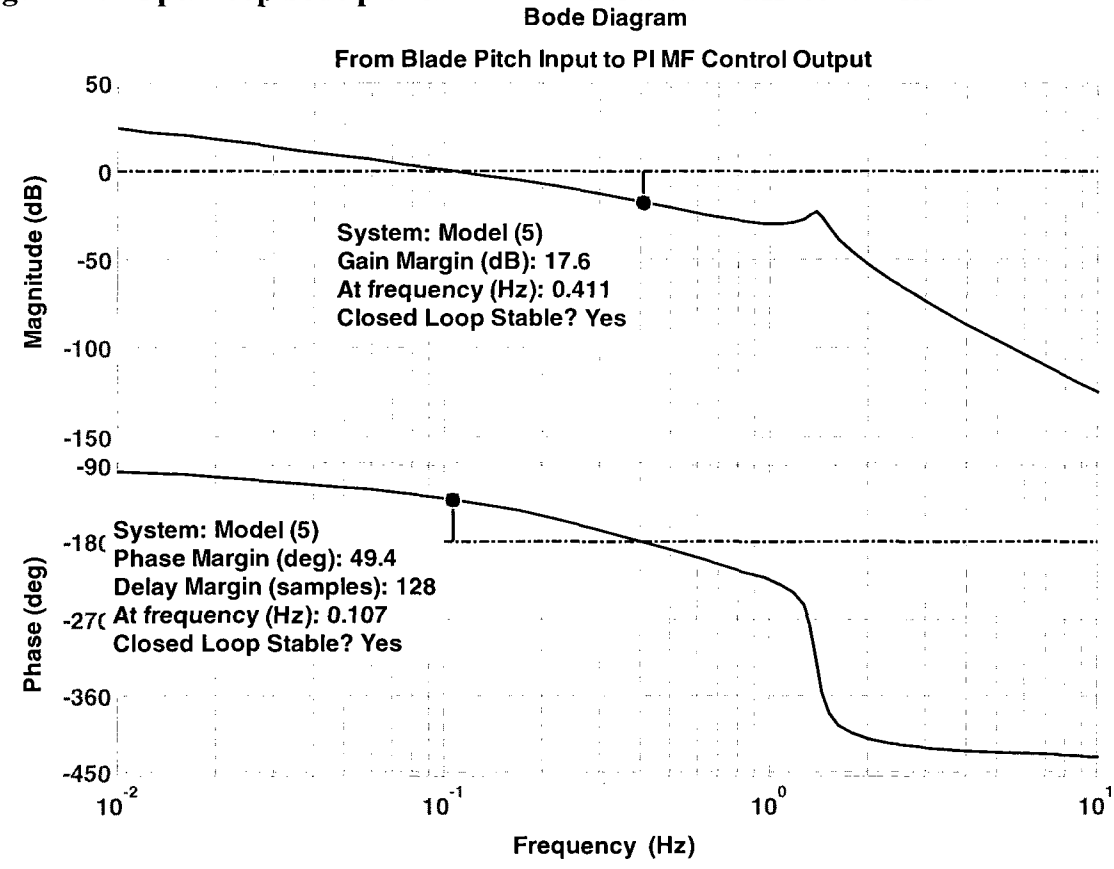

Figure 4.8- Nyquist plot of DLIN model with PI MF controller

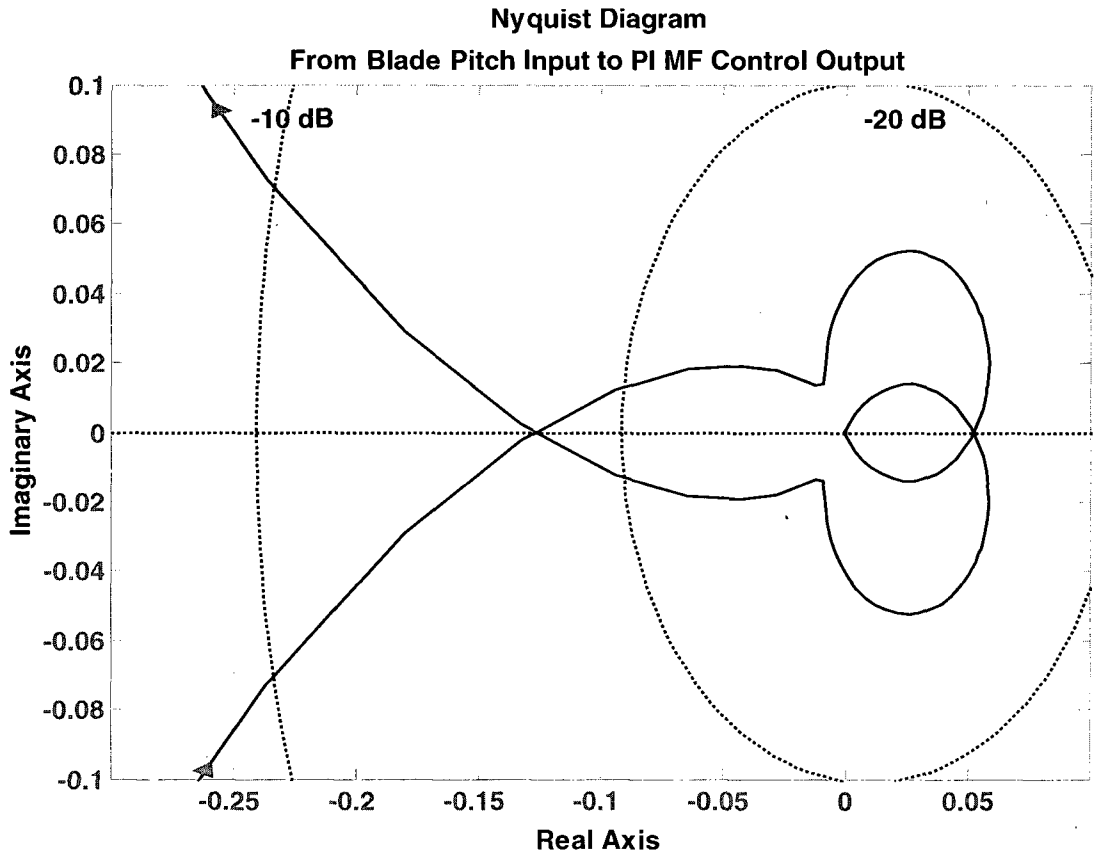

LQR Control System Description

A more advanced method of control was studied to improve regulation of speed and minimize torque variations when compared to the performance of the PI controller. The linear quadratic regulator (LQR), or optimal control, is a feedback control methodology that has many advantages over PI control. LQR control allows for easier design of multi-input multi-output (MIMO) control systems. This method also allows penalties, or weights to be applied to the regulation of each state's error signal.

Another advantage to using LQR control is that the control system development process will always ensure that there will be sufficient phase margin. Naidu proves that

"the closed-loop optimal system or LQR system has a phase margin of at least 60 degrees." [26]

The LQR controller's advantages come from utilizing full state feedback and having information about the plant embedded into the calculation of the control gains. The fact that there are gains applied to all of the error signals for the states produces a much higher order controller. This higher order controller has more poles and zeros than a PI controller. The poles and zeros are inherently placed during the control system development to meet the requirements of stability, state regulation, and ensuring at least 60 degrees of phase margin.

This method of designing a controller assumes that all states are known. This can be done by adding sensors to the wind turbine and feeding back the information known as full state feedback. If not all of the states can be measured directly, a state estimator must be developed to calculate estimates of the un-measureable states for the controller's utilization. This process takes computing power, knowledge of the plant and most importantly time. The longer the state estimator takes to settle, the less phase margin the system will have. For large scale wind turbines all the states are measurable or re-constructible with simple calculations.

The advantage of LQR control comes from knowing the model of the plant as gain calculations are plant dependent. This can be a potential drawback to LQR if the plant is not accurately modeled or known.

Application of LQR control requires that the system be linearized in the form of:

$$\Delta \dot{\boldsymbol{x}} = \boldsymbol{A}\,\Delta \boldsymbol{x} + \boldsymbol{B}\,\Delta \boldsymbol{u}. \tag{4.4}$$

Here, $\Delta \boldsymbol{x}$ is the perturbation of the state vector about the operating point, $\Delta \dot{\boldsymbol{x}}$ is the derivative of the perturbation of the state vector about the operating point, $\boldsymbol{A}$ is the state matrix, $\boldsymbol{B}$ is the input matrix and $\Delta \boldsymbol{u}$ is a vector of the input deviations from the linearized value. In this case the system is assumed to be time invariant, so $\boldsymbol{A}$ and $\boldsymbol{B}$ are constant.

The goal of the LQR control system is to regulate the states of the system to achieve a minimum quadratic performance index. For time invariant and infinite-time, or infinite-horizon, LQR system the quadratic performance index is in the form of:

$$J = \frac{1}{2}\int_{t_0}^{\infty} (\boldsymbol{x}^T(t)\boldsymbol{Q}\boldsymbol{x}(t) + \boldsymbol{u}^T(t)\boldsymbol{R}\boldsymbol{u}(t))dt. \tag{4.5}$$

[26]

Here t_0 is the start time, $\boldsymbol{Q}$ and $\boldsymbol{R}$ are symmetric positive semi-definite weighting matrices, meaning that all the eigenvalues of this matrix are positive. Therefore $\boldsymbol{x}^T(t)\boldsymbol{Q}\boldsymbol{x}(t)$ and $\boldsymbol{u}^T(t)\boldsymbol{R}\boldsymbol{u}(t)$will both always be positive and it is possible to minimize the performance index J. Note that bold characters are matrices or vectors. [26]

The optimal control $\boldsymbol{u}^*$ is given by:

$$\boldsymbol{u}^*(t) = -\boldsymbol{R}^{-1}\boldsymbol{B}'\overline{\boldsymbol{P}}\boldsymbol{x}^*(t) = -\overline{\mathbf{K}}\mathbf{x}^*(\mathrm{t}) \tag{4.6}$$

[26]

Where $\overline{\boldsymbol{P}}$ is the constant, symmetric, positive definite matrix that is the steady state solution to the matrix differential Riccati equation (DRE):

$$\frac{d\overline{\boldsymbol{P}}}{dt} = 0 = -\overline{\boldsymbol{P}}\boldsymbol{A} - \boldsymbol{A}'\overline{\boldsymbol{P}} - \boldsymbol{Q} + \overline{\boldsymbol{P}}\boldsymbol{B}\boldsymbol{R}^{-1}\boldsymbol{B}'\boldsymbol{P}. \tag{4.7}$$

[26]

The optimal state is the solution of:

$$\dot{\boldsymbol{x}}^*(t) = \left[\boldsymbol{A} - \boldsymbol{B}\boldsymbol{R}^{-1}\overline{\boldsymbol{P}}\right]\boldsymbol{x}^*(t) = \mathbf{G}\mathbf{x}^*(\mathrm{t}). \tag{4.8}$$

[26]

$$\mathbf{G} = \boldsymbol{A} - \boldsymbol{B}\boldsymbol{R}^{-1}\overline{\boldsymbol{P}}. \tag{4.9}$$

[26]

The **G** matrix has stable eigenvalues so that the closed loop optimal system is stable. Lastly, the minimum cost is given by:

$$J^* = \frac{1}{2}\boldsymbol{x}^{*\prime}(t)\overline{\boldsymbol{P}}\boldsymbol{x}^*(t). \tag{4.10}$$

[26]

The solution to this problem has been well documented in many text books. The equations were re-iterated in this document, but for full understanding and documentation one should refer to an optimal or modern control textbook. [26]

Though it is possible to solve out the Riccati equations to minimize J by hand, it is a tedious process. There are software programs that have the ability to solve these equations. MATLAB® software has built in functions to solve for the feedback gains for the LQR controller. These functions were utilized for this study.

The goal of regulating the wind turbine speed is to minimize the deviations away from the set point. Therefore $\Delta\boldsymbol{x}$ will be used instead of $\boldsymbol{x}$ in equation (4.3). The $\boldsymbol{Q}$ matrix allows penalties to be applied to these deviations from the set-point. As a quick example, if $\Delta\boldsymbol{x}$ was a 1x2 matrix of composed of Δx_1 and Δx_2:

$$\begin{aligned}\Delta\boldsymbol{x}^T\boldsymbol{Q}\Delta\boldsymbol{x} &= [\Delta x_1 \quad \Delta x_2]\begin{bmatrix} q_{1,1} & q_{1,2} \\ q_{2,1} & q_{2,2}\end{bmatrix}\begin{bmatrix}\Delta x_1 \\ \Delta x_2\end{bmatrix} \\ &= \Delta {x_1}^2 q_{1,1} + \Delta x_1 \Delta x_2 (q_{2,1} + q_{1,2}) + \Delta {x_2}^2 q_{2,2}.\end{aligned} \tag{4.11}$$

To ensure that $\boldsymbol{Q}$ is positive semi-definite $q_{1,2}$ and $q_{2,1}$ are set to zero and $q_{1,1}$ and $q_{2,2}$ are set to positive values. The remaining portion of the expression is integrated over time as part of the performance index J. Since this is the term that is wished to be

minimized, it can be seen in equation (4.11) that increasing q_{11} adds a penalty to the squared deviation of state x_1 from the set-point.

The same is true for setting the values of the $\boldsymbol{R}$ matrix. For a single input controller $\boldsymbol{R}$ is a scalar value which is a penalty on the input control signal squared. For a multi-input controller the off diagonal terms are set to zero to ensure the matrix is positive semi-definite. The diagonal terms are the penalties applied to the square of each input, similar to the penalties on the states in the $\boldsymbol{Q}$ matrix as described above.

This chapter will discuss the procedure of designing two LQR controllers. The single-input LQR controls blade pitch angle and is tested on the DLIN and FAST models. The multi-input LQR controller could only be tested on the DCVT model. The DLIN model in Simulink® is the same model as the DCVT model with switches that set the gearbox to a fixed value and the LSS spring constant to the original value. In this Simulink® file the controllers will be implemented in parallel and a switch will determine which one will be active for simulations. The set-points of each of the states is subtracted from the data stream and fed into the controllers. The data flow to these controllers in Simulink® can be seen in Figure 4.9. In Figure 4.9, 'ControlMode' is a switch that selects whether the turbine DLIN model will be simulated open loop, with the PI MF controller, the SI LQR controller or if the DCVT model will be simulated with the MI LQR controller.

Figure 4.9- Data flow to LQR controllers

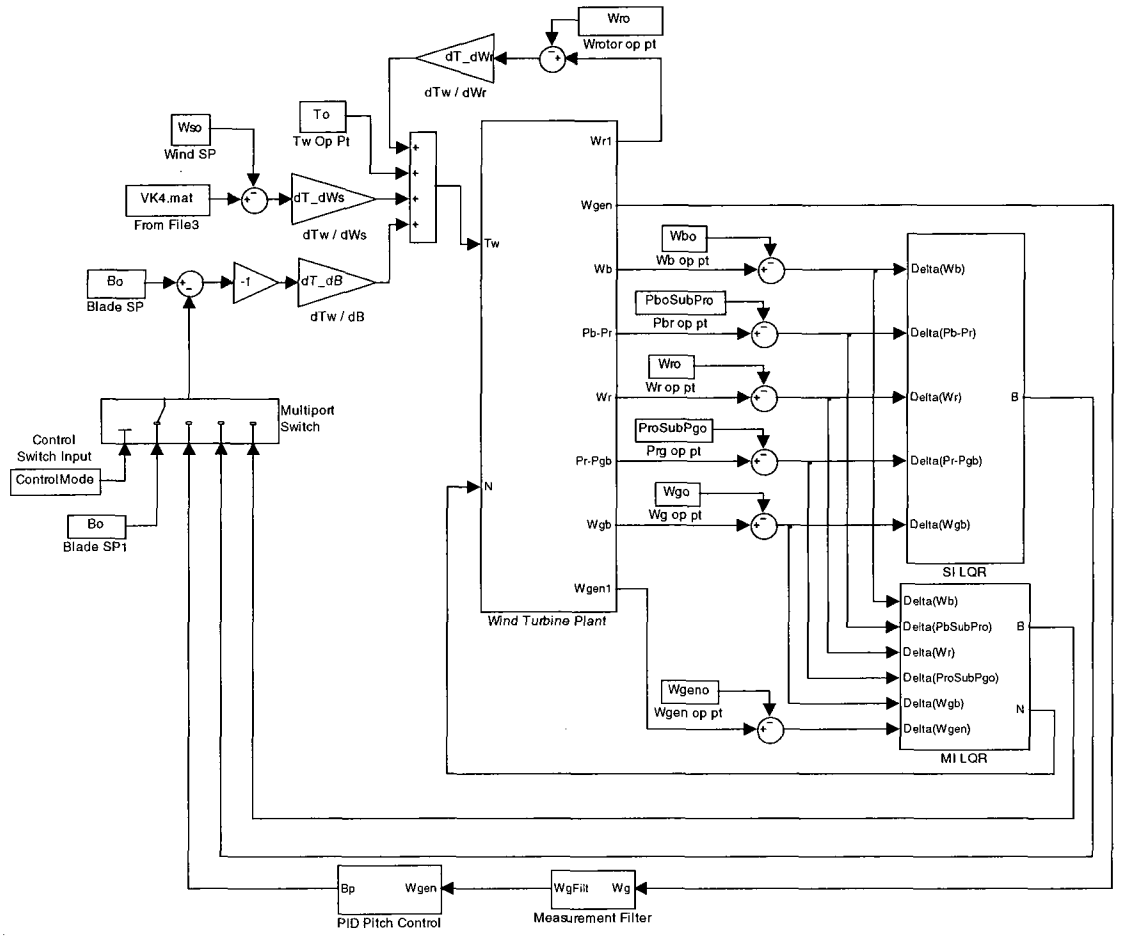

Single-Input LQR Control System

The single input LQR control system (SI LQR) was designed to control the blade pitch angle of the wind turbine model using techniques from the previous section. This controller was tested in the DLIN and FAST models. The results were directly compared to the PI controller for each model, as seen in Chapter 5.

In order to drive the steady state error of a state variable to zero, a feedback gain must be applied to the integration of the state's error. As stated earlier in this chapter, zero steady state error tracking is a feature of the PI controller. This characteristic was

desired from the LQR controller, so an additional state was included. The speed of the gearbox is the measured and regulated state. Regulating the gearbox speed also regulates the generator speed if a fixed gear ratio is assumed. The gearbox speed error is integrated and included in the state matrix.

The LQR controller allows for penalties to be applied to states and inputs. A straightforward approach may have the input as commanded blade pitch angle (β_u). The penalty ***R*** would then allow a penalty to be put on the deviation of the commanded blade pitch angle from the linearization value. An integrator was added at the input of the blade pitch actuator which turns the input command signal of the blade pitch actuator (β_u) from an input to a state. The new input is now the rate of change of the blade pitch command ($\dot{\beta}_u$). An input penalty ***R*** can now be applied to the commanded blade pitch rate ($\dot{\beta}_u$). When feedback gains are applied, the input integrator becomes a low pass filter which helps to reduce high frequency variations in pitch command.

The blade actuator and additional integrator can be seen in Figure 4.10. In Figure 4.10, the controller input is Budot, Bu is the input to the blade pitch actuator, Bdot is the rate of change of the blade pitch angle and B is the blade pitch angle output.

Figure 4.10- Blade pitch actuator with input integrator

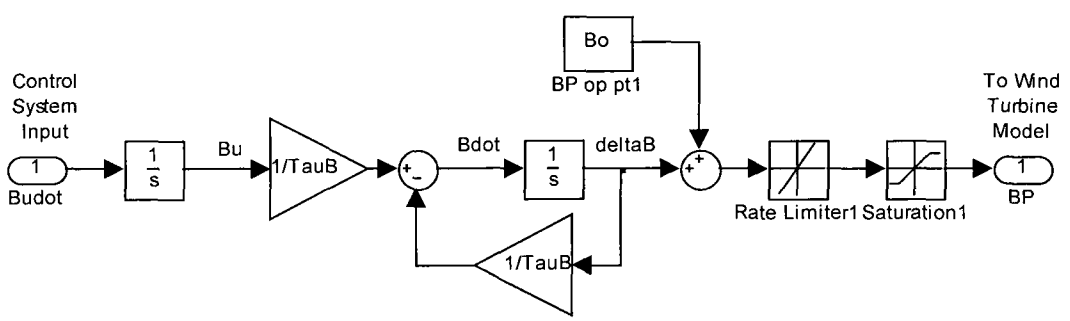

Based on the system description and equations (3.40), (3.42) and (3.44) the state differential equation was produced, seen in equations (4.13), (4.14) and (4.15) in the form of:

$$\Delta\dot{\boldsymbol{x}}_1 = \boldsymbol{A}_1\Delta\boldsymbol{x}_1 + \boldsymbol{B}_1\,\Delta\boldsymbol{u}_1. \tag{4.12}$$

$$\Delta\dot{\boldsymbol{x}}_1 = \begin{bmatrix} \Delta\ddot{\theta}_b \\ \Delta(\dot{\theta}_b - \dot{\theta}_r) \\ \Delta\ddot{\theta}_r \\ \Delta(\dot{\theta}_r - \dot{\theta}_{gb}) \\ \Delta\ddot{\theta}_{gb} \\ \Delta\dot{\theta}_{gb} \\ \Delta\dot{\beta} \\ \Delta\dot{\beta}_u \end{bmatrix}, \quad \Delta\boldsymbol{x}_1 = \begin{bmatrix} \Delta\dot{\theta}_b \\ \Delta(\theta_b - \theta_r) \\ \Delta\dot{\theta}_r \\ \Delta(\theta_r - \theta_{gb}) \\ \Delta\dot{\theta}_{gb} \\ \Delta\theta_{gb} \\ \Delta\beta \\ \Delta\beta_u \end{bmatrix}. \tag{4.13}$$

$$\boldsymbol{A}_1 = \begin{bmatrix} \frac{-D_b - B_b}{J_b} & \frac{-K_b}{J_b} & \frac{1}{J_b}\left(\frac{dT_w}{d\dot{\theta}_r} + D_b\right) & 0 & 0 & 0 & \frac{1}{J_b}\frac{dT_w}{d\beta} & 0 \\ 1 & 0 & -1 & 0 & 0 & 0 & 0 & 0 \\ \frac{D_b}{J_r} & \frac{K_b}{J_r} & \frac{-D_b - D_r - B_r}{J_r} & \frac{-K_r}{J_r} & \frac{D_r}{J_r} & 0 & 0 & 0 \\ 0 & 0 & 1 & 0 & -1 & 0 & 0 & 0 \\ 0 & 0 & \frac{D_r N^2}{J_g} & \frac{K_r N^2}{J_g} & \frac{-B_g - B_L - D_r N^2}{J_g} & 0 & 0 & 0 \\ 0 & 0 & 0 & 0 & 1 & 0 & 0 & 0 \\ 0 & 0 & 0 & 0 & 0 & 0 & -\frac{1}{\tau_b} & \frac{1}{\tau_b} \\ 0 & 0 & 0 & 0 & 0 & 0 & 0 & 0 \end{bmatrix} \tag{4.14}$$

$$\boldsymbol{B}_1 = [0,0,0,0,0,0,0,1]^T,\ \Delta\boldsymbol{u}_1 = \dot{\beta}_u \tag{4.15}$$

In order to utilize full state feedback control, all states must be available. Tachometers or decoders could be used to measure the rotational velocities of the rotor and gearbox. The integration of the gearbox error can be easily done in hardware or software. The difference in blade and rotor positions can be measured with strain gauges built into the blades. Strain gauges can also be installed on the rotor shaft to sense the

difference in rotor and gearbox position. The blade pitch angle can be sensed with a position sensor and the input to the blade actuator would be an electrical signal that would be measureable with an A/D converter. The rotational speed of the blades could be re-constructed using the rotor velocity and the blade flex.

The 'lqr' function in MATLAB® was utilized to calculate the feedback gains for a given $\boldsymbol{Q}$ matrix. This function returns the feedback gains that should be applied to each state. The implementation of these feedback gains can be seen in Figure 4.11.

Figure 4.11- SI LQR controller architecture

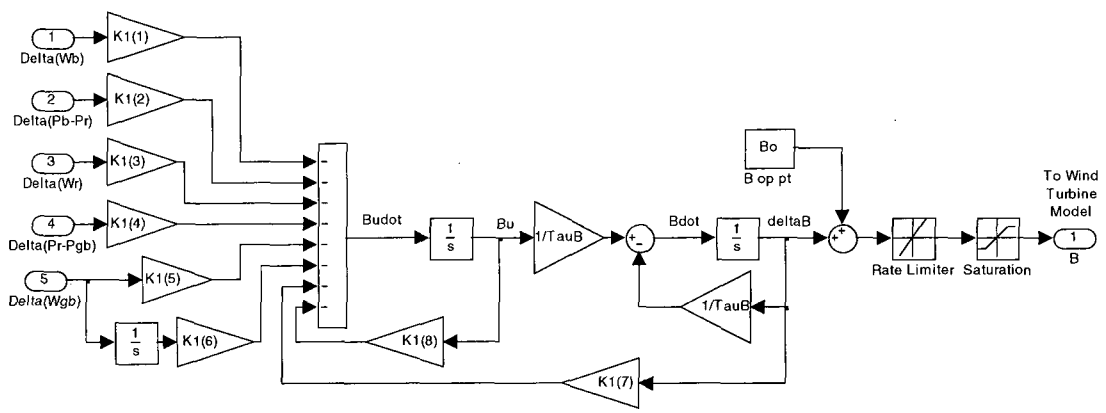

Development of specific $\boldsymbol{Q}$ matrices was done iteratively during the process of simulation and can be found in Chapter 5. The controller-plant Bode and nyquist plots cannot be generated until the $\boldsymbol{Q}$ matrix is realized and the Riccati equation is solved, so these plots can be found with the simulation results in Chapter 5.

Multi-Input LQR Control System

A control system was developed to actuate the blade pitch angle and the gear ratio. This controller could only be implemented in the derived model, as FAST has a

fixed gear ratio. The equations and the model couple the main, fixed ratio gearbox with the CVT and the multiplication of these gear ratios is expressed as the total gear ratio *N*.

An integrator was added before of the input to the CVT actuator which turns the input command signal of the CVT actuator from an input to a state in a similar manner to the integrator before the blade pitch actuator. The new input is now the rate of change of the CVT command signal, allowing a penalty to be put on the CVT slew rate. When feedback gains are implemented, the integrator turns into a low pass filter. The CVT actuator was modeled as a first order low pass filter with unity gain and a time constant τ_n. Claims have been made that the time constant of the CVT is negligible. However, to provide a conservative estimate, the time constant for the CVT is assumed to be the same as the blade pitch actuator (.2 s). A saturation limit was included to keep the CVT within the postulated range of .3-3. Since the CVT and main gearbox are coupled together as the total gear ratio *N*, the limits in the model is actually $.3*N_0$-$3*N_0$. A rate limiter is applied to the CVT. This rate limiter puts the maximum rate of change to be the entire range of the CVT divided by three seconds. The absolute value of the rate limiter is then set to $(3-.3)*N_0/3$ or $0.0093s^{-1}$. The CVT actuator and additional integrator can be seen in Figure 4.12. In Figure 4.12 Nudot is the controller input, Nu is the input to the CVT actuator, Ndot is the CVT slew rate and *N* is gear ratio.

Figure 4.12- CVT actuator with input integrator

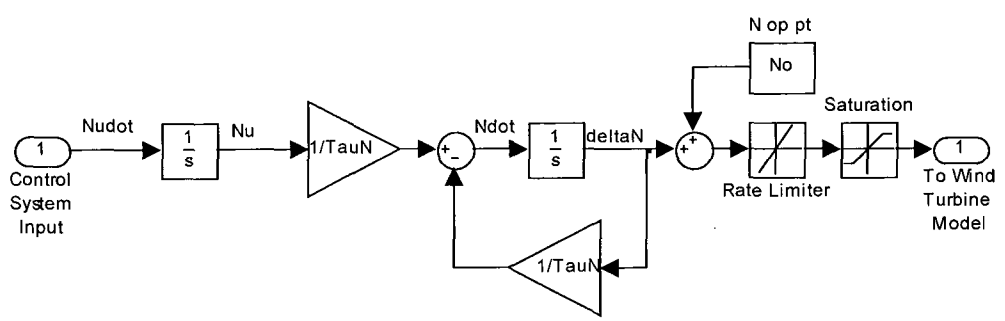

Regulating the gearbox LSS speed will no longer regulate the generator speed when the CVT is introduced to the model. An additional state must be inserted into the state vector so that a penalty may be placed on the deviation of the generator speed from the desired, or rated speed ($\Delta\dot{\theta}_{gen}$). The linearized expression for the generator acceleration, seen in equation (3.49), is implemented in the state-space equation so that the error of the generator speed is in the state vector (x_2). The SI LQR controller included a state for the integrated gearbox speed error. The same is done for the generator speed error for the MI LQR controller. The integration of the generator speed error ensures that the steady state generator speed is driven to zero. This can be seen in the state-space matrices of equations (4.16) and (4.19) and in block diagram form in Figure 4.13.

Another state is augmented to the state-space equations as the integral of the deviation of the gear ratio N from the nominal value. This state is incorporated so a penalty can be applied to $\int_0^t (\Delta N)^2 dt$. The penalty on this state will ensure that the gear ratio will return to the nominal value under steady state conditions. The gear ratio will gravitate toward the nominal value and allow the blades to operate in a similar manner to the SI LQR controller.

Equations (3.40), (3.42), (3.49), (3.54) and the CVT actuator description were written in state space representation, as seen in equations (4.16) and (4.19).

$$\Delta\dot{\boldsymbol{x}}_2 = \begin{bmatrix} \Delta\ddot{\theta}_b \\ \Delta(\dot{\theta}_b - \dot{\theta}_r) \\ \Delta\ddot{\theta}_r \\ \Delta(\dot{\theta}_r - \dot{\theta}_{gb}) \\ \Delta\ddot{\theta}_{gb} \\ \Delta\dot{\theta}_{gen} \\ \Delta\ddot{\theta}_{gen} \\ \Delta\dot{\beta} \\ \Delta\dot{\beta}_u \\ \Delta\dot{N} \\ \Delta\dot{N} \\ \Delta\dot{N}_u \end{bmatrix}, \Delta\boldsymbol{x}_2 = \begin{bmatrix} \Delta\dot{\theta}_b \\ \Delta(\theta_b - \theta_r) \\ \Delta\dot{\theta}_r \\ \Delta(\theta_r - \theta_{gb}) \\ \Delta\dot{\theta}_{gb} \\ \Delta\theta_{gen} \\ \Delta\dot{\theta}_{gen} \\ \Delta\beta \\ \Delta\beta_u \\ \int_o^t (\Delta N)dt \\ \Delta N \\ \Delta N_u \end{bmatrix}, \boldsymbol{B}_2 = \begin{bmatrix} 0 & 0 \\ 0 & 0 \\ 0 & 0 \\ 0 & 0 \\ 0 & 0 \\ 0 & 0 \\ 0 & 0 \\ 0 & 0 \\ 1 & 0 \\ 0 & 0 \\ 0 & 1 \end{bmatrix}, \Delta\boldsymbol{u}_2 = \Delta\begin{bmatrix} \dot{\beta}_u \\ \dot{N}_u \end{bmatrix} \tag{4.16}$$

Note that equation (3.54) is not directly implementable in state space since $\dot{N}$ is not one of the states in $\boldsymbol{x_2}$ of equation (4.16). However, $\dot{N}$ can be re-constructed from states N and N_u from Figure 4.12:

$$\Delta\dot{N} = \frac{1}{\tau_n}\Delta N_u - \frac{1}{\tau_n}\Delta N. \tag{4.17}$$

Substituting equation (4.17) into the last term of equation (3.54):

$$\frac{\dot{\theta}_{gb_0}}{N_0}\Delta\dot{N} = \frac{\dot{\theta}_{gb_0}}{N_0}\left(\frac{1}{\tau_n}\Delta N_u - \frac{1}{\tau_n}\Delta N\right) = \frac{\dot{\theta}_{gb_0}}{N_0\tau_n}(\Delta N_u - \Delta N). \tag{4.18}$$

The resulting state space representation of the linearized model with the CVT can be seen below in equation (4.19).

$$
\boldsymbol{A_2} = \begin{bmatrix}
\frac{-D_b - B_b}{J_b} & \frac{-K_b}{J_b} & \frac{1}{J_b}\left(\frac{dT_w}{d\dot{\theta}_r} + D_b\right) & 0 & 0 \\
1 & 0 & -1 & 0 & 0 \\
\frac{D_b}{J_r} & \frac{K_b}{J_r} & \frac{-D_b - D_r - B_r}{J_r} & \frac{-K_r}{J_r} & \frac{D_r}{J_r} \\
0 & 0 & 1 & 0 & -1 \\
0 & 0 & \frac{D_r N_0^2}{J_g} & \frac{K_r N_0^2}{J_g} & \frac{-B_g - B_L - D_r N_0^2}{J_g} \\
0 & 0 & 0 & 0 & 0 \\
0 & 0 & \frac{N_0 D_r}{J_g} & \frac{N_0 K_r}{J_g} & \left(\frac{N_0 D_r}{J_g} - \frac{(B_g + B_L)}{N_0 J_g}\right) \\
0 & 0 & 0 & 0 & 0 \\
0 & 0 & 0 & 0 & 0 \\
0 & 0 & 0 & 0 & 0 \\
0 & 0 & 0 & 0 & 0 \\
0 & 0 & 0 & 0 & 0
\end{bmatrix} \cdots
$$

(4.19)

$$
\cdots \begin{bmatrix}
0 & 0 & \frac{1}{J_b}\frac{dT_w}{d\beta} & 0 & 0 & 0 & 0 \\
0 & 0 & 0 & 0 & 0 & 0 & 0 \\
0 & 0 & 0 & 0 & 0 & 0 & 0 \\
0 & 0 & 0 & 0 & 0 & 0 & 0 \\
0 & 0 & 0 & 0 & 0 & \left(\frac{2N_0K_r}{J_g}(\theta_r - \theta_{gb})_0 - \frac{\dot{\theta}_{gb_0}}{N_0\tau_n}\right) & \frac{\dot{\theta}_{gb_0}}{N_0\tau_n} \\
0 & 1 & 0 & 0 & 0 & 0 & 0 \\
0 & 0 & 0 & 0 & 0 & \left(\frac{K_r}{J_g}(\theta_r - \theta_{gb})_0 + \frac{2(B_g + B_L)}{N_0^2 J_g}\dot{\theta}_{gb_0}\right) & 0 \\
0 & 0 & -\frac{1}{\tau_b} & \frac{1}{\tau_b} & 0 & 0 & 0 \\
0 & 0 & 0 & 0 & 0 & 0 & 0 \\
0 & 0 & 0 & 0 & 0 & 1 & 0 \\
0 & 0 & 0 & 0 & 0 & -\frac{1}{\tau_n} & \frac{1}{\tau_n} \\
0 & 0 & 0 & 0 & 0 & 0 & 0
\end{bmatrix}
$$

An analysis of the $\boldsymbol{A}_2$ and $\boldsymbol{B}_2$ matrix shows that it is not controllable. "A system described by the matrices ($\boldsymbol{A}$, $\boldsymbol{B}$) can be said to be controllable if there exists an unconstrained control u that can transfer any initial state $\mathbf{x}(0)$ to any other desired location $\mathbf{x}(t)$." [24] A controllable $\boldsymbol{A}$ matrix is required for guaranteed stability of the LQR controller. A system can be uncontrollable for two reasons. One is that some states are not connected to the input. The other is that states are linear combinations of each other. In the DCVT model, the latter is the case. The LQR equations can still be solved out and a stable solution can be achieved. This requires a careful selection of the $\boldsymbol{Q}$ and $\boldsymbol{R}$ penalties, as described in Chapter 5.

When a two input LQR controller is developed there are two sets of control gains that are produced in a 2 by n matrix, where n is the number of states. The first row of gains are applied to the deviations of the states from their set-points and fed into the first system input, the blade pitch rate input. The second row of gains is similarly applied to the second system input, or the CVT slew rate input. The realization of these feedback gains can be seen in Figure 4.13. Determination of specific $\boldsymbol{Q}$ matrices was done during the process of simulation and can be found in Chapter 5.

Figure 4.13- MI LQR controller architecture

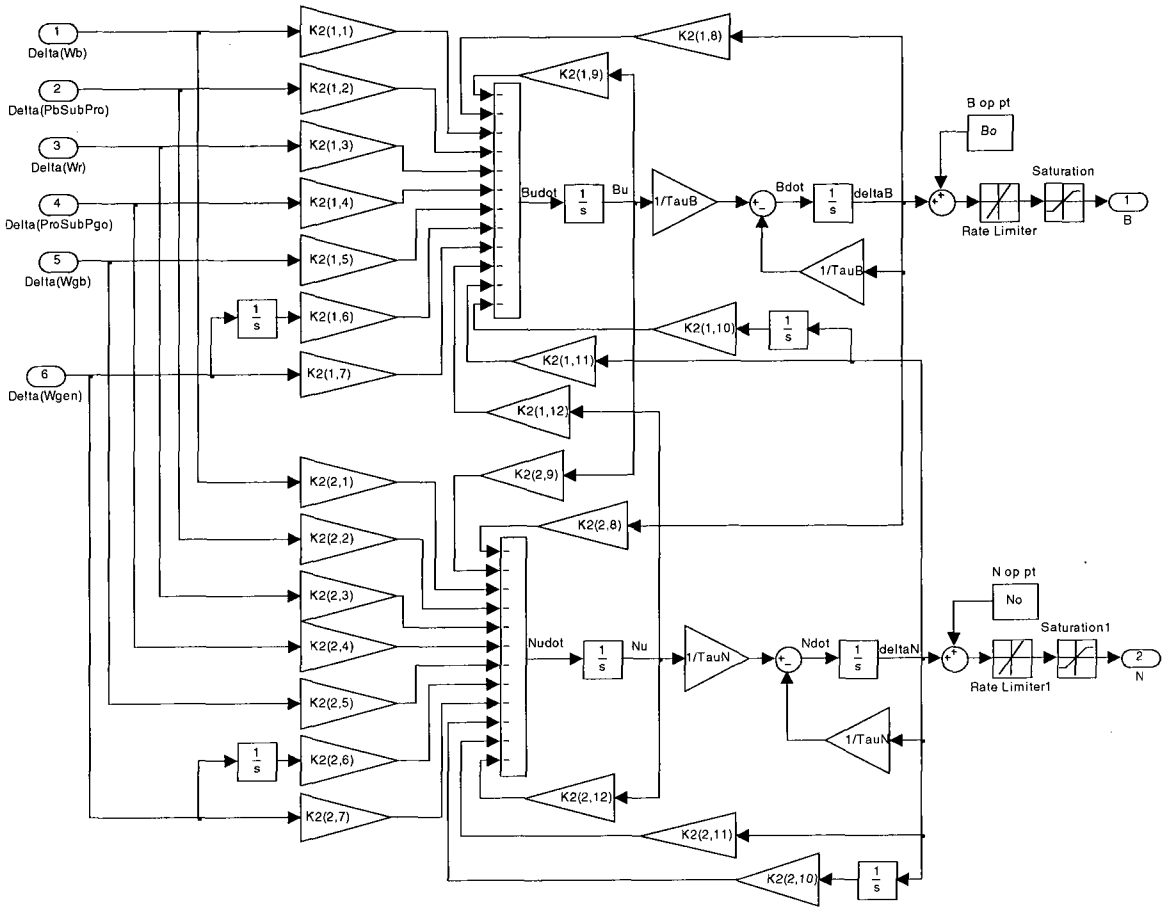

CHAPTER 5:

SIMULATIONS AND RESULTS

Simulation Overview, Assumptions and Parameters

In order to validate the control system designs in the previous chapter, many simulation experiments are performed. The simulation studies are done to develop a full understanding of the fundamental tradeoffs involved in control system design. The experiments and results are described in this chapter.

The wind is a stochastic process with non-stationary statistics. It has been studied extensively by many other researchers. A turbulent wind generating software called TurbSim was developed by NREL to create full field wind input files compatible with the FAST software. This program was used to generate wind files to test and compare the control systems in this report.

Simulation of the control systems consisted of:

- Simulation of the PI and PI MF controller on the DLIN and FAST models.
- Simulation of the single-input LQR controller on the DLIN and FAST models.
- Simulation of the multi-input LQR controller on the DCVT model

The simulations run in this chapter were for 600 seconds with a .01 second sample time. The blades and rotor shaft's initial conditions are in their relaxed state at the start of the FAST simulations. The sudden introduction of winds around 18 m/s cause significant transients as the blades and shafts flex. In this chapter all measurement

statistics were calculated for time greater than 50 seconds to exclude the effect of these transients. All plots shown will also not include the first 50 seconds.

The performance of the control systems were analyzed by reviewing statistics for each file in tabular and graphical form. These measurements were used for tuning the LQR controllers, testing the control systems and comparing their performance. The measurement statistics and descriptions can be seen in Table 5.1.

Table 5.1- Measurement statistics and descriptions

Statistic	**Description**
Max Pitch Rate, $\lvert\dot{\beta}\rvert$	Max pitch rate is analyzed to compare to the absolute limit of 8°/s
RMS Pitch Rate, $\dot{\beta}$	The RMS blade pitch rate is analyzed to understand how fast the blade is pitching throughout the simulation.
STD Blade Flex, $\theta_r - \theta_{gb}$	The standard deviation of the LSS flex is analyzed as a measure of fatigue on the LSS. The LSS flex causes the majority of all torque variations in the gearbox and generator.
RMS Gearbox Acceleration, $\ddot{\theta}_{gb}$	The RMS gearbox acceleration is analyzed as a measure of how fast the gearbox is changing speeds. The acceleration deviations are proportional to the torque variations.
RMS Gearbox Jerk, $\dddot{\theta}_{gb}$	The RMS gearbox jerk is analyzed as a measure of how fast the gearbox is accelerating or decelerating. The jerk deviations are proportional to the rate of torque variations.
RMS Speed Error, $\Delta\dot{\theta}_{gen}$	The RMS generator speed error is analyzed as a measure of how well the control system is regulating the turbine speed.
RMS Generator Acceleration, $\ddot{\theta}_{gen}$	The RMS gearbox acceleration is analyzed as a measure of how fast the generator is changing speeds. The acceleration deviations are proportional to the torque variations.
RMS Generator Jerk, $\dddot{\theta}_{gen}$	The RMS generator jerk is analyzed as a measure of how fast the generator is accelerating or decelerating. The jerk deviations are proportional to the rate of torque variations.
STD Electric Power, Epower	The standard deviation of electrical power is analyzed as a measure of variation in the electrical output of the generator.
Max Generator Speed, $\dot{\theta}_{gen}$	The maximum generator speed is analyzed as a measure of the worst regulation time for the controller.
Max Generator Acceleration, $\ddot{\theta}_{gen}$	The maximum generator acceleration is analyzed because these accelerations are due to torque variations.
Max Torque applied to the generator, T_{gen}	The maximum torque applied to the generator via the HSS is analyzed as a measure of the potential damage done by delivering too much torque to the generator.

Wind Input Files

A software package from NREL called TurbSim was used to generate wind input files to be used in this simulation. "TurbSim is a stochastic, full-field, turbulent-wind simulator. It uses a statistical model (as opposed to a physics-based model) to numerically simulate time series of three-component wind-speed vectors at points in a two-dimensional vertical rectangular grid that is fixed in space." [27] TurbSim generates full field wind files with wind speeds that vary across the rotor plane. The TurbSim wind files are compatible with the FAST model. The FAST model was then run in Simulink to output the hub height wind speed as a MATLAB .mat file. The wind file was used as the wind speed input for simulations of the DLIN and DCVT models. Two wind files were generated for simulations, VK4 and VK5. Table 5.2 contains important TurbSim input parameters of these wind files. The full TurbSim input file used to generate the VK4 wind file can be seen in Appendix B. Refer to the TurbSim User's Guide for more information on the input parameters and how the software works. [27]

Table 5.2- TurbSim input parameters

Input Parameters	**VK4**	**VK5**
Length	600 seconds	600 seconds
Sample time	.01 seconds	.01 seconds
Turbulence Model	IEC von Karman	IEC von Karman
IEC Standard	1	1
IEC Turbulence %	5	2
IEC Turbulence Model	"NTM"=normal	"NTM"=normal
IEC ETM "c" parameter	1 m/s	1 m/s
Power Law Exponent	0	0
Surface roughness length	.001 m	.001m
URef - Mean (total) wind speed	18 m/s	18 m/s

Table 5.3- TurbSim hub-height wind statistics

Hub Height Wind Speed Statistics	VK4	VK5
Mean	17.98803 m/s	18.01036 m/s
RMS	17.24245 m/s	17.24752 m/s
Standard Deviation	0.868341 m/s	0.375256 m/s
-3 dB frequency	3.329 Hz	2.338 Hz
Max, Min	21.08, 14.96 m/s	19.18, 16.73 m/s

The primary difference between these files is that VK5 has a smaller standard deviation than VK4. A smaller standard deviation causes smaller variations in wind speed from the linearized wind speed of 18 m/s. The two wind files allowed the simulation of the controllers when operating close to the linearization point and over a wider operating region. A different set of random numbers was used to generate each wind file so that they did not temporally correlate with each other.

A 100 second segment of the output file 'VK4' can be seen in Figure 5.1. If the entire 600 second time series was plotted the wind speed variations would be compressed to such an extent that it would be difficult to see the temporal wind speed variations.

Figure 5.1- TurbSim generated hub height wind speed

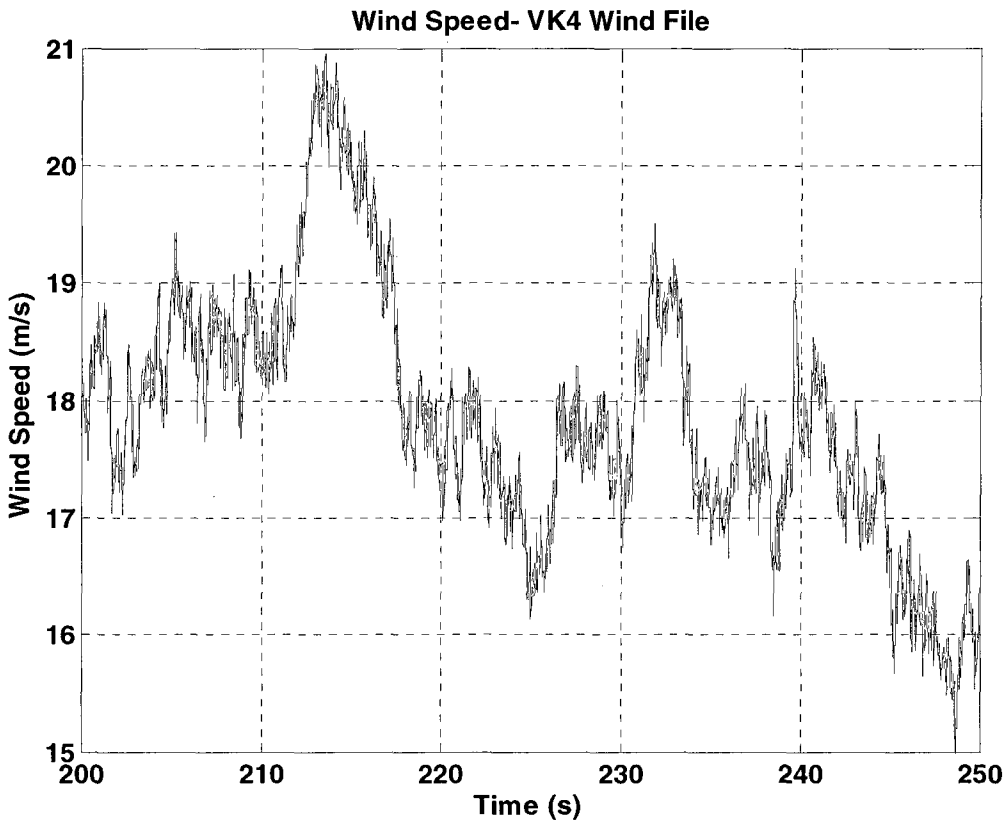

The power spectral density (PSD) of the wind input files was taken using MATLAB®. A plot of the PSD for wind file VK4 can be seen in Figures 5.2. There was a large spike in the PSD plot at DC because the mean wind speed was approximately 18 m/s. The maximum frequency on the PSD is 50 Hz, or half of the sampling frequency, as the sample time is .01 seconds. The power at DC and high frequencies is not shown in Figure 5.2 to show a higher resolution at low frequencies. The -3dB power point for wind input files of VK4 and VK5 are 3.3 Hz and 2.3 Hz respectively. Most of the energy in the wind is contained within frequencies below the -3dB values. These frequencies are within the pass-band of the wind turbine bode plot seen in Figure 3.9 which indicates that these frequencies will propagate through the wind turbine and affect the gearbox and generator.

Figure 5.2- PSD plot of wind input VK4

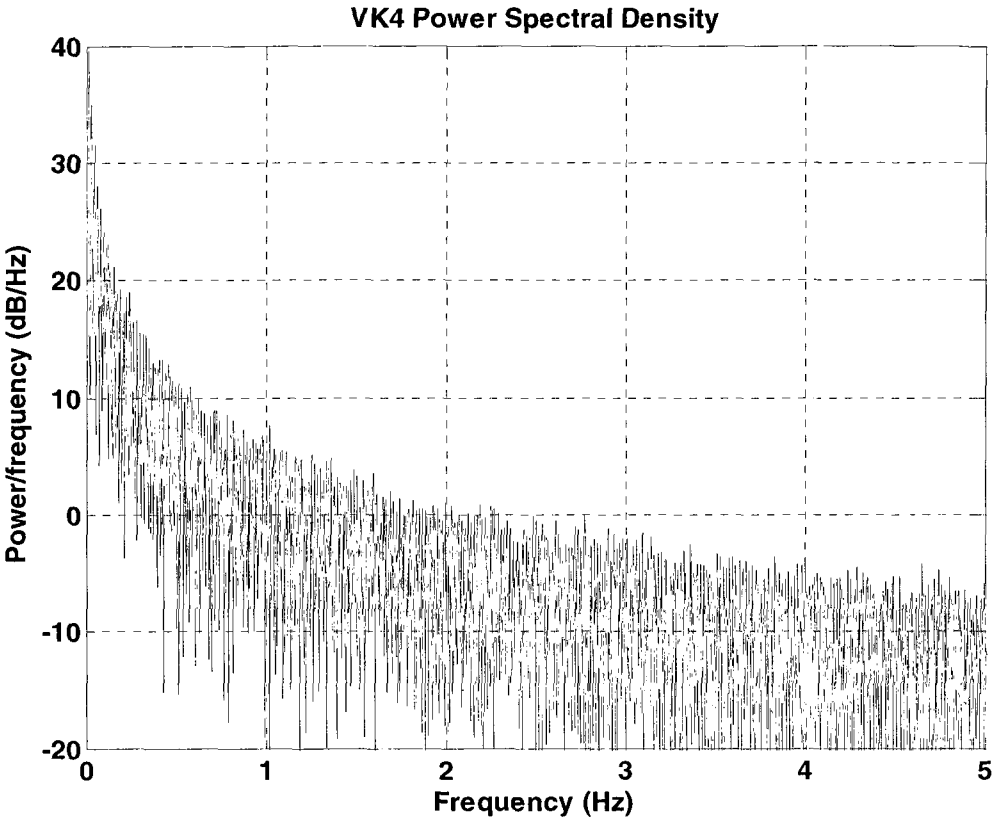

PI Controller Simulations

The gain scheduled PI controller described in Chapter 4 was simulated in the DLIN and FAST models with both wind input files. This is the control methodology most commonly used in industry and will be used as a baseline to compare other controllers. The simulations were performed with the DLIN model employing constant generator back-torque. Simulations were run with both models with and without the measurement filter. A comparison of the results can be seen in Table 5.4.

Table 5.4- PI control simulation statistics with VK4 wind

Model	**DLIN**	**DLIN**	**FAST**	**FAST**
Controller	**PI**	**PI MF**	**PI**	**PI MF**
Max Blade Pitch Rate, $\lvert\dot{\beta}\rvert$ (deg/s)	2.18994	1.82759	1.05896	0.592072
RMS Blade Pitch Rate, $\dot{\beta}$ (deg/s)	0.56759	0.457655	0.269736	0.17002
STD LSS Flex, $\theta_r - \theta_{gb}$ (rad)	0.000197	0.000183	0.000115	0.000112
RMS Agb, $\ddot{\theta}_{gb}$ (rad/s^2)	0.032711	0.030348	0.019036	0.018594
RMS Jgb, $\dddot{\theta}_{gb}$ (rad/s^3)	0.329185	0.278624	0.23226	0.217052
RMS Wgen Error, $\Delta\dot{\theta}_{gen}$ (rad/s)	1.608996	2.030974	0.705112	0.838789
RMS Agen, $\ddot{\theta}_{gen}$ (rad/s^2)	3.172973	2.943741	1.846444	1.803609
RMS Jgen, $\dddot{\theta}_{gen}$ (rad/s^3)	31.93096	27.02655	22.52922	21.05408
STD Epower (watts)	68356.19	86285.44	29957.14	35637.3
Max Wgen, $\dot{\theta}_{gen}$ (rad/s)	127.8737	129.1434	124.9318	125.3629
Max Agen, $\ddot{\theta}_{gen}$ (rad/s^2)	12.91773	10.37726	6.609782	7.735137
Max Gen Torque, T_{gen} (N-m)	49993.12	48636.21	46623.94	47225.01

A bar graph was created to visually depict each of the statistics, seen in Figure 5.3. The plot was normalized to the statistics of the DLIN model with the PI and no measurement filter. When the gearbox acceleration and jerk statistics are normalized they are the same as the acceleration and jerk of the generator when a fixed gearbox is used. The gearbox statistics were not included in Figure 5.3 to improve the readability of the data.

Figure 5.3- Normalized PI control simulation statistics with VK4 wind

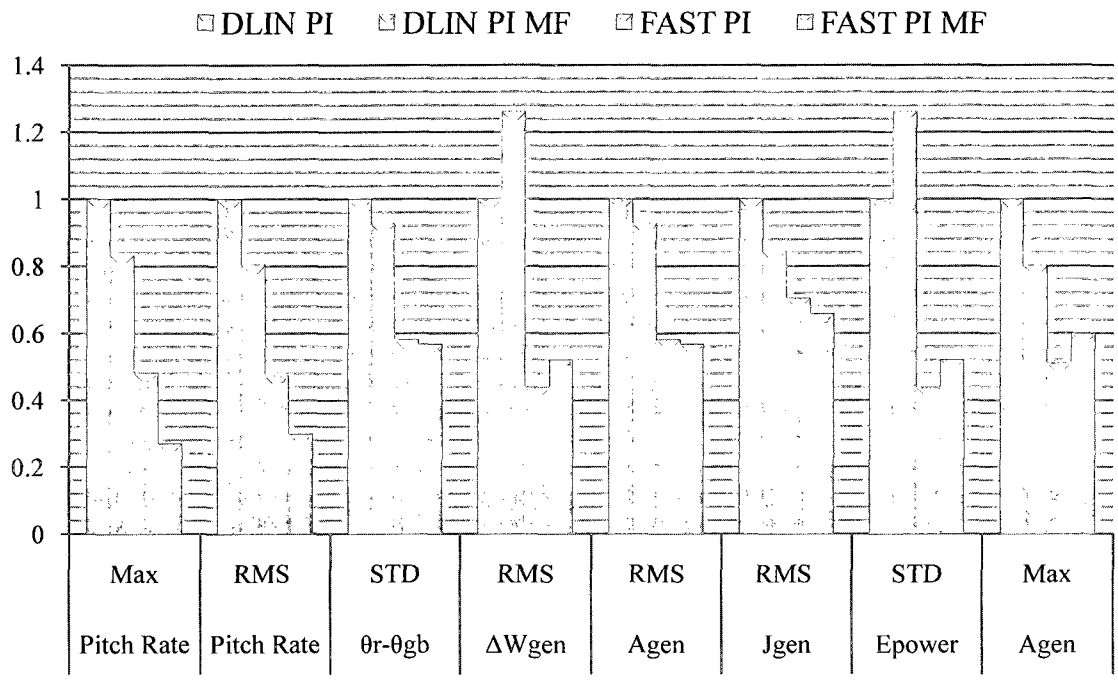

It can be seen in Figure 5.3 that the FAST model pitched the blades less and experienced lower RMS accelerations and jerks. This can be attributed to the simplification of the blade dynamics in the linear model. There were many un-modeled non-linear aerodynamics not included in this model.

It can also be seen that introducing the measurement filter caused both models to reduce RMS blade pitch rates, RMS accelerations at the expense of reduced regulation of speed and power. The PI controller with the measurement filter (PI MF) was the baseline which the LQR controllers were compared. The PI MF controller minimized the RMS accelerations better than the PI controller alone.

Figure 5.4 shows the regulation of the generator speed relative to the variation in wind speed and blade pitch angle for the DLIN model with PI MF control experiencing VK4 winds. All variables in Figure 5.4 are normalized to their peak value. It can be seen

that the blade pitch angle is tracking the wind speed. The 40% variation in the wind velocity is regulated to a 10% variation in generator speed.

Figure 5.4- Simulation outputs over time for DLIN- PI MF with VK4 wind

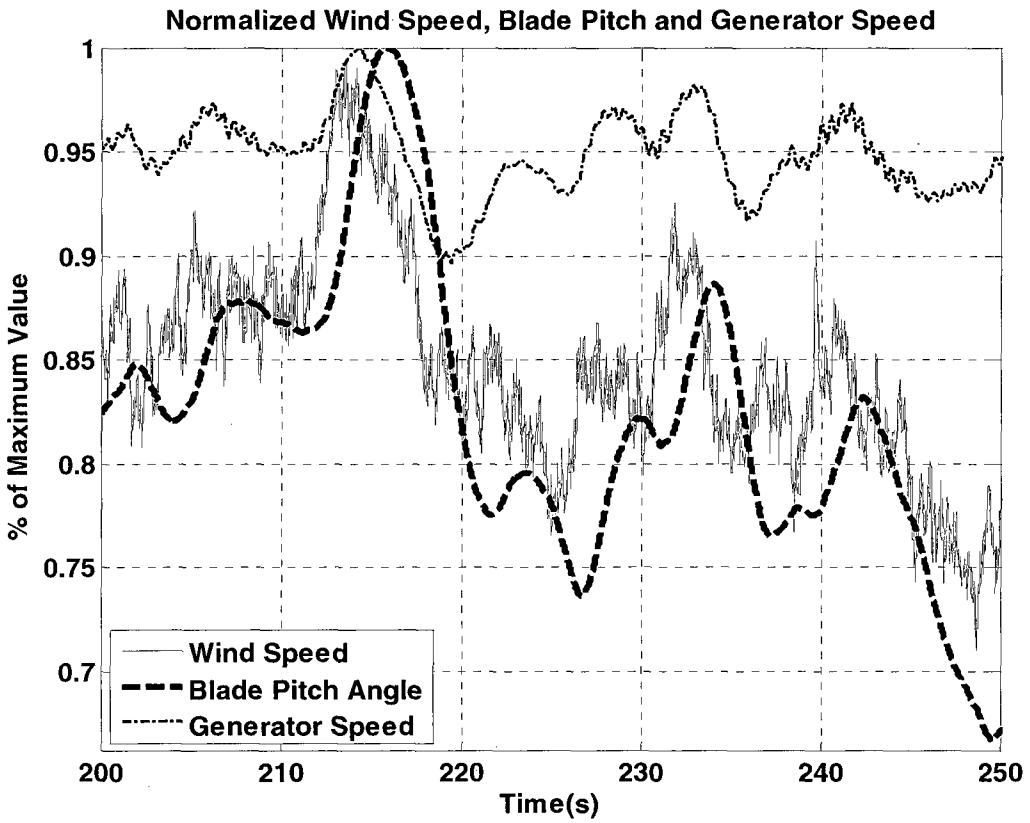

The closed loop Bode diagram of PI MF controller and the open loop Bode plot of the wind turbine plant from wind speed input to HSS velocity output can be seen in Figure 5.5. Notice that the resonant peak of the wind turbine is outside of the controller's bandwidth. This is a result of adding the measurement filter to the PI controller. It was undesirable for the PI controller to actuate the blades at these frequencies and potentially excite the natural modes of the blades and drivetrain. An overlay of the power spectral density (PSD) plot of the VK4 wind input file shows that there is still significant power in the wind at frequencies outside the bandwidth of the

controller, where the resonant frequency of the wind turbine lies. This can be seen in Figure 5.6. Figure 5.7 shows the plots of Figure 5.6 with the power spectral density of the generator accelerations that resulted from simulating the DLIN model with the PI MF controller in VK4 winds. It can be seen in Figure 5.7 that there is significant power in the generator accelerations outside of the PI MF controller's bandwidth. This means that the controller cannot react fast enough to attenuate these frequencies.

Figure 5.5- DLIN open loop and DLIN- PI MF closed loop Bode plots

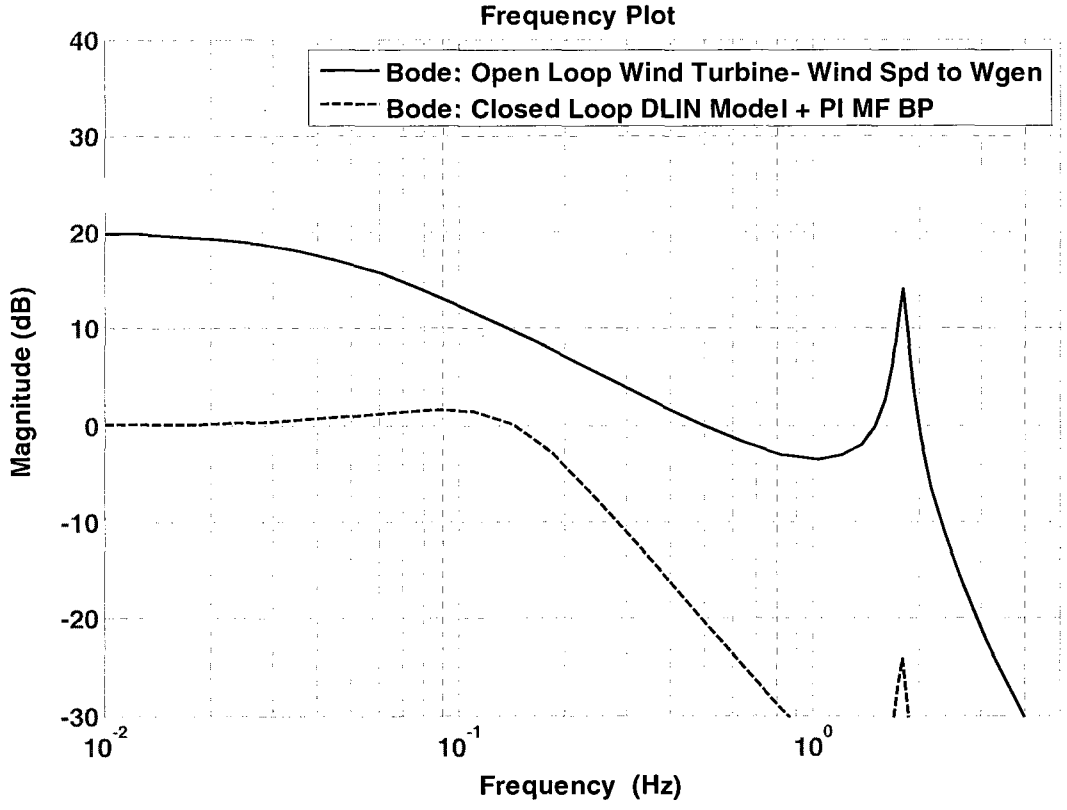

The same simulations were run with wind input VK5. Results can be seen in Table 5.5 and Figure 5.8. These simulation results were similar to those found in Table 5.4 and Figure 5.4 scaled down by approximately 60%. This scaling is due to the similar frequency content of both wind input files and, with the smaller standard deviation of wind input file VK5.

Figure 5.6- DLIN- PI MF Bode plots with VK4 wind PSD overlay

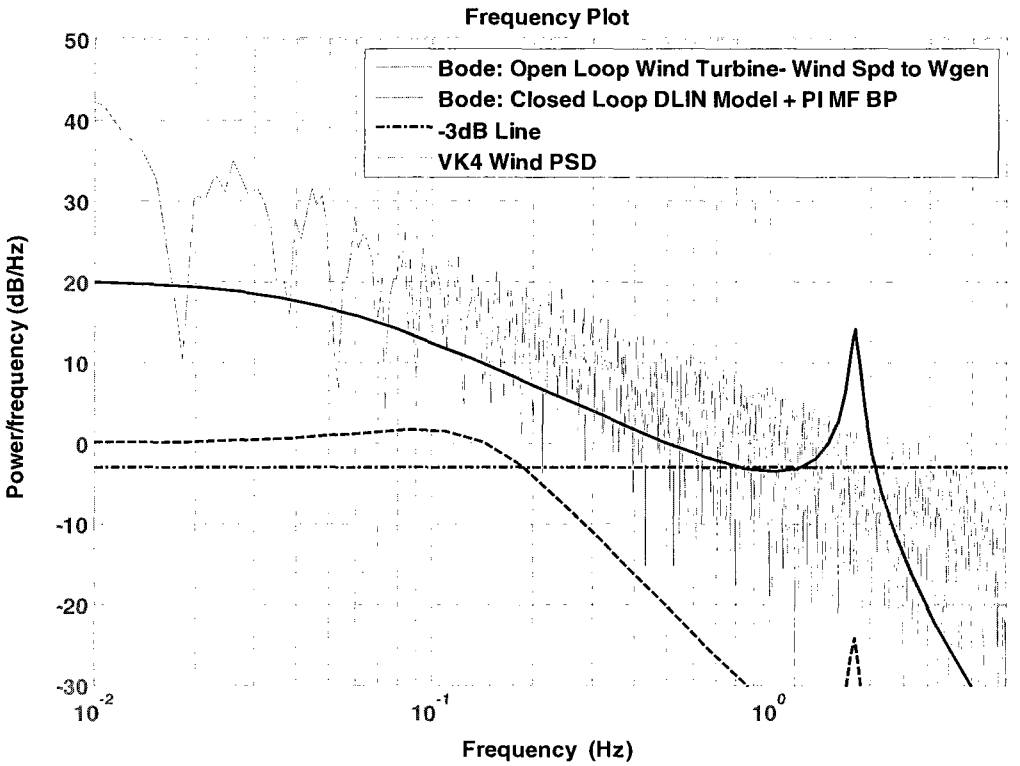

Figure 5.7- DLIN PI MF Bode plots, VK4 wind PSD and Agen PSD overlay

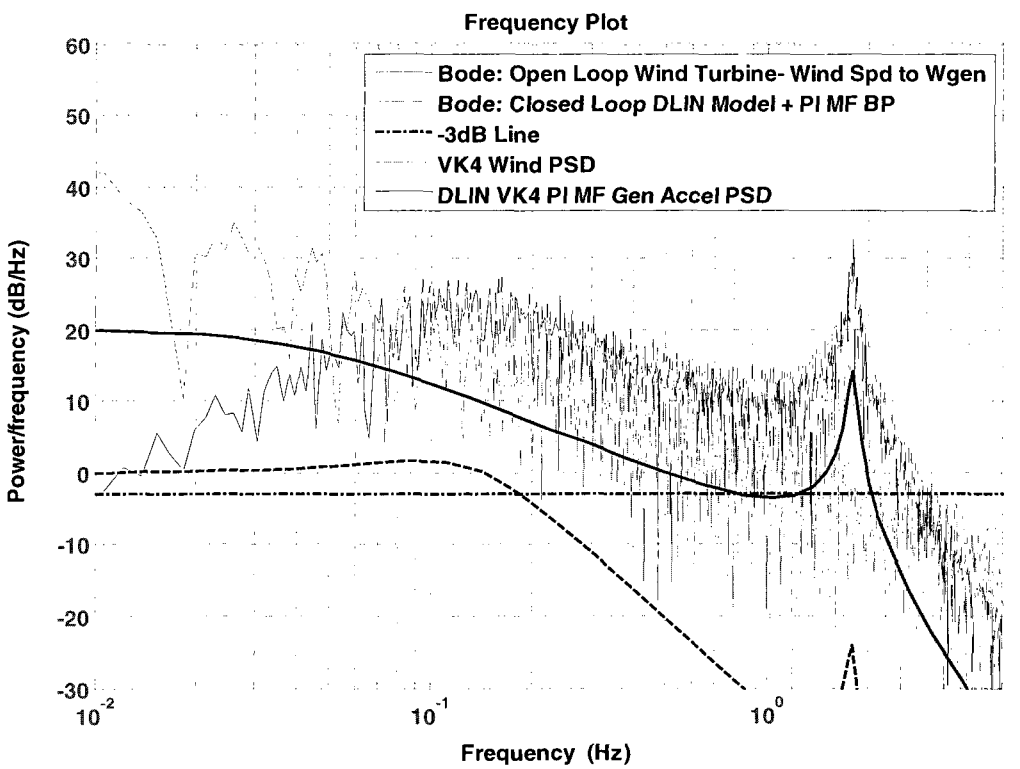

Table 5.5- PI control simulation statistics with VK5 wind input

Model	DLIN	DLIN	FAST	FAST
Controller	**PI**	**PI MF**	**PI**	**PI MF**
Max Blade Pitch Rate, $\lvert\dot{\beta}\rvert$ (deg/s)	0.941662	0.575371	0.472482	0.261731
RMS Blade Pitch Rate, $\dot{\beta}$ (deg/s)	0.228631	0.185824	0.11148	0.074325
STD LSS Flex, $\theta_r - \theta_{gb}$ (rad)	7.91E-05	7.32E-05	4.75E-05	4.65E-05
RMS Agb, $\ddot{\theta}_{gb}$ (rad/s^2)	0.013115	0.012121	0.007888	0.007711
RMS Jgb, $\dddot{\theta}_{gb}$ (rad/s^3)	0.131957	0.111198	0.096453	0.090041
RMS Wgen Error, $\Delta\dot{\theta}_{gen}$ (rad/s)	0.678677	0.848749	0.29358	0.360304
RMS Agen, $\ddot{\theta}_{gen}$ (rad/s^2)	1.272156	1.175706	0.765105	0.747999
RMS Jgen, $\dddot{\theta}_{gen}$ (rad/s^3)	12.79986	10.78618	9.355942	8.734022
STD Epower (watts)	28834	36059.6	12473.73	15308.76
Max Wgen, $\dot{\theta}_{gen}$ (rad/s)	125.0073	125.3194	123.8277	124.0943
Max Agen, $\ddot{\theta}_{gen}$ (rad/s^2)	5.316585	4.594295	3.228364	3.078083
Max Gen Torque, T_{gen} (N-m)	45933.22	45547.44	44817.87	44737.6

Figure 5.8- Normalized PI control simulation statistics with VK5 wind

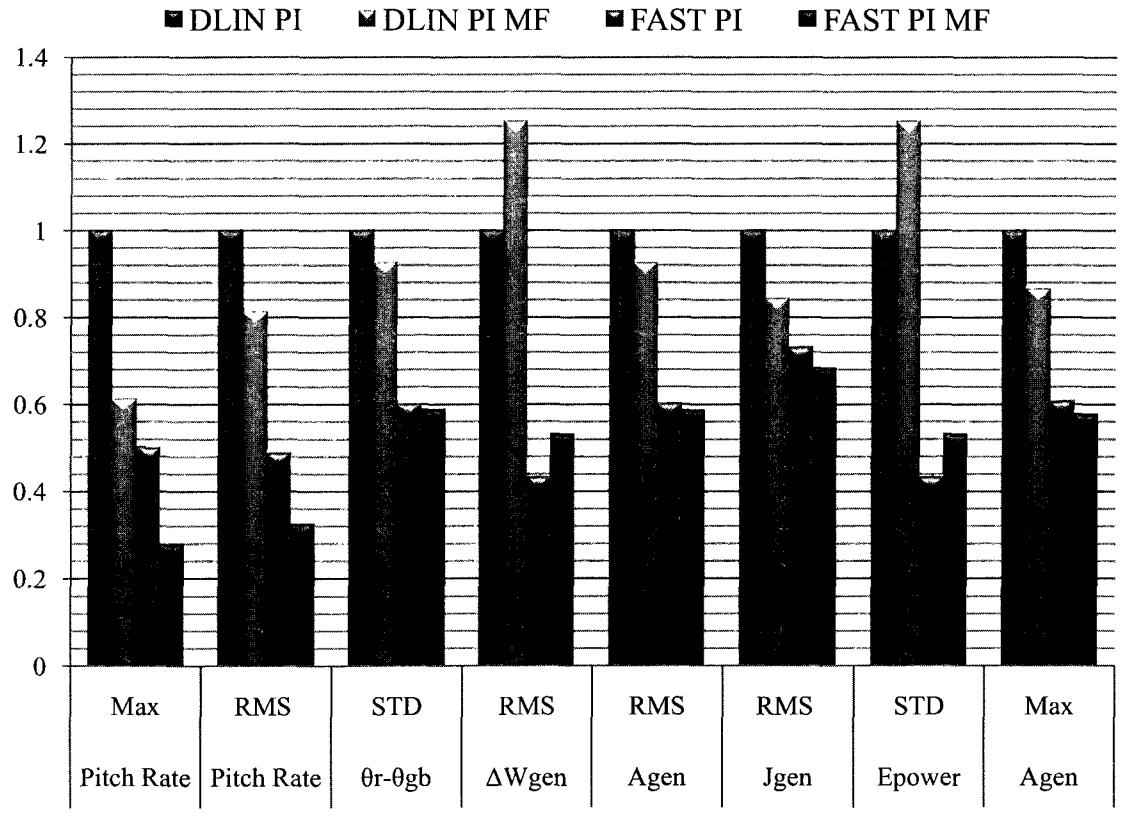

Single-Input LQR Controller Simulation Results

The single input LQR controller designed in Chapter 4 was then tuned for desired performance. The tuning of the controller was an iterative process of varying the control system parameters and simulating the DLIN model until the output was desired.

The single input LQR control system development has nine variables to alter, eight in the $\boldsymbol{Q}$ state penalty matrix and one as the $\boldsymbol{R}$ input penalty. The goal of the LQR controller is to minimize the performance index. It can be seen in equation (4.5) that the values of $\boldsymbol{Q}$ and $\boldsymbol{R}$ are chosen relative to one another. The penalty applied to state x_i depends on the ratio of $q_{i,i}$ to $\boldsymbol{R}$. An initial value of .01 was set to $\boldsymbol{R}$ as a starting point and the state penalties in $\boldsymbol{Q}$ were tuned. The penalty variables can be seen in equation (5.1).

$$\boldsymbol{Q}_1 = \begin{bmatrix} q_{1,1} & 0 & 0 & 0 & 0 & 0 & 0 & 0 \\ 0 & q_{2,2} & 0 & 0 & 0 & 0 & 0 & 0 \\ 0 & 0 & q_{3,3} & 0 & 0 & 0 & 0 & 0 \\ 0 & 0 & 0 & q_{4,4} & 0 & 0 & 0 & 0 \\ 0 & 0 & 0 & 0 & q_{5,5} & 0 & 0 & 0 \\ 0 & 0 & 0 & 0 & 0 & q_{6,6} & 0 & 0 \\ 0 & 0 & 0 & 0 & 0 & 0 & q_{7,7} & 0 \\ 0 & 0 & 0 & 0 & 0 & 0 & 0 & q_{8,8} \end{bmatrix}, \boldsymbol{R}_1 = r_1 \tag{5.1}$$

A description of each of the penalty variables can be seen in Table 5.6. In this table 'error' means the deviations away from the linearization point.

Table 5.6- Description of Q and R penalties for SI LQR controller

Penalty	Associated State	Description
$q_{1,1}$	$\Delta\dot{\theta}_b$	Penalty on blade tip rotational speed error
$q_{2,2}$	$\Delta(\theta_b - \theta_r)$	Penalty on blade flex error
$q_{3,3}$	$\Delta\dot{\theta}_r$	Penalty on rotor speed error
$q_{4,4}$	$\Delta(\theta_r - \theta_{gb})$	Penalty on LSS flex error
$q_{5,5}$	$\Delta\dot{\theta}_{gb}$	Penalty on gearbox speed error
$q_{6,6}$	$\int_0^T (\Delta\theta_{gen})dt$	Penalty on integrated gearbox speed error
$q_{7,7}$	$\Delta\beta$	Penalty on blade pitch actuator input deviation from β_0
$q_{8,8}$	$\Delta\beta_u$	Penalty on blade pitch actuator input deviation from β_0
r_1	$\Delta\dot{\beta}_u$	Penalty on rate of change of blade actuator input

The initial values of $\boldsymbol{Q}$ were entered as all zero except for the penalty on the gearbox speed error and the integrated gearbox speed error. Penalties on other states were then introduced and increased until their inclusion made a desirable difference in the output statistics.

The goal of the control system is to reduce generator torque variations and regulate the generator speed. The control system must pitch the blades to shed aerodynamic torque due to the wind. No penalty was put on the deviations of the blade pitch angle or blade pitch actuator input from the nominal blade pitch angle. The penalties $q_{7,7}$ and $q_{8,8}$ were left at zero to allow the blades to track the wind.

The controller was then tuned to meet the primary goal of reducing torque regulations and secondary goal of speed regulation. The constraint requirement was to keep the RMS blade pitch rates similar to that of the PI controller. When the tuning of the $\boldsymbol{Q}$ matrix was complete r_1 was then increased to produce similar RMS pitch rates as that of the PI controller. Table 5.4 shows that the PI pitch rates were not close to the absolute

maximum of 8°/s. The controller could pitch the blades at a much faster rate. Slower pitch rates are desirable in order to not excite the natural modes of the turbine.

A tradeoff existed between blade pitch rates, speed regulation and torque deviation regulation. For example, to some extent increasing the penalties on the blade and LSS flex proved to reduce torque variations at the gearbox and generator at the expense of increasing speed variation and blade pitch rate. The LQR controller can be tuned in many ways with different criteria. One set of penalties can be seen in Table 5.7. The large difference in scale of the penalty weights is due to the units of each state variable. The feedback gains were calculated and can be seen in Table 5.7. Gain k_1 represents the feedback gain applied to the measurement of the first state, as seen in Figure 4.8. The closed loop eigenvalues of $(\boldsymbol{A}_1\text{-}\boldsymbol{B}_1{*}\boldsymbol{K}_1)$ were also calculated and included in Table 5.7.

Table 5.7- Penalties and associated gains for SI LQR controller

State Penalties		State Feedback Gains		Eigenvalues
$q_{1,1}$	10	k_1	15.5852	-34.5+ 113.6i
$q_{2,2}$	3000000	k_2	1492.1561	-34.5-113.6i
$q_{3,3}$	400	k_3	-1.65	-1.14+9.41i
$q_{4,4}$	10000000	k_4	1531.9355	-1.14-9.41i
$q_{5,5}$	800	k_5	-129.9769	-3.81+0.81i
$q_{6,6}$	50	k_6	-25	-3.81-0.81i
$q_{7,7}$	0	k_7	0.8418	-1.22
$q_{8,8}$	0	k_8	2.9014	-0.17
r_1	.08			

The measurement filter was not used when simulating the SI LQR controller. The augmented state in front of the blade pitch input creates a low pass filter when the k_8 gain is fed back around to the control input, as seen in Figure 4.12. This feedback gain is

dependent on the penalties of the controller, as is the input filter. For the set of penalties and gains in Table 5.7 the normalized low pass filter has a cutoff frequency at approximately .4 Hz. The normalized Bode diagram for the SI LQR filter can be seen in Figure 5.9.

Figure 5.9- Normalized Bode diagram of SI LQR low pass input filter

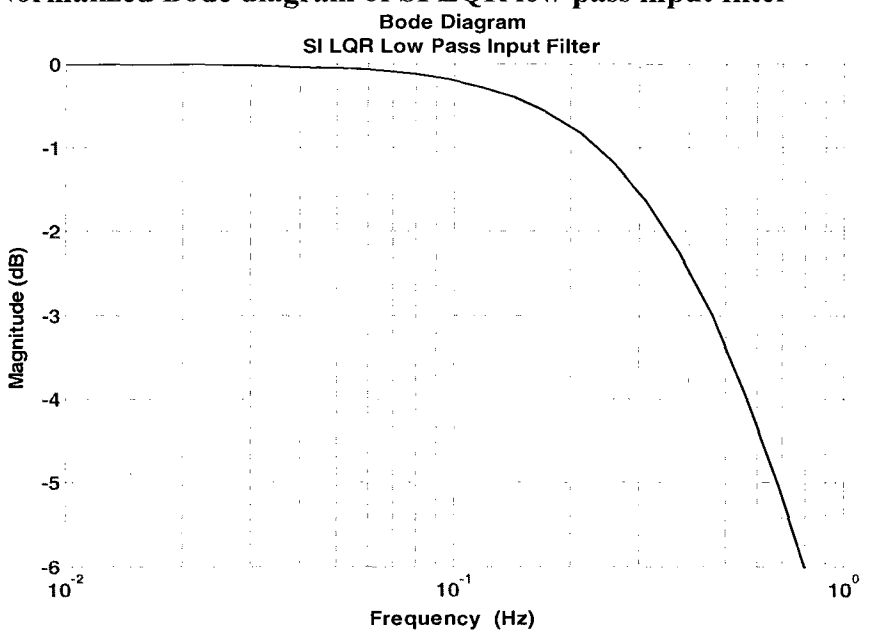

The SI LQR controller does a better job regulating torque variations (accelerations) and the generator speed than the PI MF controller. The simulation statistics of the SI LQR controller compared with the baseline PI MF controller can be seen in Table 5.8. The SI LQR statistics are normalized by those of the PI MF for easy comparison of percent change in output statistics as seen in Figure 5.10. Comparisons are made with the PI MF controller since the measurement filter aided in reducing RMS accelerations compared to the PI controller alone.

It can be seen in Figure 5.10 that the SI LQR controller proved to have lower RMS generator acceleration, generator jerk, gearbox acceleration, gearbox jerk, and

standard deviation of LSS twisting and provide better power and speed regulation at the expense of slightly higher pitch rates.

Table 5.8 - PI MF and SI LQR controller simulation statistics on DLIN model

Controller	**PI MF**	**SI LQR**	**PI MF**	**SI LQR**
Wind	**VK4**	**VK4**	**VK5**	**VK5**
Max Blade Pitch Rate, $\lvert\dot{\beta}\rvert$ (deg/s)	1.82759	1.874009	0.575371	0.682602
RMS Blade Pitch Rate, $\dot{\beta}$ (deg/s)	0.457655	0.48549	0.185824	0.195031
STD LSS Flex, $\theta_r - \theta_{gb}$ (rad)	0.000183	0.000165	7.32E-05	6.59E-05
RMS Agb, $\ddot{\theta}_{gb}$ (rad/s^2)	0.030348	0.02735	0.012121	0.010912
RMS Jgb, $\dddot{\theta}_{gb}$ (rad/s^3)	0.278624	0.25321	0.111198	0.10083
RMS Wgen Error, $\Delta\dot{\theta}_{gen}$ (rad/s)	2.030974	1.864993	0.848749	0.793649
RMS Agen, $\ddot{\theta}_{gen}$ (rad/s^2)	2.943741	2.652968	1.175706	1.058437
RMS Jgen, $\dddot{\theta}_{gen}$ (rad/s^3)	27.02655	24.5614	10.78618	9.780522
STD Epower (watts)	86285.44	79221.23	36059.6	33718.32
Max Wgen, $\dot{\theta}_{gen}$ (rad/s)	129.1434	128.6918	125.3194	125.6352
Max Agen, $\ddot{\theta}_{gen}$ (rad/s^2)	10.37726	10.26347	4.594295	4.307566
Max Gen Torque, T_{gen} (N-m)	48636.21	48575.43	45547.44	45394.29

Figure 5.10- Normalized PI MF and SI LQR control performance on DLIN model

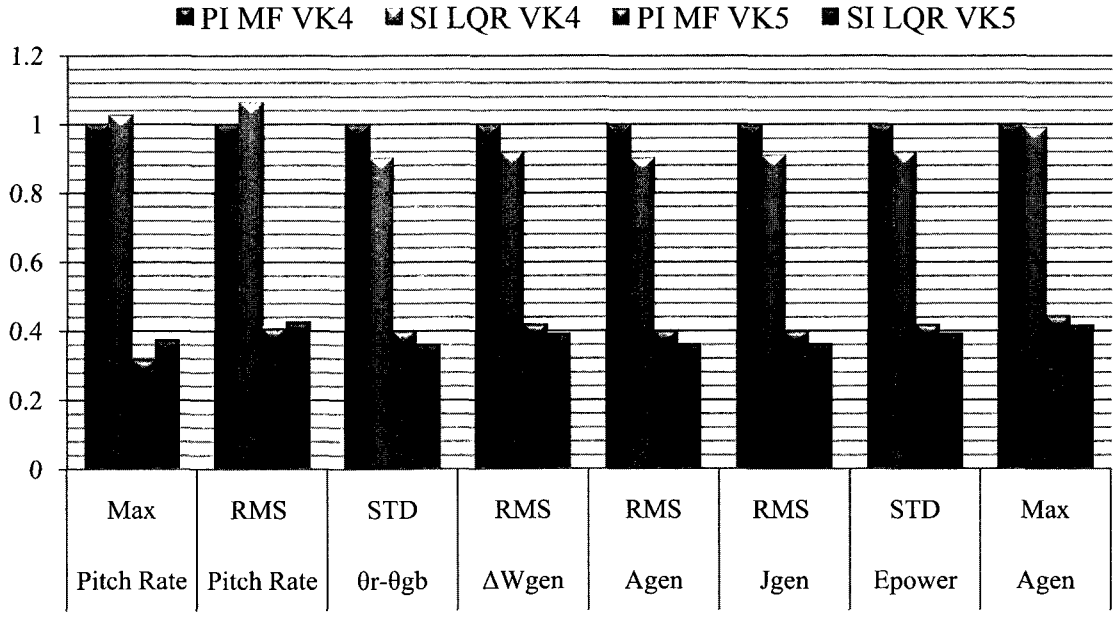

The open loop Bode plot and nyquist plot were analyzed for the SI LQR controller as seen in Figures 5.11 and 5.12. The Bode and nyquist plots for the PI MF controller with the DLIN model can be seen Chapter 4. The PI MF controller had a gain margin of 17.6 dB and a phase margin is 49.4°, as seen in Figure 4.7 and 4.8. The SI LQR controller had a gain margin of 14.7 dB and a phase margin of 74.3°. The SI LQR controller has substantial gain margin and significantly more phase margin than the PI MF controller.

Figure 5.11- Bode plot of DLIN model with SI LQR controller

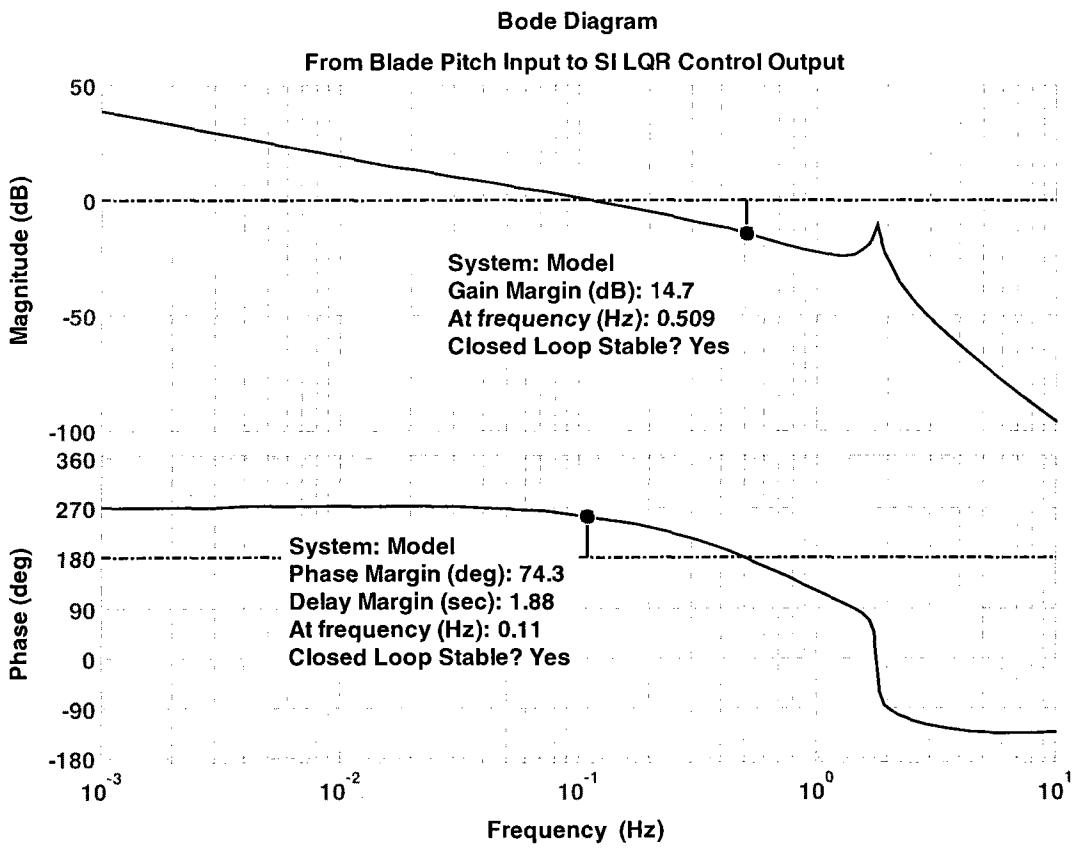

Figure 5.12- Nyquist plot of DLIN model with SI LQR controller

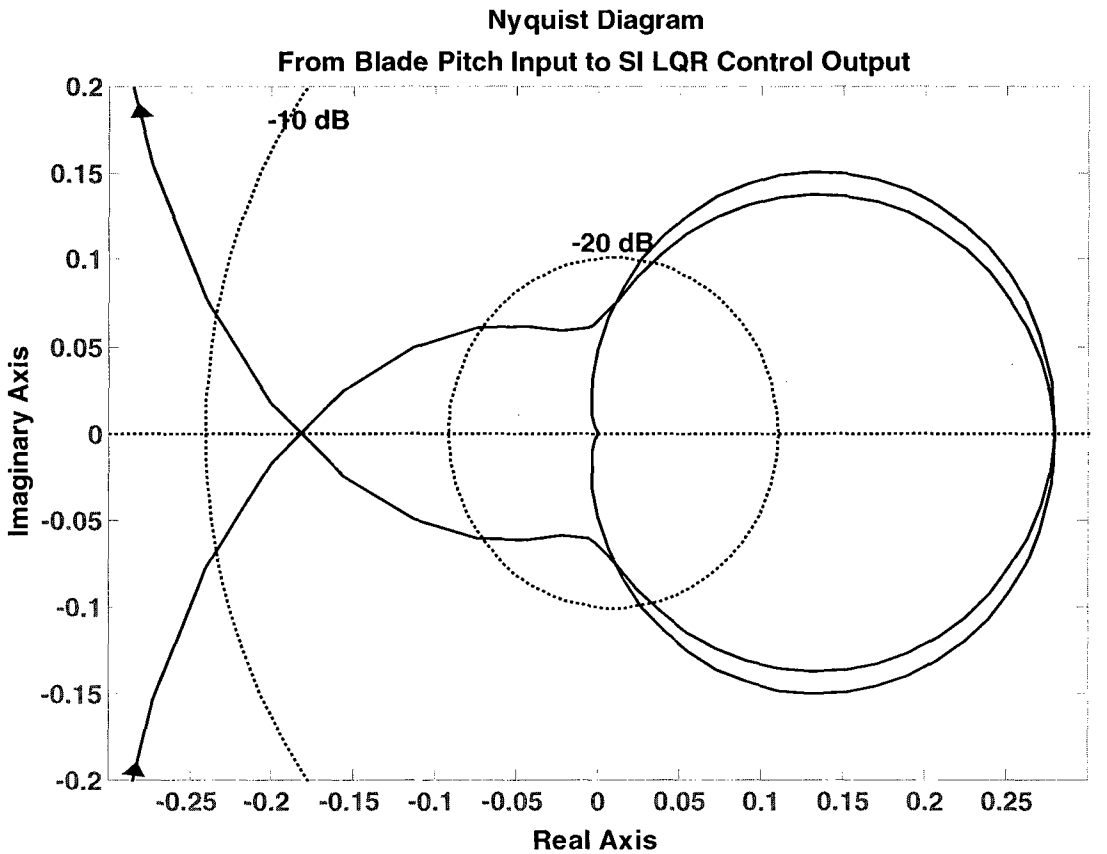

Figure 5.13 shows the regulation of the generator speed relative to the variation in wind speed and blade pitch angle for the DLIN model with SI LQR control experiencing VK4 winds. This plot resembles Figure 5.5 very closely.

Figure 5.13- Simulation output over time for DLIN- SI LQR with VK4 wind

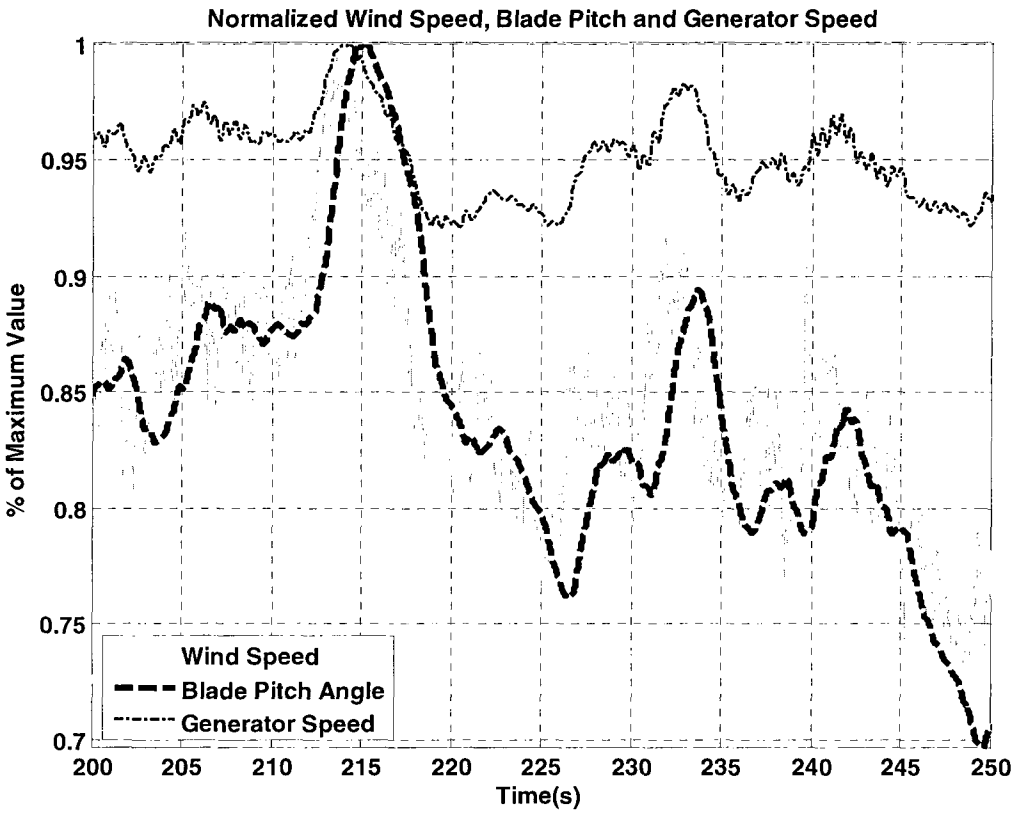

It is difficult to get significant reduction of torque variations even when using an advanced controller that utilizes full state feedback control and perfect knowledge of the model. This difficulty is due to the propagation time of the torque variations along the drivetrain. A close look at an overlay of the rotational speeds of the blade and gearbox can be seen in Figure 5.14.

Figure 5.14- Propagation of torque along the drivetrain

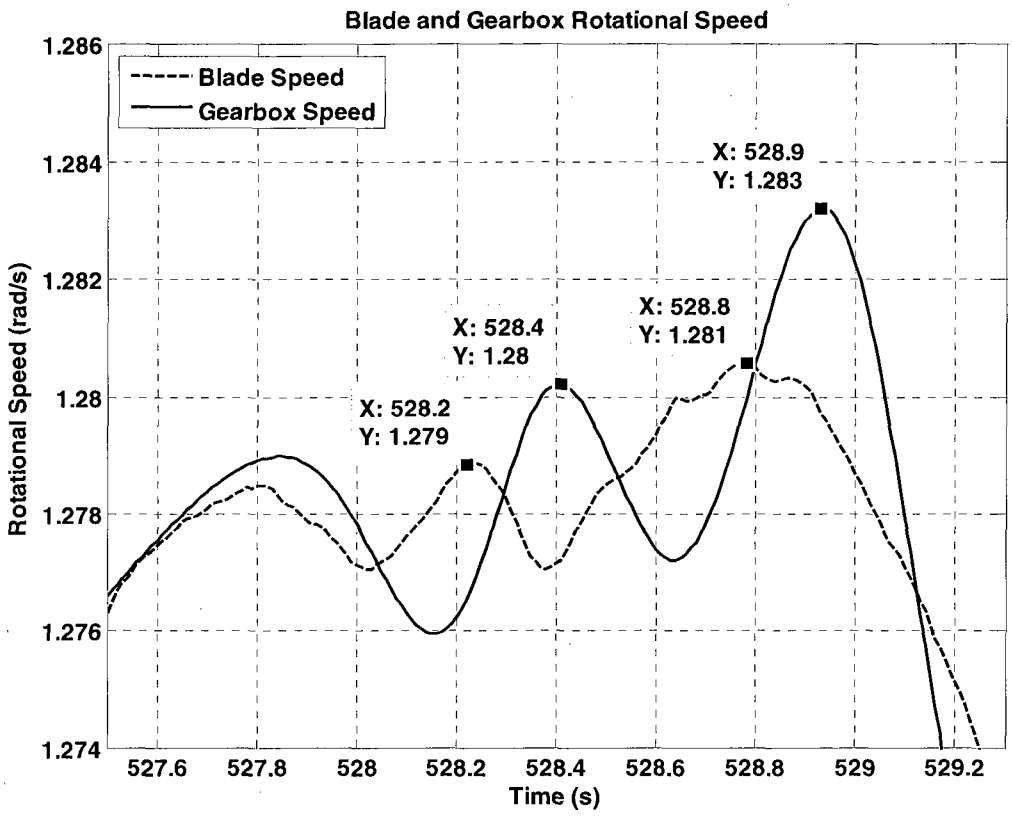

Figure 5.14 shows the propagation time from blade to gearbox takes less than 0.2 seconds. The maximum pitch rate reached in simulations was 1.9°/s. This short propagation delay means that the blades can pitch less than 0.38 ° in the time that the energy is delivered to the gearbox and generator. This change in pitch from the controller would be responding to a torque that has already been delivered to the turbine drivetrain. The change in pitch angle could therefore only assist in mitigating future torque variations. An actuator with a faster slew rate that is closer to the load is required to significantly mitigate these torque variations. The next section of this chapter will focus on the multi-input LQR controller which can adjust the gear ratio of the CVT.

Multi-Input LQR Controller Simulation Results

The multi-input LQR controller described in Chapter 4 was tuned on the DCVT model. This controller was more difficult to choose penalties for, since there were twelve penalties in the $\boldsymbol{Q}$ matrix and two in the $\boldsymbol{R}$ matrix. The $\boldsymbol{Q}$ and $\boldsymbol{R}$ matrices are defined in equations (5.2) and (5.3). The description of the $\boldsymbol{Q}$ and $\boldsymbol{R}$ matrix penalties can be seen in Table 5.9.

$$\boldsymbol{Q}_2 = \begin{bmatrix} q_{1,1} & 0 & 0 & 0 & 0 & 0 & 0 & 0 & 0 & 0 & 0 & 0 \\ 0 & q_{2,2} & 0 & 0 & 0 & 0 & 0 & 0 & 0 & 0 & 0 & 0 \\ 0 & 0 & q_{3,3} & 0 & 0 & 0 & 0 & 0 & 0 & 0 & 0 & 0 \\ 0 & 0 & 0 & q_{4,4} & 0 & 0 & 0 & 0 & 0 & 0 & 0 & 0 \\ 0 & 0 & 0 & 0 & q_{5,5} & 0 & 0 & 0 & 0 & 0 & 0 & 0 \\ 0 & 0 & 0 & 0 & 0 & q_{6,6} & 0 & 0 & 0 & 0 & 0 & 0 \\ 0 & 0 & 0 & 0 & 0 & 0 & q_{7,7} & 0 & 0 & 0 & 0 & 0 \\ 0 & 0 & 0 & 0 & 0 & 0 & 0 & q_{8,8} & 0 & 0 & 0 & 0 \\ 0 & 0 & 0 & 0 & 0 & 0 & 0 & 0 & q_{9,9} & 0 & 0 & 0 \\ 0 & 0 & 0 & 0 & 0 & 0 & 0 & 0 & 0 & q_{10,10} & 0 & 0 \\ 0 & 0 & 0 & 0 & 0 & 0 & 0 & 0 & 0 & 0 & q_{11,11} & 0 \\ 0 & 0 & 0 & 0 & 0 & 0 & 0 & 0 & 0 & 0 & 0 & q_{12,12} \end{bmatrix} \tag{5.2}$$

(5.3)

$$\boldsymbol{R}_2 = \begin{bmatrix} r_{1,1} & 0 \\ 0 & r_{2,2} \end{bmatrix} \tag{5.4}$$

Careful selection of the $\boldsymbol{Q}_2$ and $\boldsymbol{R}_2$ penalties was required to ensure stability of the controller. Recall that the linearized $\boldsymbol{A}_2$ matrix is uncontrollable, as discussed in Chapter 4. The process of choosing the $\boldsymbol{Q}_2$ and $\boldsymbol{R}_2$ penalties began with choosing values of $r_{1,1}$ and $r_{2,2}$ that were inversely proportional to a moderate control signal for blade pitch and gear ratio. This was done to keep the blade pitch rate and CVT slew rates at appropriate levels without one of these inputs supplying the majority of the control effort. A penalty

was applied to $q_{10,10}$ to ensure the CVT would return to the nominal value under steady state conditions as described in Chapter 4. Penalties were also applied to the generator speed error and the integration of the generator speed error to ensure speed regulation and zero steady state tracking error for generator speed. The penalties on blade pitch and blade pitch command were left at 0. The penalties on blade, rotor and gearbox speed error were also left at zero as they will vary independently of the generator speed with a variable gear ratio. Penalties on blade and LSS flex were applied and the controller was tuned for desired performance. The resulting penalties, gains and eigenvalues can be seen in Table 5.10.

Table 5.9- Description of Q and R penalties for MI LQR controller

Penalty	Associated State	Description
$q_{1,1}$	$\Delta\dot{\theta}_b$	Penalty on blade tip rotational speed error
$q_{2,2}$	$\Delta(\theta_b - \theta_r)$	Penalty on blade flex error
$q_{3,3}$	$\Delta\dot{\theta}_r$	Penalty on rotor speed error
$q_{4,4}$	$\Delta(\theta_r - \theta_{gb})$	Penalty on LSS flex error
$q_{5,5}$	$\Delta\dot{\theta}_{gb}$	Penalty on gearbox speed error
$q_{6,6}$	$\Delta\dot{\theta}_{gen}$	Penalty on generator speed error
$q_{7,7}$	$\int_0^T (\Delta\theta_{gen})dt$	Penalty on integrated generator speed error
$q_{8,8}$	$\Delta\beta$	Penalty on blade pitch actuator input deviation from β_0
$q_{9,9}$	$\Delta\beta_u$	Penalty on blade pitch actuator input deviation from β_0
$q_{10,10}$	$\int_0^T (\Delta N)dt$	Penalty on integrated gear ratio deviation from N_0
$q_{11,11}$	ΔN	Penalty on gear ratio deviation from N_0
$q_{12,12}$	ΔN_u	Penalty on gear ratio actuator input deviation from N_0
$r_{1,1}$	$\Delta\dot{\beta}_u$	Penalty on rate of change of blade actuator input
$r_{2,2}$	$\Delta\dot{N}_u$	Penalty on rate of change of gear ratio actuator input

Table 5.10- Penalties and associated gains for MI LQR controller

State Penalties		State Feedback Gains				Eigenvalues
$q_{1,1}$	0	$k_{1,1}$	-73.2132	$k_{2,1}$	-0.4065	-34.46 + 113.61*i*
$q_{2,2}$	3000000	$k_{1,2}$	160.8921	$k_{2,2}$	-1.5872	-34.46 - 113.61*i*
$q_{3,3}$	0	$k_{1,3}$	-0.1818	$k_{2,3}$	0.0012	-6.03 + 13.75*i*
$q_{4,4}$	100000000	$k_{1,4}$	114.2826	$k_{2,4}$	-2.0785	-6.03 - 13.75*i*
$q_{5,5}$	0	$k_{1,5}$	102.2491	$k_{2,5}$	0.3734	-12.37
$q_{6,6}$	.5	$k_{1,6}$	-0.1573	$k_{2,6}$	-0	-5.00
$q_{7,7}$	10	$k_{1,7}$	-0.9344	$k_{2,7}$	0.0001	-2.44
$q_{8,8}$	0	$k_{1,8}$	0.396	$k_{2,8}$	0.0004	-0.87
$q_{9,9}$	0	$k_{1,9}$	1.8357	$k_{2,9}$	-0.0015	-0.60 + 0.42*i*
$q_{10,10}$	200000	$k_{1,10}$	-0.4985	$k_{2,10}$	0.0097	-0.60 - 0.42*i*
$q_{11,11}$	10	$k_{1,11}$	-14370.48	$k_{2,11}$	-4.7614	-0.22
$q_{12,12}$	10	$k_{1,12}$	-384.0105	$k_{2,12}$	20.2679	-5.6E-09
$r_{1,1}$	20					
$r_{2,2}$	5000000					

The augmentation of additional states by adding integrators in front of the blade pitch and CVT actuators in Chapter 4 allowed penalties to be placed on the rate of change of the blade pitch and CVT command signals. These extra states also created tunable low pass filters at each controller input when feedback gains were applied as seen in Figure 4.14. Gain $k_{1,9}$ determined the blade pitch rate command filter and gain $k_{2,12}$ determined the CVT slew rate command filter. The normalized Bode plot of the two input filters can be seen in Figure 5.15. The cutoff frequency of the blade pitch rate command filter was .25 Hz, similar to that of the measurement filter used with the PI controller. The cutoff frequency of the CVT slew rate command filter was 3Hz. This allowed the CVT to slew faster than the blade pitch. The natural frequencies of the blade and LSS are within this bandwidth. This means that the accuracy of the linearized system A matrix is important. Proper system representation in this A matrix can lead to damping of the drivetrain and

blade modes. If the system is not sufficiently characterized in the A matrix, the controller could cause excitation of these natural modes.

Figure 5.15- Normalized Bode plot of MI LQR low pass input filters

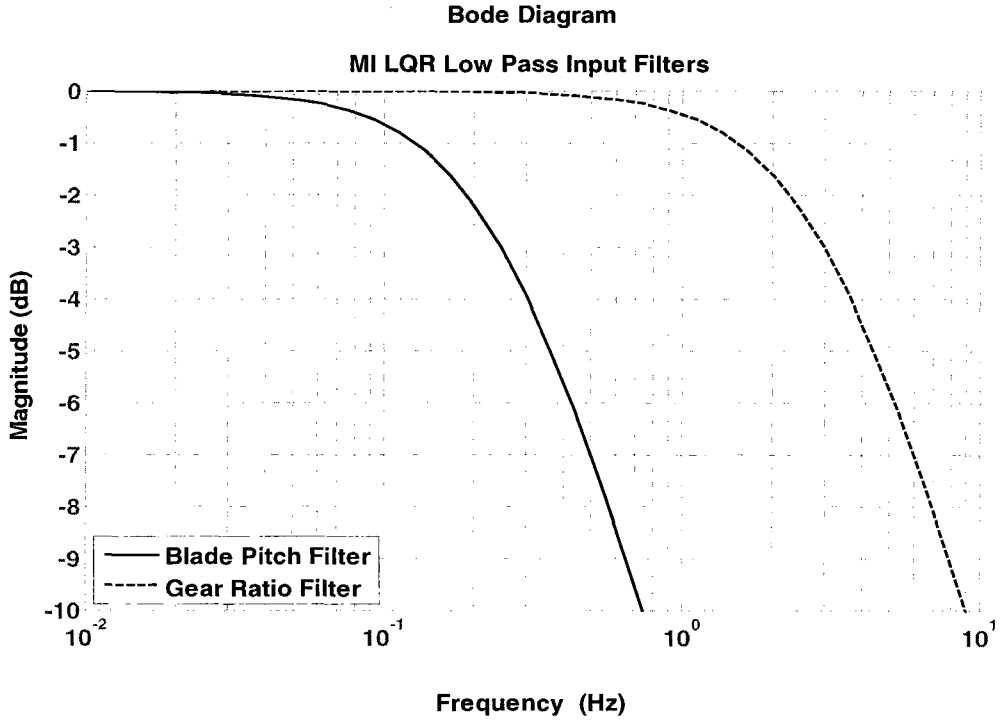

The DCVT model was then simulated with the MI LQR controller. Results are compared to the PI MF controller for each wind condition, as seen in Table 5.11 and Figure 5.16. With a variable gear ratio the RMS gearbox acceleration and jerk are not proportional to those of the generator. The RMS gearbox acceleration and jerk are included in Figure 5.16.

It can be seen that the state-space A_2 matrix was an accurate enough representation of the DCVT model, as the controller worked very effectively to mitigate RMS accelerations and jerks while maintaining a much tighter regulation of generator speed and electric power. The controller also significantly reduced the maximum

generator speed, torque and acceleration. There was no sacrifice in RMS blade pitch rate to achieve these goals.

Table 5.11- PI MF and MI LQR controller simulation statistics on DCVT model

Controller	PI MF	SI LQR	PI MF	SI LQR
Wind	**VK4**	**VK4**	**VK5**	**VK5**
Max Blade Pitch Rate, $\lvert\dot{\beta}\rvert$ (deg/s)	1.82759	1.471721	0.575371	0.513954
RMS Blade Pitch Rate, $\dot{\beta}$ (deg/s)	0.457655	0.404149	0.185824	0.163631
STD LSS Flex, $\theta_r - \theta_{gb}$ (rad)	0.000183	0.000171	7.32E-05	7.4E-05
RMS Agb, $\ddot{\theta}_{gb}$ (rad/s^2)	0.030348	0.018604	0.012121	0.007413
RMS Jgb, $\dddot{\theta}_{gb}$ (rad/s^3)	0.278624	0.12543	0.111198	0.049736
RMS Wgen Error, $\Delta\dot{\theta}_{gen}$ (rad/s)	2.030974	1.091669	0.848749	0.458492
RMS Agen, $\ddot{\theta}_{gen}$ (rad/s^2)	2.943741	1.124683	1.175706	0.447562
RMS Jgen, $\dddot{\theta}_{gen}$ (rad/s^3)	27.02655	5.173212	10.78618	2.053426
STD Epower (watts)	86285.44	46384.1	36059.6	19448.31
Max Wgen, $\dot{\theta}_{gen}$ (rad/s)	129.1434	126.3505	125.3194	124.2251
Max Agen, $\ddot{\theta}_{gen}$ (rad/s^2)	10.37726	4.47631	4.594295	1.538915
Max Gen Torque, T_{gen} (N-m)	48636.21	45484.42	45547.44	43915.51

Figure 5.16- Normalized simulation statistics for MI LQR controller

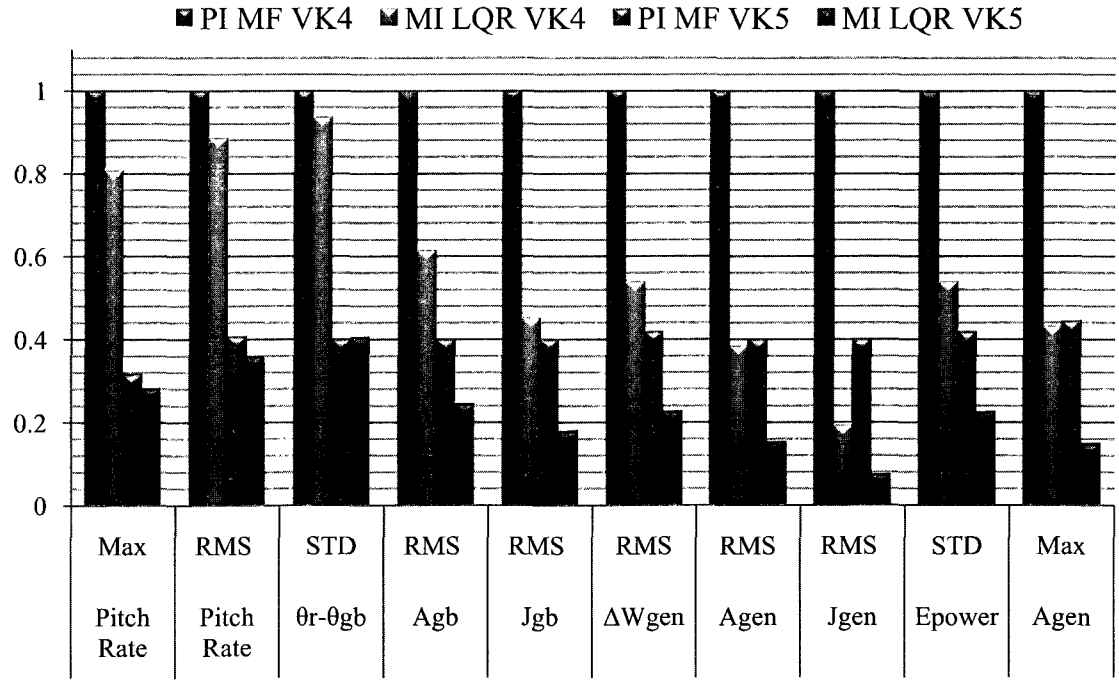

Figure 5.17 shows the generator accelerations of the PI MF controller and the MI LQR controllers plotted on the same set of axis. Reductions in accelerations are easily visible.

Figure 5.17- Generator accelerations of PI MF and MI LQR

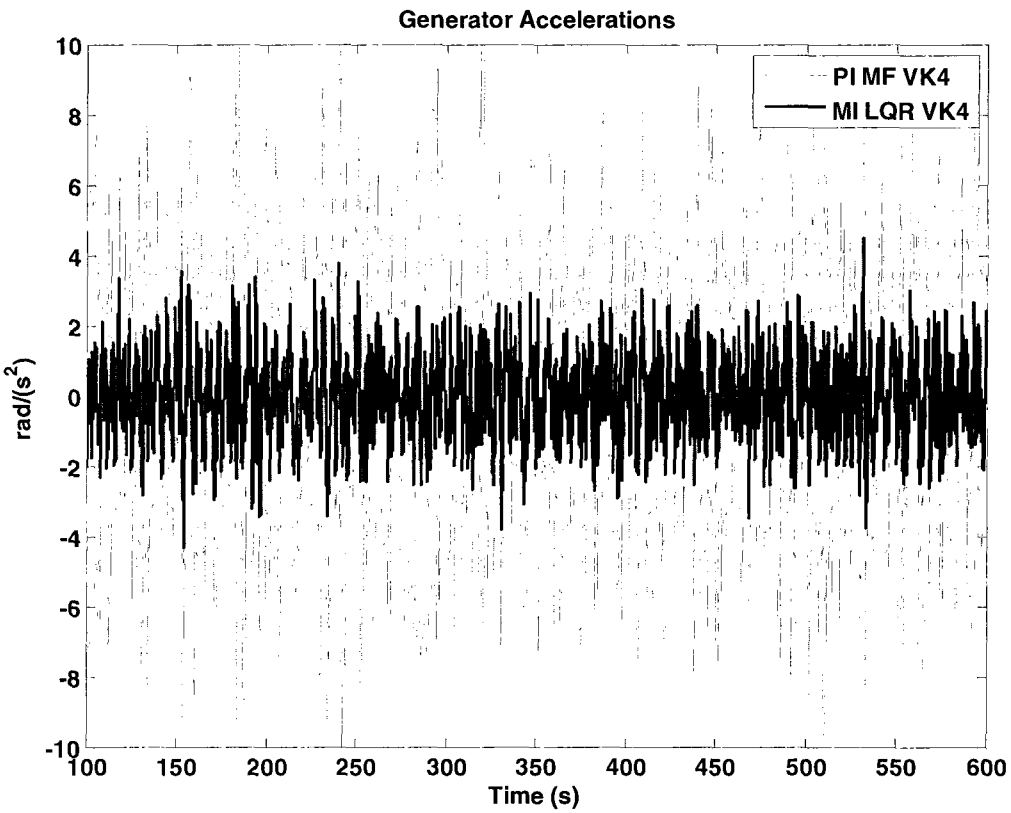

There are no standards to compare the statistics of the gear ratio or the CVT slew rate. It is useful to view a plot of the gear ratio variations over time to gain understanding of how the CVT is working. This plot can be seen in Figure 5.18, plotted as the inverse of the gear ratio for easier reference. Analyzing the plot as the inverse of the gear ratio sets the nominal gear ratio to 97 and the maximum and minimum limits of the gear ratio to 323 and 32 respectively. It can be seen in Figure 5.18 that the gear ratio does not come

close to its limits and instead varies closer to the nominal gear ratio transforming the load while the blades still pitch to shed the power at the source side.

Figure 5.18- Gear ratio inverse during simulation with MI LQR controller

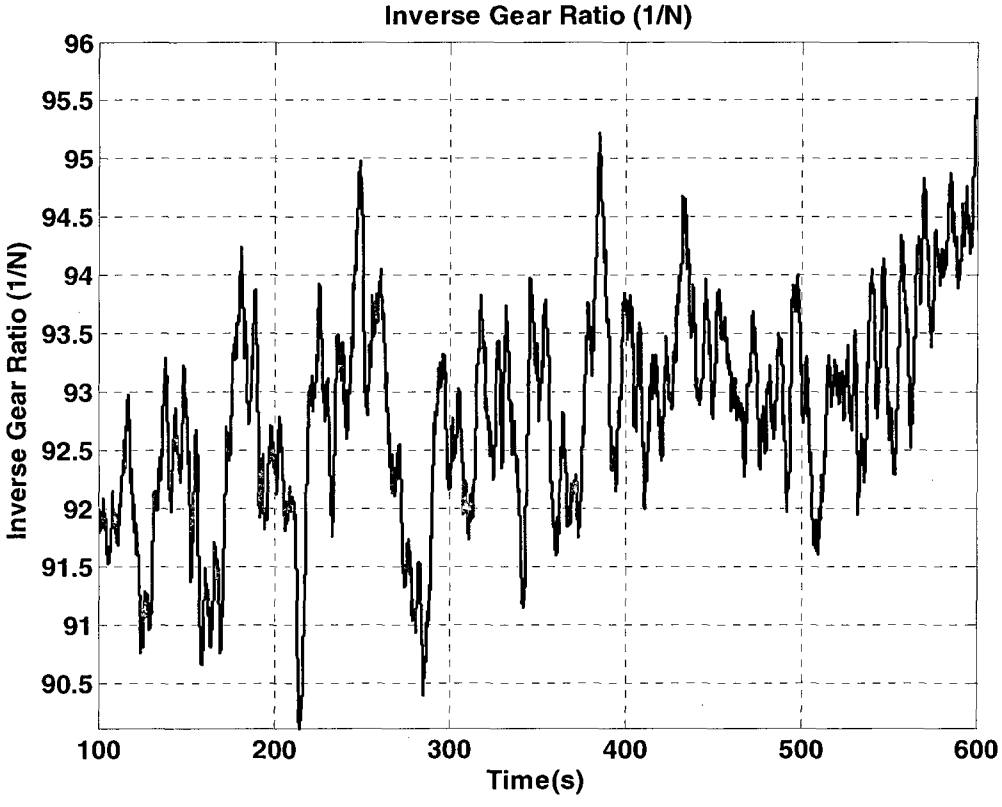

Figure 5.19 shows the wind speed, blade pitch, generator speed and gear ratio over time for the simulation of the DCVT model with MI LQR controller and VK4 wind input file. It can be seen that the blade pitch angle tracks the wind speed to limit aerodynamic torque while the gear ratio tracks the generator speed and regulates LSS flex, which in turn regulates the accelerations.

Figure 5.19- Simulation output over time for MI LQR and VK4 wind

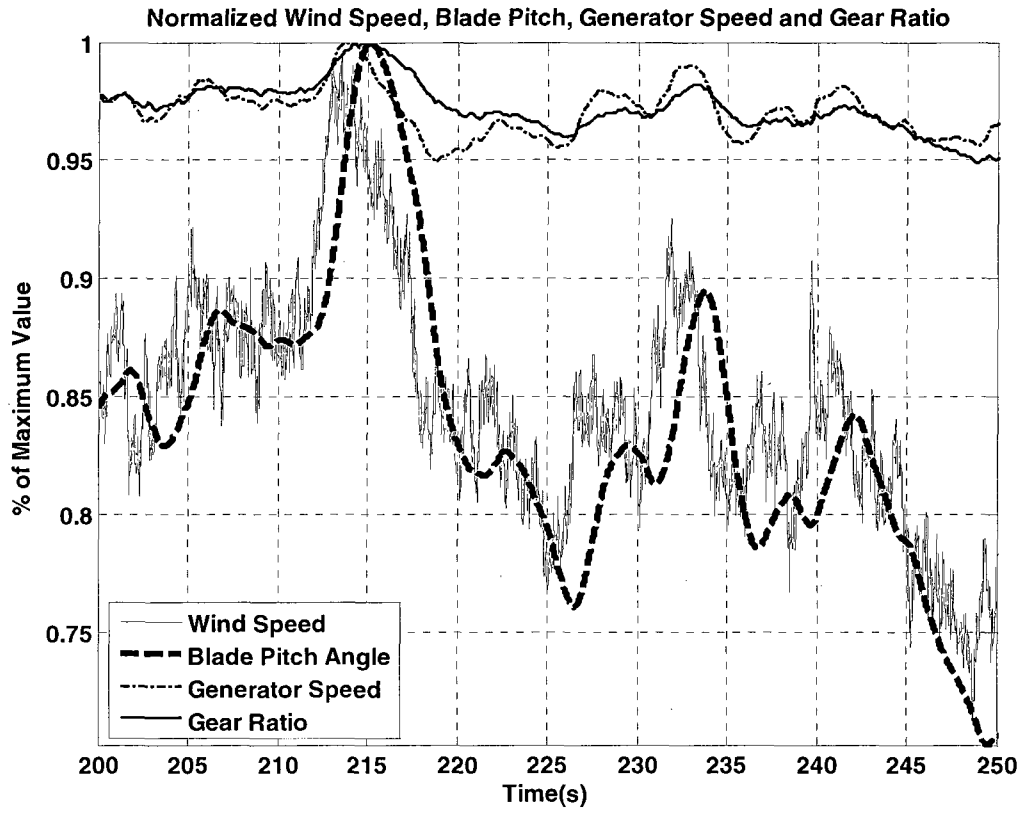

A half meter per second increase in wind was simulated at 60 seconds. The step responses of the PI MF, SI LQR and MI LQR controllers were analyzed. The steady state tracking of a step response for each controller can be seen in Figure 5.20. The generator speed with the PI MF controller experienced some overshoot and more oscillations than the other two controllers as the speed rose and fell quickly in response to the step input. The generator speed with the SI LQR controller also experienced a sharp increase and high frequency oscillations. The SI LQR controller damped some of the oscillations, but took longer to reach steady state as it returned smoothly to the rated speed. The MI LQR controller damped out almost all generator speed oscillations. The

generator speed with the MI LQR controller did not experience a radical change as the other two controllers. The MI LQR controller also took longer to reach steady state, but it did so in a smooth, vibration free trajectory.

Figure 5.20- Wind speed step response of controllers on derived models

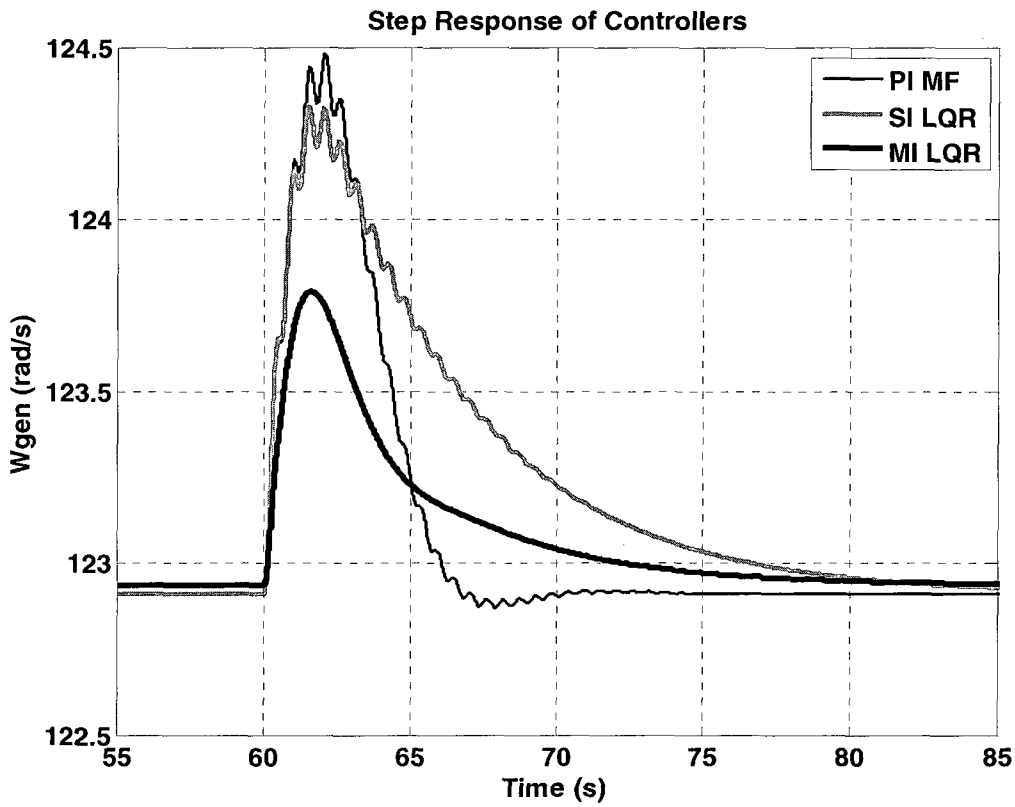

Comparison of PI MF and SI LQR controllers in FAST

The SI LQR controller described earlier in this chapter was simulated with the non-linear FAST model and compared to the PI MF controller. Results can be seen in Table 5.12 and Figure 5.21. The SI LQR was tested on the FAST model to observe the performance of this controller on a different model with non-linearities that it was not designed for. The SI LQR controller was robust enough to control the non-linear turbine

model and remain stable. There are similarities between the FAST and DLIN step responses and bode plots at the linearization point as seen in Chapter 3. The models do not match each other as well when perturbed with dynamic simulations, as seen in Figures 5.4 and 5.7. Table 5.12 shows the SI LQR controller commanded almost twice the RMS pitch rate as the PI MF controller with no reduction in RMS accelerations or speed regulation. The one advantage of the SI LQR controller was the reduction in maximum acceleration and maximum torque. It is clear that the FAST model differed significantly enough from the linearized model in dynamic simulations to degrade the performance of the controller. A normalized plot of the statistics in Table 5.12 can be seen in Figure 5.21.

Table 5.12- PI MF and SI LQR controller simulation statistics on FAST model

Controller	**PI MF**	**SI LQR**	**PI MF**	**SI LQR**
Wind	**VK4**	**VK4**	**VK5**	**VK5**
Max Blade Pitch Rate, $\lvert\dot{\beta}\rvert$ (deg/s)	0.592072	1.216091	0.261731	0.49279
RMS Blade Pitch Rate, $\dot{\beta}$ (deg/s)	0.17002	0.332143	0.074325	0.136033
STD LSS Flex, $\theta_r - \theta_{gb}$ (rad)	0.000112	0.000113	4.65E-05	4.76E-05
RMS Agb, $\ddot{\theta}_{gb}$ (rad/s^2)	0.018594	0.018715	0.007711	0.007887
RMS Jgb, $\dddot{\theta}_{gb}$ (rad/s^3)	0.217052	0.213409	0.090041	0.089693
RMS Wgen Error, $\Delta\dot{\theta}_{gen}$ (rad/s)	0.838789	0.879259	0.360304	0.372599
RMS Agen, $\ddot{\theta}_{gen}$ (rad/s^2)	1.803609	1.815308	0.747999	0.764998
RMS Jgen, $\dddot{\theta}_{gen}$ (rad/s^3)	21.05408	20.70071	8.734022	8.700249
STD Epower (watts)	35637.3	37352.51	15308.76	15831.12
Max Wgen, $\dot{\theta}_{gen}$ (rad/s)	125.3629	125.6347	124.0943	124.1406
Max Agen, $\ddot{\theta}_{gen}$ (rad/s^2)	7.735137	6.623737	3.078083	3.627521
Max Gen Torque, T_{gen} (N-m)	47225.01	46631.39	44737.6	45031.07

Figure 5.21- Normalized simulation statistics for SI LQR controller in FAST

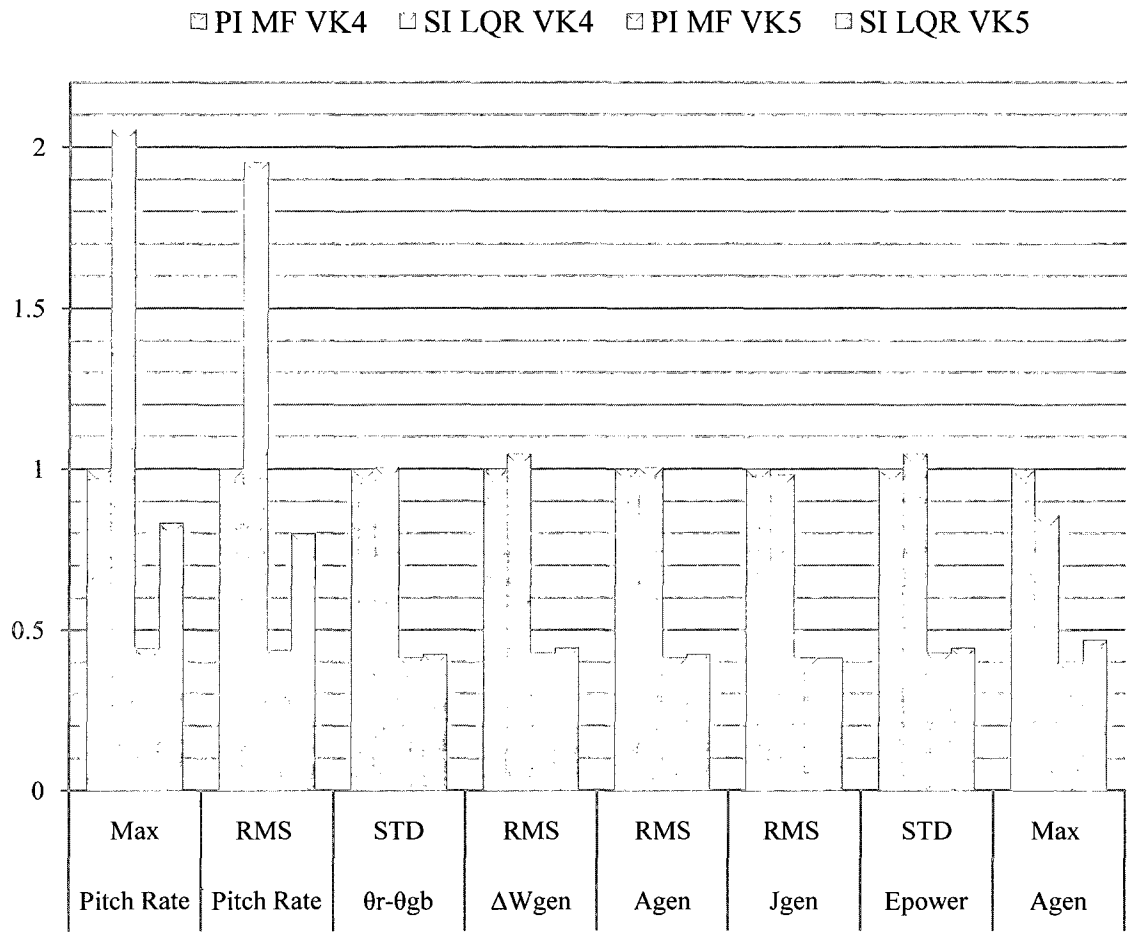

Attempts were made to tune the SI LQR controller with the FAST model. Results of these attempts can be seen in Table 5.13 and Figure 5.22. The first attempt was to regulate the torques and accelerations in FAST. This controller was denoted as SI LQR-FTq. The controller was then tuned for speed regulation, denoted as SI LQR-FSpd.

Table 5.13 - SI LQR controller simulation statistics tuned to FAST model

Controller	**PI MF**	**SI LQR-FTq**	**PI MF-FSpd**
Wind	**VK4**	**VK4**	**VK4**
Max Blade Pitch Rate, $\lvert\dot{\beta}\rvert$ (deg/s)	0.592072	0.582331	0.691586
RMS Blade Pitch Rate, $\dot{\beta}$ (deg/s)	0.17002	0.178882	0.201337
STD LSS Flex, $\theta_r - \theta_{gb}$ (rad)	0.000112	0.00011	0.000116
RMS Agb, $\ddot{\theta}_{gb}$ (rad/s^2)	0.018594	0.018204	0.019256
RMS Jgb, $\dddot{\theta}_{gb}$ (rad/s^3)	0.217052	0.206839	0.225917
RMS Wgen Error, $\Delta\dot{\theta}_{gen}$ (rad/s)	0.838789	1.484042	0.662236
RMS Agen, $\ddot{\theta}_{gen}$ (rad/s^2)	1.803609	1.765815	1.867844
RMS Jgen, $\dddot{\theta}_{gen}$ (rad/s^3)	21.05408	20.06337	21.91399
STD Epower (watts)	35637.3	63042.75	28136.21
Max Wgen, $\dot{\theta}_{gen}$ (rad/s)	125.3629	126.8653	124.815
Max Agen, $\ddot{\theta}_{gen}$ (rad/s^2)	7.735137	6.187921	6.698258
Max Gen Torque, T_{gen} (N-m)	47225.01	46398.62	46671.2

Compared to PI MF the SI LQR-FTq controller decreased RMS accelerations by 2%, RMS jerks by 4.7% and 20% smaller maximum acceleration at the expense of using 5% higher RMS pitch rates, and a 77% increases in RMS speed error and power fluctuations.

With The SI LQR-Fspd it was possible to achieve 21% better speed and power regulation and 13% reduction in maximum acceleration compared to the PI MF controller. This simulation sacrificed 18% more RMS blade pitch, 3.56% higher RMS accelerations and 4.08% higher RMS jerks. It is clear that the primary advantages of the LQR controller comes from building an accurate model of the specific system into the control algorithm.

Figure 5.22- Normalized simulation statistics for SI LQR tuned with FAST

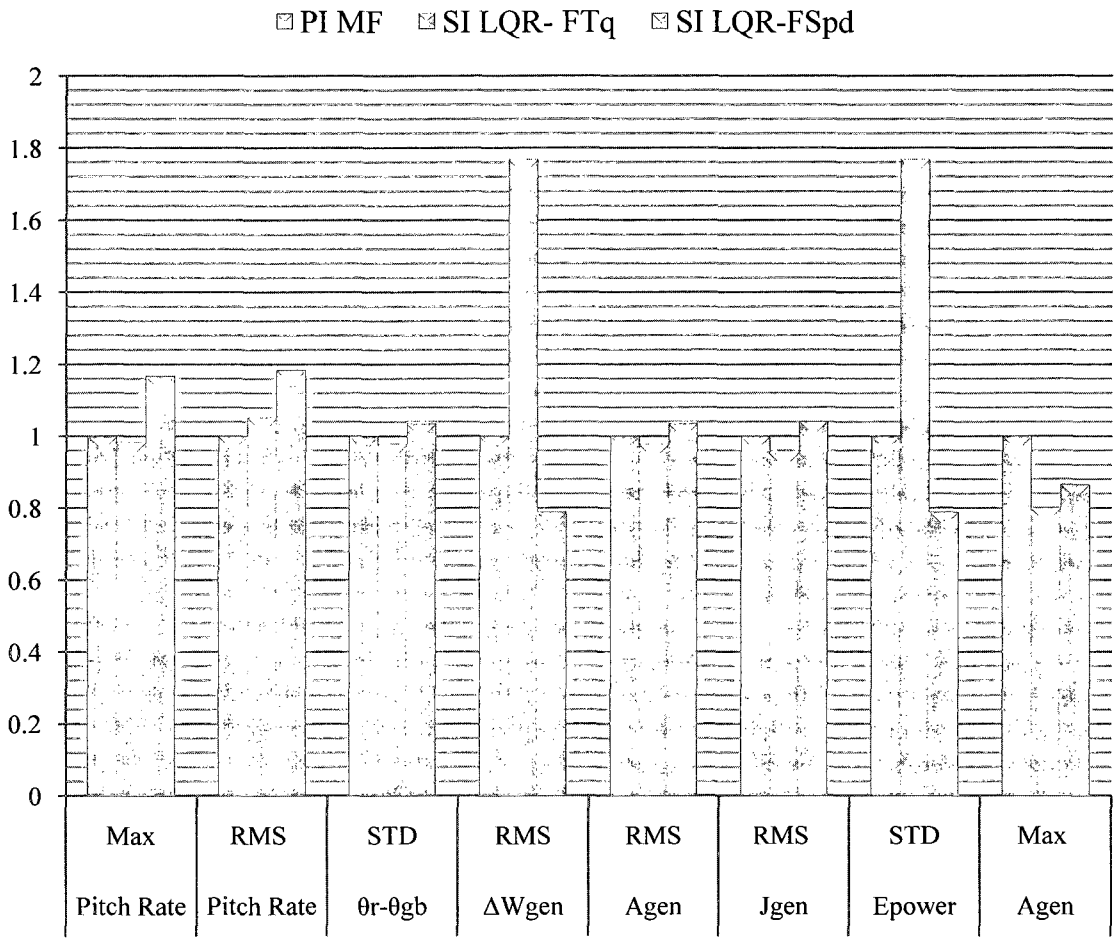

CHAPTER 6:

CONCLUSIONS

Conclusions of Study

This study focused on controlling a wind turbine in Region 3 using full state feedback linear quadratic regulator (LQR) controllers. The control goals were to minimize drivetrain torque variations while maintaining generator speed regulation without significant increases in blade pitch rate when compared to industry standard proportional-integral control with a measurement filter (PI MF controller). A single-input blade pitch LQR (SI LQR) controller was designed and simulated on a derived wind turbine model. A magnetic continuously variable transmission (CVT) was added to the wind turbine model and a multi-input LQR (MI LQR) controller was developed and simulated.

Several original contributions were made by this study. A new linear model of a wind turbine was developed largely based on the NREL FAST 5MW wind turbine model. A unique SI LQR controller was developed for the linear model. This LQR controller utilized additional states augmented to the plant state-space matrices to add penalty to the blade pitch rate and ensure zero steady state tracking error. New equations for the generator and gearbox accelerations with a variable gear ratio were derived and implemented in the linear model. Properties of a magnetic CVT were assumed and included in the model. The new equations were linearized and incorporated into new

state-space matrices. The development of the MI LQR controller also augmented additional states to the new state-space matrices. These states were added to regulate generator speed error, ensure zero steady state generator speed error, ensure that the CVT would be driven back to the nominal gear ratio, and add penalties to the blade pitch rate and CVT slew rate.

The results of this study indicate that utilization of full state feedback and a blade pitch LQR controller has potential to add some damping to torque variations along the drivetrain if an accurate model of the plant is known. Simulations of the SI LQR controller with the derived linear model show a decrease in RMS gearbox and generator accelerations and a decrease in RMS gearbox and generator jerk when compared to the baseline PI MF controller. The SI LQR controller also improved RMS speed regulation and used slightly higher RMS blade pitch rates. The SI LQR controller showed less than 10% reduction in RMS accelerations, even when the state-space matrices used for calculating LQR control gains exactly matched the model. Performance improvements of the SI LQR controller were limited by the slow blade pitch rate, low bandwidth of the controller input, and a very fast propagation of torque variations along the drivetrain.

This study also shows that the implementation of a magnetic continuously variable transmission in a wind turbine has potential to significantly mitigate torque variations along the turbine's drivetrain if the turbine is accurately modeled and the CVT is sufficiently fast. Simulations of the MI LQR controller show that the controller pitches the turbine blades in a similar manner to that of the SI LQR, using the blades to control the power extracted from the wind. The MI LQR controller actuates the CVT, shifting the load of the generator to minimize speed error and torque variations. The CVT is

allowed a larger controller bandwidth to be able to mitigate the vibrations in the drivetrain. This is advisable only if the turbine plant model is well known. If an accurate model of the wind turbine is not known then a high bandwidth controller such as the CVT has the potential to excite the natural frequencies of the turbine blades and drive train.

The SI LQR controller that was tuned for the linear model was tested on the NREL FAST 5MW wind turbine model. This is a different model than the controller was designed for. The controller worked and remained stable, but required high RMS blade pitch rates and did not regulate torque variations better than the PI controller. Significantly superior performance was not achieved when iteratively tuning the SI LQR controller in FAST when compared to the PI MF controller. These results stress the importance of developing an accurate model of the wind turbine plant to reap the benefits of the LQR controller.

This study is the first step of ongoing research of developing control systems to mitigate torque variations in the turbine drivetrain. In the model used for this study, measuring blade flex allows the controller less than .2 seconds before the torque variations arrive at the generator. If blade pitch is the only control input and the earliest measurement is the flexing of the blades, the controller is responding retro-actively to torques delivered to the drivetrain. Using a CVT that has a fast slew rate can intercept the torque variations as they propagate along the drivetrain.

The results of the DCVT model and MI LQR controller show that one of the major sources of premature gearbox failures could potentially be significantly reduced using a smart multi-input control design. By reducing torque variations, maintenance

costs can be reduced, which makes wind energy more cost competitive with other energy sources.

Suggestions for Future Study

This study is a preliminary investigation into reducing torque variations in wind turbine drivetrains. The results of this research show that model accuracy is very important when utilizing LQR feedback control given the states measured. Future work should be done to improve the fidelity of the model. This research also indicates that magnetic CVTs have potential to mitigate torque variations. Further research should be done in the area of magnetic CVT implementation in wind turbines. Future work should also incorporate all regions of wind turbine control. It would also be important to test the control systems under extreme conditions to observe performance under worst-case scenarios.

Developing a higher fidelity model is an important next step for this research. Modeling the turbine blades and aerodynamic forces more accurately and including higher order blade dynamics would significantly improve the derived model. This study combined the blades into one rotational inertia, one spring and one damper. The simplification of the blades allowed for one single wind speed input. A more accurate model would utilize spatial variations of wind speed and finite element analysis to calculate the aerodynamic forces on the blades, as FAST does. This could be done by deriving more accurate aerodynamic equations for inclusion in the model. The aerodynamic equations could then be linearized for inclusion in the LQR gain

calculations. Testing could then be done with the LQR controller for analysis of system performance.

Another future direction would be to develop an accurate model of a magnetic CVT. This study models simplified dynamics of a magnetic CVT as a fixed spring and a low pass filter as the actuator. There has not been a 5MW magnetic CVT developed yet. The dynamic equations of a lower power magnetic CVTs could be studied and scaled up to the 5MW size. If simulations were run with a scaled up model of an actual magnetic CVT in the high speed shaft of a high fidelity wind turbine model, one could make a more accurate estimate to the potential benefit of implementing such a device in a real wind turbine.

This study assumes that the generator torque control provides constant generator back-torque at the load end of the high speed shaft. Studies have analyzed the use of a CVT to eliminate the power electronics and connect the generator directly to the grid. This is done by using the CVT to regulate generator rotational velocity, producing a regulated frequency voltage signal. This area of research could be incorporated into this model by developing a complete generator model. [14]

FAST is a high fidelity model that includes blade aerodynamics. The CVT and MI LQR were not tested with FAST, as the FAST wind turbine model has a fixed gear ratio. A prior study has shown that the gearbox and generator can be pulled out of the FAST model and simulated externally. This allowed for research on a controllable mechanical CVT for Region 2 fixed speed control. [14] Incorporating the CVT in FAST requires a generator model be developed, which was beyond the scope of this research.

Future work could incorporate the CVT and generator models with the FAST model to analyze the performance of the MI LQR on a higher fidelity non-linear model.

Much of the discussion of future work in this section involves including many non-linearities into the model. The LQR controller's advantage comes from knowing the system's linearized equations and incorporating them into the control methodology for more intelligent, advanced control. The non linearities may have significant effects when the turbine deviates from the operating point. It may be worth linearizing the wind turbine plant about several operating points and providing a methodology for a smooth transition between the operating regions.

The model could also include accurate drivetrain and blade flex sensor models with noisy measurements. This would allow for more realistic feedback data. The controller would also be directly implementable in a real wind turbine. A Kalman filter could be developed to mitigate sensor noise.

Wind speed states could be augmented into the state-space matrix. This would allow for data from a Kalman filter, anemometer or LIDAR to be used to predict or measure the wind speed before it reaches the rotor plane. The advanced knowledge of the wind could give the LQR controllers a significant advantage. The controller could then utilize the advanced measurements to actuate the control inputs earlier than the controllers presented in this thesis. This would reduce the problem of the controller responding retro-actively by allowing for blade actuation before winds reach the rotor. Many high frequency torque variations will still get through the blades, but the controller can actively damp the natural frequencies of the turbine components. The combination of

earlier information and an accurate state-space matrix built into the controller could provide large reduction in torque variations.

Future work could be done to correlate the reduction of gearbox and generator accelerations to the lifetime of the components. This would allow for more quantitative results that can translate to financial savings from the protection of the gearboxes. Statistics regarding the number of failed gearboxes, the cost of the sensors, gearbox and CVT could be included in future studies. This would allow for a cost benefit analysis to study whether or not the LQR controller and CVT are worth implementing in a real wind turbine.

LIST OF REFERENCES

1. **Danish Wind Industry Association.** Danish Wind Industry Association- Guided Tour. *Danish Wind Industry Association Website.* [Online] June 1, 2003. [Cited: May 20, 2010.] http://www.talentfactory.dk/en/tour/wres/index.htm.

2. **Masters, Gilbert M.** *Renewable and Efficient Electric Power Systems.* Hoboken, New Jersey : John Wiley & Sons, Inc., 2004.

3. **U.S. Department of Energy- Energy Efficiency & Renewable Energy.** History of Wind Energy. [Online] September 12, 2005. [Cited: March 20, 2009.] http://www1.eere.energy.gov/windandhydro/wind_history.html.

4. **National Renewable Energy Laboratory.** NREL: Overview. [Online] December 14, 2007. [Cited: April 10, 2010.] http://www.nrel.gov/overview.

5. **American Wind Energy Association.** AWEA Market Update Factsheet. *American Wind Energy Association Website.* [Online] April 27, 2009. [Cited: April 5, 2010.] http://www.awea.org/pubs/factsheets/Market_Update_Factsheet.pdf.

6. **Jonkman, J., et al.** *Definition of a 5-MW Wind Turbine for Offshore System Development.* Golden : National Renewable Energy Laboratory, 2009. Technical Report.

7. **Pao, Lucy Y. and Johnson, Kathryn.** *A Tutorial on the Dynamics and Control of Wind Turbines and Wind Farms.* St. Louis : American Controls Conference, 2009. Conference Paper.

8. **Boyle, Godfrey.** *Renewable Electricity and the Grid.* Trowbridge : Cromwell Press, 2007.

9. **Allen, Robert D.** NASA Wind Tunnels. [Online] February 01, 2004. [Cited: April 10, 2010.] http://oea.larc.nasa.gov/PAIS/WindTunnel.html.

10. **Wright, Alan D.** *Modern Control Design for Flexible Wind Turbines.* Boulder : National Renewable Energy Laboratory, 2004. Technical Report.

11. **Musial, W., Butterfield, S. and McNiff, B.** *Improving Wind Turbine Gearbox Reliability.* Golden : National Renewable Energy Laboratory, 2007. Conference Paper.

12. **Dunne, Fiona, et al.** *Combining Standard Feedback Controllers with Feedforward Blade Pitch Control for Load Mitigation in Wind Turbines.* Orlando : American Institute of Aeronautics and Astronautics, 2009. Conference Paper.

13. **Laks, Jason, et al.** *Blade Pitch Control with Prevew Wind Measurments.* Orlando : American Institute of Aeronautics and Astronautics, 2009. Conference Paper.
14. *Methods for Controlling a Wind Turbine System with a Continuously Variable Transmission in Region 2.* **Johnson, K. and Rex, A.** 3, s.l. : Journal of Solar Energy Engineering, 2009, Journal of Solar Energy Engineering, Vol. 131, No. 3, Vol. 130, pp. 031012-1-031012-8.

15. **AAER Inc.** AAER A-2000 Wind Turbine. *AAER Wind Energy.* [Online] May 8, 2010. [Cited: May 8, 2010.] http://www.aaer.ca/page.asp?intNodeID=33733.
16. **Jonkman, J. M. and Buhl, M. L. Jr.** *FAST User's Guide.* Golden : National Renewable Energy Laboratory, 2005. Technical Report.

17. **Wright, Allan D. and Fingersh, L. J.** *Advanced Control Design for Wind Turbines-Part I:Control Design, Implementation, and Initial Tests.* Golden : National Renewable Energy Laboratory, 2008. Technical Report.

18. **Magnomatics Ltd.** Magnomatics. [Online] April 17, 2010. [Cited: April 17, 2010.] http://www.magnomatics.com/.

19. **Kirby, Chris and Atallah, Kais.** *Online Webex Meeting.* [interv.] Jacob Aho. March 11, 2010.

20. **Rex, Andrew H. and Johnson, E. Kathryn.** *Model Development of a Wind Turbine System with a Continuously Variable Transmission for Design of Region 2 Speed Control.* Reno : AIAA, 2008. Conference Paper.

21. **Cotrell, J.** *Assessing the Potential of a Mechanical Continuously Variable Transmission for Wind Turbines.* Golden : National Renewable Energy Laboratory, 2005. Conference Paper.

22. **National Renewable Energy Laboratory.** NWTC Design Codes: FAST. [Online] March 31, 2010. [Cited: April 01, 2010.] http://wind.nrel.gov/designcodes/simulators/fast/.

23. **Franklin, Gene F., Powell, J. David and Emami-Naeini, Abbas.** *Feedback Control of Dynamic Systems, Fourth Edition.* Upper Saddle River : Prentice Hall, 2002.

24. **Brogan, William L.** *Modern Control Theory, Third Edition.* Upper Saddle River : Prentice Hall, 1991.

25. **Dorf, Richard C. and Bishop, Robert H.** *Modern Control Systems, 9th ed.* Upper Saddle River : Prentice Hall, 2001.

26. **Naidu, Desineni Subbaram.** *Optimal Control Systems.* Boca Raton : CRC Press, 2003.

27. **Jonkman, B. J.** *TurbSim User's Guide: Version 1.50.* Golden : National Renewable Energy Laboratory, 2009. Technical Report.

APPENDIX A:

FAST INPUT FILE

```
---------------------------------------------------------------------
------- FAST INPUT FILE -------------------------------------------------
NREL 5.0 MW Baseline Wind Turbine- JPA Thesis Version
Properties from Dutch Offshore Wind Energy Converter (DOWEC) 6MW Pre-Design (10046_009.pdf) and REpower 5M 5MW (5m_uk.pdf);
Compatible with FAST v6.0.
---------------------- SIMULATION CONTROL --------------------------------
False     Echo       - Echo input data to "echo.out" (flag)
  1       ADAMSPrep  - ADAMS preprocessor mode {1: Run FAST, 2: use FAST as a preprocessor to create an ADAMS model, 3: do both} (switch)
  1       AnalMode   - Analysis mode {1: Run a time-marching simulation, 2: create a periodic linearized model} (switch)
  3       NumBl      - Number of blades (-)
600       TMax       - Total run time (s)
  0.01    DT         - Integration time step (s)
---------------------- TURBINE CONTROL -----------------------------------
  0       YCMode     - Yaw control mode {0: none, 1: user-defined from routine UserYawCont, 2: user-defined from Simulink} (switch)
  0       TYCOn      - Time to enable active yaw control (s) [unused when YCMode=0]
  2       PCMode     - Pitch control mode {0: none, 1: user-defined from routine PitchCntrl, 2: user-defined from Simulink} (switch)
  0.0     TPCOn      - Time to enable active pitch control (s) [unused when PCMode=0]
  1       VSContrl   - Variable-speed control mode {0: none, 1: simple VS, 2: user-defined from routine UserVSCont, 3: user-defined from Simulink}
(switch)
 800      VS_RtGnSp  - Rated generator speed for simple variable-speed generator control (HSS side) (rpm) [used only when VSContrl=1]
 43093.55 VS_RtTq    - Rated generator torque/constant generator torque in Region 3 for simple variable-speed generator control (HSS side)
(N-m) [used only when VSContrl=1]
  .0255764 VS_Rgn2K  - Generator torque constant in Region 2 for simple variable-speed generator control (HSS side) (N-m/rpm^2) [used only
when VSContrl=1]
  10      VS_SlPc    - Rated generator slip percentage in Region 2 1/2 for simple variable-speed generator control (%) [used only when VSContrl=1]
  1       GenModel   - Generator model {1: simple, 2: Thevenin, 3: user-defined from routine UserGen} (switch) [used only when VSContrl=0]
True      GenTiStr   - Method to start the generator {T: timed using TimGenOn, F: generator speed using SpdGenOn} (flag)
True      GenTiStp   - Method to stop the generator {T: timed using TimGenOf, F: when generator power = 0} (flag)
9999.9    SpdGenOn   - Generator speed to turn on the generator for a startup (HSS speed) (rpm) [used only when GenTiStr=False]
  0       TimGenOn   - Time to turn on the generator for a startup (s) [used only when GenTiStr=True]
9999.9    TimGenOf   - Time to turn off the generator (s) [used only when GenTiStp=True]
  1       HSSBrMode  - HSS brake model {1: simple, 2: user-defined from routine UserHSSBr} (switch)
9999.9    THSSBrDp   - Time to initiate deployment of the HSS brake (s)
9999.9    TiDynBrk   - Time to initiate deployment of the dynamic generator brake [CURRENTLY IGNORED] (s)
9999.9    TTpBrDp(1) - Time to initiate deployment of tip brake 1 (s)
9999.9    TTpBrDp(2) - Time to initiate deployment of tip brake 2 (s)
9999.9    TTpBrDp(3) - Time to initiate deployment of tip brake 3 (s) [unused for 2 blades]
9999.9    TBDeplSp(1) - Deployment-initiation speed for the tip brake on blade 1 (rpm)
9999.9    TBDeplSp(2) - Deployment-initiation speed for the tip brake on blade 2 (rpm)
9999.9    TBDeplSp(3) - Deployment-initiation speed for the tip brake on blade 3 (rpm) [unused for 2 blades]
9999.9    TYawManS   - Time to start override yaw maneuver and end standard yaw control (s)
9999.9    TYawManE   - Time at which override yaw maneuver reaches final yaw angle (s)
  0.0     NacYawF    - Final yaw angle for yaw maneuvers (degrees)
9999.9    TPitManS(1) - Time to start override pitch maneuver for blade 1 and end standard pitch control (s)
9999.9    TPitManS(2) - Time to start override pitch maneuver for blade 2 and end standard pitch control (s)
9999.9    TPitManS(3) - Time to start override pitch maneuver for blade 3 and end standard pitch control (s) [unused for 2 blades]
9999.9    TPitManE(1) - Time at which override pitch maneuver for blade 1 reaches final pitch (s)
9999.9    TPitManE(2) - Time at which override pitch maneuver for blade 2 reaches final pitch (s)
9999.9    TPitManE(3) - Time at which override pitch maneuver for blade 3 reaches final pitch (s) [unused for 2 blades]
 15.98    BlPitch(1) - Blade 1 initial pitch (degree
 15.98    BlPitch(2) - Blade 2 initial pitch (degrees)
 15.98    BlPitch(3) - Blade 3 initial pitch (degrees) [unused for 2 blades]
 15.98    B1PitchF(1) - Blade 1 final pitch for pitch maneuvers (degrees)
 15.98    B1PitchF(2) - Blade 2 final pitch for pitch maneuvers (degrees)
 15.98    B1PitchF(3) - Blade 3 final pitch for pitch maneuvers (degrees) [unused for 2 blades]
---------------------- ENVIRONMENTAL CONDITIONS --------------------------
  0 Gravity   - 9.80665 Gravitational acceleration (m/s^2)
```

```
---------- FEATURE FLAGS ----------
False      FlapDOF1   - First flapwise blade mode DOF (flag)
False      FlapDOF2   - Second flapwise blade mode DOF (flag)
True       EdgeDOF    - First edgewise blade mode DOF (flag)
False      TeetDOF    - Rotor-teeter DOF (flag) [unused for 3 blades]
True       DrTrDOF    - Drivetrain rotational-flexibility DOF (flag)
True       GenDOF     - Generator DOF (flag)
False      YawDOF     - Yaw DOF (flag)
False      TwFADOF1   - First fore-aft tower bending-mode DOF (flag)
False      TwFADOF2   - Second fore-aft tower bending-mode DOF (flag)
False      TwSSDOF1   - First side-to-side tower bending-mode DOF (flag)
False      TwSSDOF2   - Second side-to-side tower bending-mode DOF (flag)
True       CompAero   - Compute aerodynamic forces (flag)
False      CompNoise  - Compute aerodynamic noise (flag)
---------- INITIAL CONDITIONS ----------
  0.0      OoPDefl    - Initial out-of-plane blade-tip displacement (meters)
  0.0      IPDefl     - Initial in-plane blade-tip deflection (meters)
  0.0      TeetDefl   - Initial or fixed teeter angle (degrees) [unused for 3 blades]
  0.0      Azimuth    - Initial azimuth angle for blade 1 (degrees)
 12.1      RotSpeed   - Initial or fixed rotor speed (rpm)
  0.0      NacYaw     - Initial or fixed nacelle-yaw angle (degrees)
  0.0      TTDspFA    - Initial fore-aft tower-top displacement (meters)
  0.0      TTDspSS    - Initial side-to-side tower-top displacement (meters)
---------- TURBINE CONFIGURATION ----------
 63.0      TipRad     - The distance from the rotor apex to the blade tip (meters)
  1.5      HubRad     - The distance from the rotor apex to the blade root (meters)
  1        PSpnElN    - Number of the innermost blade element which is still part of the pitchable portion of the blade for partial-span pitch control [1 to
BldNodes] [CURRENTLY IGNORED] (-)
  0.0      UndSling   - Undersling length [distance from teeter pin to the rotor apex] (meters) [unused for 3 blades]
  0.0      HubCM      - Distance from rotor apex to hub mass [positive downwind] (meters)
 -5.01910  OverHang   - Distance from yaw axis to rotor apex [3 blades] or teeter pin [2 blades] (meters)
  1.9      NacCMxn    - Downwind distance from the tower-top to the nacelle CM (meters)
  0.0      NacCMyn    - Lateral distance from the tower-top to the nacelle CM (meters)
  1.75     NacCMzn    - Vertical distance from the tower-top to the nacelle CM (meters)
 87.6      TowerHt    - Height of tower above ground level [onshore] or MSL [offshore] (meters)
  1.96256  Twr2Shft   - Vertical distance from the tower-top to the rotor shaft (meters)
  0.0      TwrRBHt    - Tower rigid base height (meters)
 -5.0      ShftTilt   - Rotor shaft tilt angle (degrees)
  0.0      Delta3     - Delta-3 angle for teetering rotors (degrees) [unused for 3 blades]
 -2.5      PreCone(1) - Blade 1 cone angle (degrees)
 -2.5      PreCone(2) - Blade 2 cone angle (degrees)
 -2.5      PreCone(3) - Blade 3 cone angle (degrees) [unused for 2 blades]
  0.0      AzimB1Up   - Azimuth value to use for I/O when blade 1 points up (degrees)
---------- MASS AND INERTIA ----------
  0.0      YawBrMass  - Yaw bearing mass (kg)
 240.00E3  NacMass    - Nacelle mass (kg)
 56.78E3   HubMass    - Hub mass (kg)
  0.0      TipMass(1) - Tip-brake mass, blade 1 (kg)
  0.0      TipMass(2) - Tip-brake mass, blade 2 (kg)
  0.0      TipMass(3) - Tip-brake mass, blade 3 (kg) [unused for 2 blades]
2607.89E3  NacYIner   - Nacelle inertia about yaw axis (kg m^2)
 534.116   GenIner    - Generator inertia about HSS (kg m^2)
 115.926E3 HubIner    - Hub inertia about rotor axis [3 blades] or teeter axis [2 blades] (kg m^2)
---------- DRIVETRAIN ----------
 100.0     GBoxEff    - Gearbox efficiency (%)
  94.4     GenEff     - Generator efficiency [ignored by the Thevenin and user-defined generator models] (%)
  97.0     GBRatio    - Gearbox ratio (-)
False      GBRevers   - Gearbox reversal {T: if rotor and generator rotate in opposite directions} (flag)
 28.1162E3 HSSBrTqF   - Fully deployed HSS-brake torque (N-m)
  0.6      HSSBrDT    - Time for HSS-brake to reach full deployment once initiated (sec) [used only when HSSBrMode=1]
           DynBrkFi   - File containing a mech-gen-torque vs HSS-speed curve for a dynamic brake [CURRENTLY IGNORED] (quoted string)
 867.637E6 DTTorSpr   - Drivetrain torsional spring (N-m/rad)
 6.215E6   DTTorDmp   - Drivetrain torsional damper (N-m/(rad/s))
---------- SIMPLE INDUCTION GENERATOR ----------
10         SIG_SlPc   - Rated generator slip percentage (%) [used only when VSContrl=0 and GenModel=1]
1173.7     SIG_SySp   - Synchronous (zero-torque) generator speed (rpm) [used only when VSContrl=0 and GenModel=1]
43093.55   SIG_RtTq   - Rated torque (N-m) [used only when VSContrl=0 and GenModel=1]
10         SIG_PORt   - Pull-out ratio (Tpullout/Trated) (-) [used only when VSContrl=0 and GenModel=1]
---------- THEVENIN-EQUIVALENT INDUCTION GENERATOR ----------
9999.9     TEC_Freq   - Line frequency [50 or 60] (Hz) [used only when VSContrl=0 and GenModel=2]
```

```
9998      TEC_NPol    - Number of poles [even integer > 0] (-) [used only when VSContrl=0 and GenModel=2]
9999.9    TEC_SRes    - Stator resistance (ohms) [used only when VSContrl=0 and GenModel=2]
9999.9    TEC_RRes    - Rotor resistance (ohms) [used only when VSContrl=0 and GenModel=2]
9999.9    TEC_VLL     - Line-to-line RMS voltage (volts) [used only when VSContrl=0 and GenModel=2]
9999.9    TEC_SLR     - Stator leakage reactance (ohms) [used only when VSContrl=0 and GenModel=2]
9999.9    TEC_RLR     - Rotor leakage reactance (ohms) [used only when VSContrl=0 and GenModel=2]
9999.9    TEC_MR      - Magnetizing reactance (ohms) [used only when VSContrl=0 and GenModel=2]
---------- PLATFORM ----------
 0        PtfmModel   - Platform model {0: none, 1: onshore, 2: fixed bottom offshore, 3: floating offshore} (switch)
          PtfmFile    - Name of file containing platform properties (quoted string) [unused when PtfmModel=0]
---------- TOWER ----------
 20       TwrNodes    - Number of tower nodes used for analysis (-)
"NRELOffshrBsline5MW_Tower_Onshore.dat"    TwrFile    - Name of file containing tower properties (quoted string)
---------- NACELLE-YAW ----------
9028.32E6 YawSpr      - Nacelle-yaw spring constant (N-m/rad)
 19.16E6  YawDamp     - Nacelle-yaw damping constant (N-m/(rad/s))
 0.0      YawNeut     - Neutral yaw position--yaw spring force is zero at this yaw (degrees)
---------- FURLING ----------
False     Furling     - Read in additional model properties for furling turbine (flag)
          FurlFile    - Name of file containing furling properties (quoted string) [unused when Furling=False]
---------- ROTOR-TEETER ----------
 0        TeetMod     - Rotor-teeter spring/damper model {0: none, 1: standard, 2: user-defined from routine UserTeet} (switch) [unused for 3 blades]
 0.0      TeetDmpP    - Rotor-teeter damper position (degrees) [used only for 2 blades and when TeetMod=1]
 0.0      TeetDmp     - Rotor-teeter damping constant (N-m/(rad/s)) [used only for 2 blades and when TeetMod=1]
 0.0      TeetCDmp    - Rotor-teeter rate-independent Coulomb-damping moment (N-m) [used only for 2 blades and when TeetMod=1]
 0.0      TeetSStP    - Rotor-teeter soft-stop position (degrees) [used only for 2 blades and when TeetMod=1]
 0.0      TeetHStP    - Rotor-teeter hard-stop position (degrees) [used only for 2 blades and when TeetMod=1]
 0.0      TeetSSSp    - Rotor-teeter soft-stop linear-spring constant (N-m/rad) [used only for 2 blades and when TeetMod=1]
 0.0      TeetHSSp    - Rotor-teeter hard-stop linear-spring constant (N-m/rad) [used only for 2 blades and when TeetMod=1]
---------- TIP-BRAKE ----------
 0.0      TBDrConN    - Tip-brake drag constant during normal operation, Cd*Area (m^2)
 0.0      TBDrConD    - Tip-brake drag constant during fully-deployed operation, Cd*Area (m^2)
 0.0      TpBrDT      - Time for tip-brake to reach full deployment once released (sec)
---------- BLADE ----------
"NRELOffshrBsline5MW_Blade.dat"    BldFile(1)  - Name of file containing properties for blade 1 (quoted string)
"NRELOffshrBsline5MW_Blade.dat"    BldFile(2)  - Name of file containing properties for blade 2 (quoted string)
"NRELOffshrBsline5MW_Blade.dat"    BldFile(3)  - Name of file containing properties for blade 3 (quoted string) [unused for 2 blades]
---------- AERODYN ----------
"NRELOffshrBsline5MW_AeroDyn.ipt"    ADFile    - Name of file containing AeroDyn input parameters (quoted string)
---------- NOISE ----------
          NoiseFile   - Name of file containing aerodynamic noise input parameters (quoted string) [used only when CompNoise=True]
---------- ADAMS ----------
"NRELOffshrBsline5MW_ADAMSSpecific.dat"    ADAMSFile   - Name of file containing ADAMS-specific input parameters (quoted string) [unused
when ADAMSPrep=1]
---------- LINEARIZATION CONTROL ----------
"NRELOffshrBsline5MW_Linear.dat"    LinFile    - Name of file containing FAST linearization parameters (quoted string) [unused when
AnalMode=1]
---------- OUTPUT ----------
True      SumPrint    - Print summary data to "<RootName>.fsm" (flag)
True      TabDelim    - Generate a tab-delimited tabular output file. (flag)
"ES10.3E2" OutFmt     - Format used for tabular output except time.  Resulting field should be 10 characters. (quoted string)  [not checked for
validity!]
 0.0      TStart      - Time to begin tabular output (s)
 1        DecFact     - Decimation factor for tabular output {1: output every time step} (-)
 1.0      SttsTime    - Amount of time between screen status messages (sec)
-3.09528  NcIMUxn     - Downwind distance from the tower-top to the nacelle IMU (meters)
 0.0      NcIMUyn     - Lateral distance from the tower-top to the nacelle IMU (meters)
 2.23336  NcIMUzn     - Vertical distance from the tower-top to the nacelle IMU (meters)
 1.912    ShftGagL    - Distance from rotor apex [3 blades] or teeter pin [2 blades] to shaft strain gages [positive for upwind rotors] (meters)
 0        NTwGages    - Number of tower nodes that have strain gages for output [0 to 9] (-)
          TwrGagNd    - List of tower nodes that have strain gages [1 to TwrNodes] (-) [unused if NTwGages=0]
 3        NBlGages    - Number of blade nodes that have strain gages for output [0 to 9] (-)
 5,9,13   BldGagNd    - List of blade nodes that have strain gages [1 to BldNodes] (-) [unused if NBlGages=0]
          OutList     - The next line(s) contains a list of output parameters.  See OutList.txt for a listing of available output channels, (-)
"WindVxi"                    - Longitudinal wind speeds
"LSSTipPxa, LSSTipVxa, LSSTipAxa"                    - Low Speed shaft pos,vel,acc
"LSSGagPxa, LSSGagVxa, LSSGagAxa"                    - LSS strain gauges, pos, vel, acc
"HSShftV, HSShftA"                    - HSS vel, acc
"TSR"                    - Rotor Blade Tip seed Ratio
"LSShftFxa, LSShftMxa"          -Rotor thrust force, LSS Torque
```

"RotPwr" -Rotor Power (LSS Power),
"HSShftTq, HSShftPwr" -HSS Shaft Torque, Power,
"GenPwr , GenTq" - Electrical generator power and torque
"TipDyc1, TipDyc2, TipDyc3" -In plan tip deflection
"PtchPMzc1" -Blade pitch angle, degrees
END of FAST input file (the word "END" must appear in the first 3 columns of this last line).

APPENDIX B:

TURBSIM INPUT FILE- VK4

TurbSim Input File. Valid for TurbSim v1.50, 25-Sep-2009; for Certification Test #5 (SMOOTH Spectrum, formatted FF files, Coherent Structures).

```
---------Runtime Options-----------------------------------
7453241        RandSeed1     - First random seed  (-2147483648 to 2147483647)
"RanLux"       RandSeed2     - Second random seed (-2147483648 to 2147483647) for intrinsic pRNG, or an alternative pRNG: "RanLux" or
"RNSNLW"
True           WrBHHTP       - Output hub-height turbulence parameters in GenPro-binary form?  (Generates RootName.bin)
True           WrFHHTP       - Output hub-height turbulence parameters in formatted form?  (Generates RootName.dat)
False          WrADHH        - Output hub-height time-series data in AeroDyn form?  (Generates RootName.hh)
False          WrADFF        - Output full-field time-series data in TurbSim/AeroDyn form? (Generates RootName.bts)
True           WrBLFF        - Output full-field time-series data in BLADED/AeroDyn form?  (Generates RootName.wnd)
False          WrADTWR       - Output tower time-series data? (Generates RootName.twr)
False          WrFMTFF       - Output full-field time-series data in formatted (readable) form?  (Generates RootName.u, RootName.v, RootName.w)
False          WrACT         - Output coherent turbulence time steps in AeroDyn form? (Generates RootName.cts)
False          Clockwise     - Clockwise rotation looking downwind? (used only for full-field binary files - not necessary for AeroDyn)
 0             ScaleIEC      - Scale IEC turbulence models to exact target standard deviation? [0=no additional scaling; 1=use hub scale uniformly;
2=use individual scales]

--------Turbine/Model Specifications-----------------------
7              NumGrid_Z     - Vertical grid-point matrix dimension
7              NumGrid_Y     - Horizontal grid-point matrix dimension
0.01           TimeStep      - Time step [seconds]
600.0          AnalysisTime  - Length of analysis time series [seconds] (program will add time if necessary: AnalysisTime = MAX(AnalysisTime,
UsableTime+GridWidth/MeanHHWS) )
600.0          UsableTime    - Usable length of output time series [seconds] (program will add GridWidth/MeanHHWS seconds)
126            HubHt         - Hub height [m] (should be > 0.5*GridHeight)
140.00         GridHeight    - Grid height [m]
140.00         GridWidth     - Grid width [m] (should be >= 2*(RotorRadius+ShaftLength))
0              VFlowAng      - Vertical mean flow (uptilt) angle [degrees]
0              HFlowAng      - Horizontal mean flow (skew) angle [degrees]

--------Meteorological Boundary Conditions-------------------
"IECVKM"       TurbModel     - Turbulence model ("IECKAI"=Kaimal, "IECVKM"=von Karman, "GP_LLJ", "NWTCUP", "SMOOTH", "WF_UPW",
"WF_07D", "WF_14D", or "NONE")
1              IECstandard   - Number of IEC 61400-x standard (x=1,2, or 3 with optional 61400-1 edition number (i.e. "1-Ed2") )
5              IECturbc      - IEC turbulence characteristic ("A", "B", "C" or the turbulence intensity in percent) ("KHTEST" option with NWTCUP, not
used for other models)
NTM            IEC_WindType  - IEC turbulence type ("NTM"=normal, "xETM"=extreme turbulence, "xEWM1"=extreme 1-year wind,
"xEWM50"=extreme 50-year wind, where x=wind turbine class 1, 2, or 3)
1              ETMc          - IEC ETM "c" parameter [m/s] (or "default")
PL             WindProfileType - Wind profile type ("JET"=Low-level jet,"LOG"=Logarithmic,"PL"=Power law, or "default")
126            RefHt         - Height of the reference wind speed [m]
18             URef          - Mean (total) wind speed at the reference height [m/s]
260            ZJetMax       - Jet height [m] (used only for JET wind profile, valid 70-490 m)
0              PLExp         - Power law exponent  (or "default")
.001           Z0            - Surface roughness length [m] (or "default")

--------Non-IEC Meteorological Boundary Conditions------------
default        Latitude      - Site latitude [degrees] (or "default")
1              RICH_NO       - Gradient Richardson number
.1             UStar         - Friction or shear velocity [m/s] (or "default")
.1             ZI            - Mixing layer depth [m] (or "default")
none           PC_UW         - Mean hub u'w' Reynolds stress (or "default" or "none")
none           PC_UV         - Mean hub u'v' Reynolds stress (or "default" or "none")
none           PC_VW         - Mean hub v'w' Reynolds stress (or "default" or "none")
default        IncDec1       - u-component coherence parameters (e.g. "10.0  0.3e-3" in quotes) (or "default")
default        IncDec2       - v-component coherence parameters (e.g. "10.0  0.3e-3" in quotes) (or "default")
```

```
default      IncDec3      - w-component coherence parameters (e.g. "10.0  0.3e-3" in quotes) (or "default")
default      CohExp       - Coherence exponent (or "default")

--------Coherent Turbulence Scaling Parameters----------
".\EventData"  CTEventPath    - Name of the path where event data files are located
"les"        CTEventFile    - Type of event files ("random", "les" or "dns")
false        Randomize      - Randomize disturbance scale and location? (true/false)
1.0          DistScl        - Disturbance scale (ratio of dataset height to rotor disk).
0.5          CTLy           - Fractional location of tower centerline from right (looking downwind) to left side of the dataset.
0.5          CTLz           - Fractional location of hub height from the bottom of the dataset.
600          CTStartTime    - Minimum start time for coherent structures in RootName.cts [seconds]

================================================
NOTE: Do not add or remove any lines in this file!
================================================
```

APPENDIX C:

MATLAB SCRIPT FILE

```
% Wind Turbine 5MW Model Parameters %
clear all
clc
format compact

%% Switch Inputs

RUNALL=1; % 0=no, 1=Runs this file, simulink file and plot file

Filtout=1; %Switch 0=No Filter,1=implement measurement filter
ControlMode=4; %1=Open Loop, 2=PI, 3=LQR, 4=LQR with VGB
TgSwitch=1;  %0=Frictional, 1=Constant Tg
GainSched=1; %Gain scheduling switch 0=no 1=yes
WindNum=4;  % Specify which wind input file to use

SM=0;
Plots=0 % Switch, 0=off, 1=on
Write=0 % Switch, 0=off, 1=write stats data to .xls file

%% Simulation Parameters
Ts=.01;
Tmax=600;

if WindNum==1;
    Tmax=200;
end

if WindNum==2;
    Tmax=150;
end

%% Q1

Q1=zeros(8,8);
Q1(1,1)=10;      %Penalty on Blade Speed Error
Q1(2,2)=3000000;  %Penalty on Blade Pos-Rotor Pos Error
Q1(3,3)=400;     %Penalty on Rotor Speed Error
Q1(4,4)=10000000;  %Penalty on Rotor Pos-GB Pos Error
Q1(5,5)=800;     %Penalty on GB Speed Error
Q1(6,6)=50;      %Penalty on Int(EWgb)
Q1(7,7)=0;        %Penalty on BP
Q1(8,8)=0;       %Penalty on Bu
R1=.08;           %Penalty to be put on Budot

%% DEFINE Q2
```

```
Q2=zeros(11,11);

Q2(1,1)=0;        %Penalty on Blade Speed
Q2(2,2)=3000000;     %Penalty on Blade Pos-Rotor Pos
Q2(3,3)=0;        %Penalty on Rotor Speed
Q2(4,4)=100000000;     %Penalty on Rotor Pos-GB Pos
Q2(5,5)=0;        %Penalty on GB Speed
Q2(6,6)=.5;         %Penalty on Int(EWgen)
Q2(7,7)=10;         %Penalty on Gen Speed Error
Q2(8,8)=0;     %Penalty on BP
Q2(9,9)=0;     %Penalty on Bu
Q2(10,10)=200000;    %Penalty on Int(deltaN)
Q2(11,11)=10;     %Penalty on deltaN
Q2(12,12)=10;    %Penalty on deltaNu
R2=[20,0;0,5000000]; %Penalty to be put on Budot and Nudot

%% PI Variables

Bo=15.98; %Blade Pitch in Degrees

Kio=0.008068634; %in rad/rad
Kpo=.01882681; %in rad/rad/s

Kio=Kio*(180/pi)%/(2*pi/60);  %Convert to deg/(rad)
Kpo=Kpo*(180/pi)%/(2*pi/60);  %Convert to deg/(rad/s)

Tk=6.302336; % Bp at which power halfs

% Gains for Const Pid
Kp=Kpo/(1+Bo/Tk);
Ki=Kio/(1+Bo/Tk);
Kd=0;

%% Some IC's

No=1/97; % GB ratio wlss/whss
Wso=18; % wind in meters per second
Wbo=12.1*pi/30;  %Blade Speed
Wro=12.1*pi/30;  %Rotor Speed
Wgo=12.1*pi/30;  %Gb Speed
Wgeno=12.1*pi/30/No;  %Gen Speed

Po=5.296610e+006 % Rated Mechanical Power in Watts
LSSTrated=Po/Wbo
HSSTrated=Po/Wgeno

%% Turbine Dynamic Variables

wn=1.0793*2*pi/sqrt(1-.00477465^2)
Mb=17740*3;
Jb = 1.176E7*3;
Bb = .5*.00477465*wn*Jb%.477465*wn*Jb  %Mb*10%0;%.9*Mb*3;
Db = 1.5*.00477465*wn*Jb%.0632*Jb;
Kb = wn^2*Jb; %(1.0793*2*pi)^2*Jb;

Mr= 110000
Jr = 1.15E5;     %Kg*m^2
```

```
Br = .1*Mr;
Dr = 6.215E6;
Kr = 867.637E6;

Mg=0
Jg = 5.34116E2;      %Kg*m^2
Bg = 0;
BL = Po/(Wgo/No)^2;  %5MW/(1.2671 rad/sec)^2/(N0^2)
GenEff=94.4
if ControlMode==4
    Kr=Kr*.5;
end

TauB=.2; % Time constant of blade actuator  %PAGE 33 of MCDFWT
TauN=.2;

Bpr=8;  %Maximum Blade Pitch Rate
NdotMax=(3*No-.3*No)/3;

roots([Jr Dr Kr])
roots([Jb Db Kb])
%roots([JG BG])

%% Operating Point

To=Po/Wro+Wro*Br+Wbo*Bb+Wgeno*Bg;
dT_dB=-9.1991e+005  %Sensitivity of Tw due to blade pitch (Nm/degree)
dT_dWr=-1.0941e+007 %Sensitivity of Tw due to rotor speed (Nm/degree/s)
dT_dWs=1.2074e+006;
PboSubPro=2.63E-3;
ProSubPgo=4.8208E-3;
Tgo=Po/Wgeno; %Rated gen tq

%% Linearized System

A1=[(-Db-Bb)/Jb, -Kb/Jb, (dT_dWr+Db)/Jb, 0, 0, 0, dT_dB/Jb,0;...
    1, 0, -1, 0, 0, 0, 0,0;...
    Db/Jr, Kb/Jr, (-Br-Db-Dr)/Jr, -Kr/Jb, Dr/Jr, 0, 0,0;...
    0, 0, 1, 0, -1, 0, 0,0;...
    0, 0, Dr*No^2/Jg, Kr*No^2/Jg, (-Bg-BL-Dr*No^2)/Jg, 0, 0,0;...
    0, 0, 0, 0, 1, 0, 0,0;...
    0, 0, 0, 0, 0, 0, -1/TauB,1/TauB;...
    0, 0, 0, 0, 0, 0, 0, 0];

B1=[ 0; 0; 0; 0; 0; 0; 0; 1];
C1=[1,1,1,1,1,1,1,1];
D1=0;

sys1=ss(A1,B1,C1,D1);

minreal(sys1);

% Is Controllable
[n,n]=size(A1);
Cont=B1;
for m=1:n-1
    Cont=cat(2,Cont,A1^m*B1);
```

```
end
if rank(Cont)==n
    disp('Is Controllable')
else
    disp('NOT Controllable')
end

% Is Observable?
Obs=C1';
for m=1:n-1
    Obs=cat(2,Obs,(A1')^m*C1');
end
rank(Obs)
if rank(Obs)==n
    disp('Is Observable')
else
    disp('NOT OBSERVABLE')
end

%% LQR
Qeigen=eig(Q1);
[m,n]=size(Qeigen);
for n=1:m
    if Qeigen(n)<0
        disp('ERROR: Q is not positive semi-definite')
    end
end

[K1, S1, E1]=lqr(A1,B1,Q1,R1)

%% DCVT System

A2=[(-Db-Bb)/Jb, -Kb/Jb, (dT_dWr+Db)/Jb, 0, 0, 0,
0,dT_dB/Jb,0,0,0,0;...
    1, 0, -1, 0, 0, 0, 0,0,0,0,0,0;...
    Db/Jr, Kb/Jr, (-Br-Db-Dr)/Jr, -Kr/Jb, Dr/Jr, 0,0, 0,0,0,0,0;...
    0, 0, 1, 0, -1, 0, 0,0,0,0,0,0;...
    0, 0, Dr*No^2/Jg, Kr*No^2/Jg, (-Bg-BL-Dr*No^2)/Jg, 0,0,
0,0,0,2*No*Kr*ProSubPgo/Jg-Wgo/(No*TauN),Wgo/(No*TauN);...
    0, 0, 0, 0, 0, 0,1, 0,0,0,0,0;...
    0, 0, Dr*No/Jg, Kr*No/Jg, (-Bg-BL-Dr*No^2)/(No*Jg), 0,0,
0,0,0,Kr*ProSubPgo/Jg+Wgo*2*(Bg+BL)/(No^2*Jg),0;...
    0, 0, 0, 0, 0, 0, 0,-1/TauB,1/TauB,0,0,0;...
    0, 0, 0, 0, 0, 0,0, 0,0,0,0,0;...
    0, 0, 0, 0, 0, 0,0, 0,0,0,1,0;...
    0, 0, 0, 0, 0, 0,0, 0, 0,0,-1/TauN,1/TauN;...
    0, 0, 0, 0, 0, 0, 0,0, 0,0,0,0];

B2=[ 0,0; 0,0; 0,0; 0,0; 0,0; 0,0; 0,0; 0,0; 1,0; 0,0; 0,0; 0,1];

C2=[1,1,1,1,1,1,1,1,1,1,1,1];

D2=0;

sys2=ss(A2,B2,C2,D2);

minreal(sys2);
```

```
% Is Controllable
[n,n]=size(A2);
Cont2=B2;
for m=1:n-1
    Cont2=cat(2,Cont2,A2^m*B2);
end
if rank(Cont2)==n
    disp('Is Controllable')
else
    disp('NOT Controllable')
end


% Is Observable?
Obs=C2';
for m=1:n-1
    Obs=cat(2,Obs,(A2')^m*C2');
end
rank(Obs)
if rank(Obs)==n
    disp('Is Observable')
else
    disp('NOT OBSERVABLE')
end


%% LQR 2

Qeigen2=eig(Q2);
[m,n]=size(Qeigen2);
for n=1:m
    if Qeigen2(n)<0
        disp('ERROR: Q is not positive semi-definite')
    end
end
[K2, S2, E2]=lqr(A2,B2,Q2,R2)

%%
if RUNALL==1
sim('Wind_Turbine_5MW_Model')
PlotModelOutput
end

beep
```

APPENDIX D:

SIMULINK® MODELS

Main Simulink File

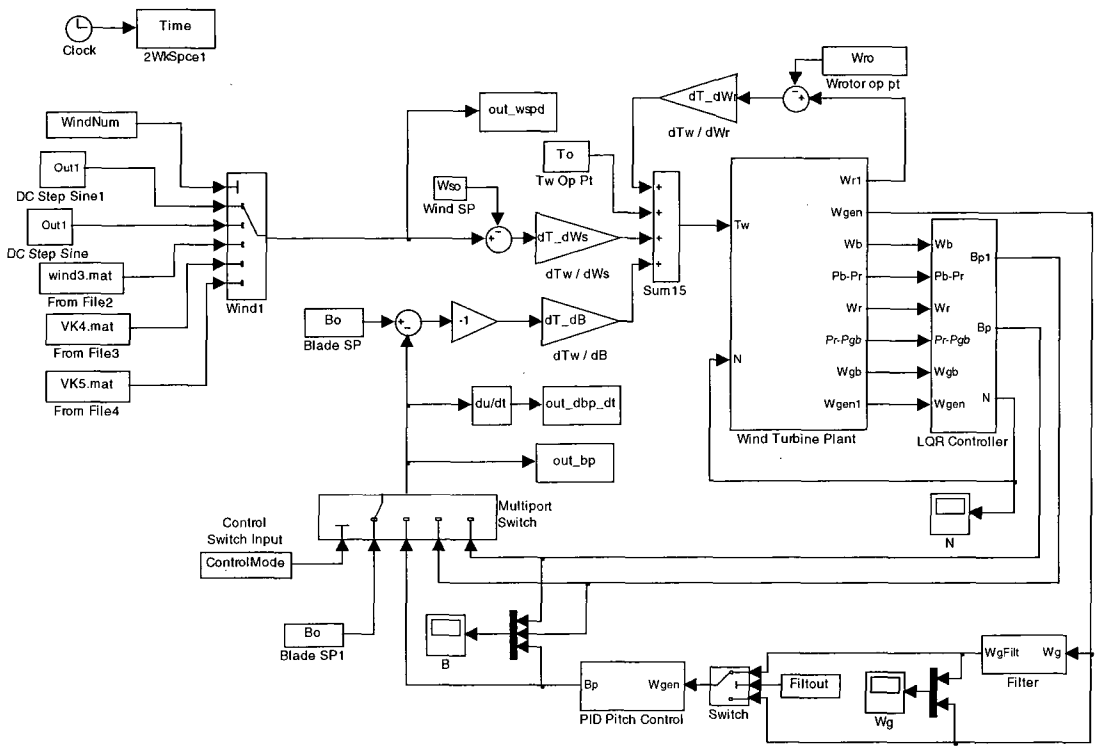

PID Controller

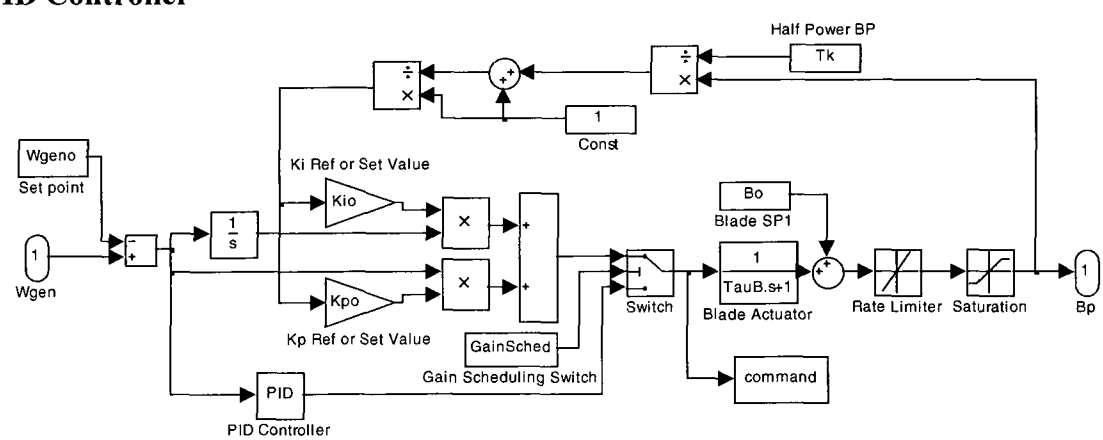

Wind Turbine Plant

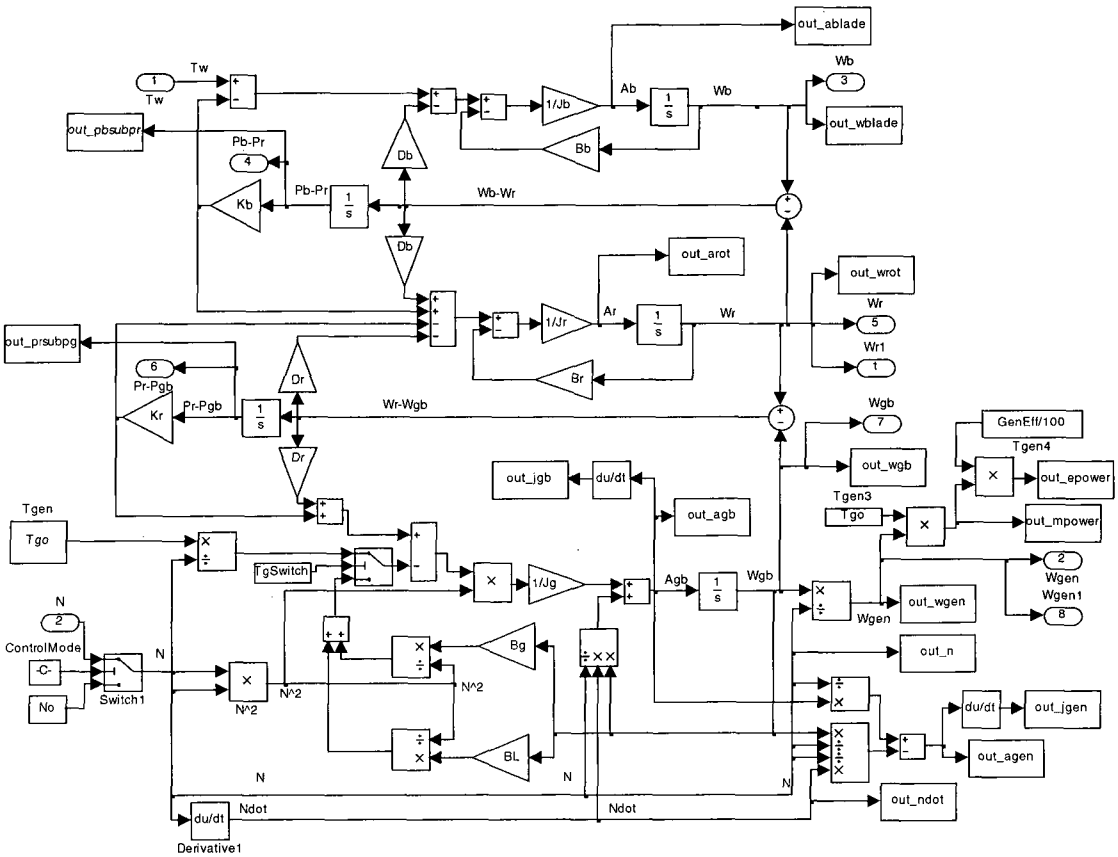

Measurement Filter

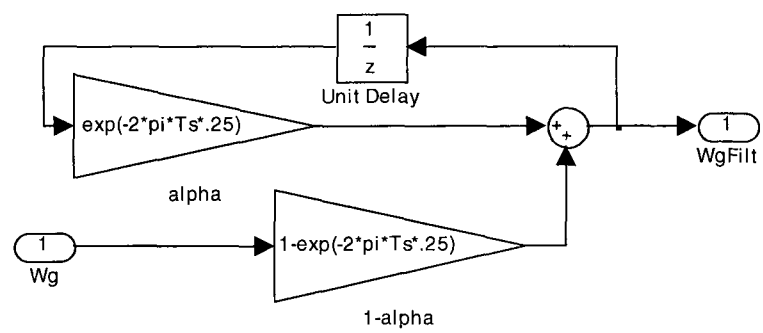

Filter as described on p17 of 5MW Manual

LQR Controller

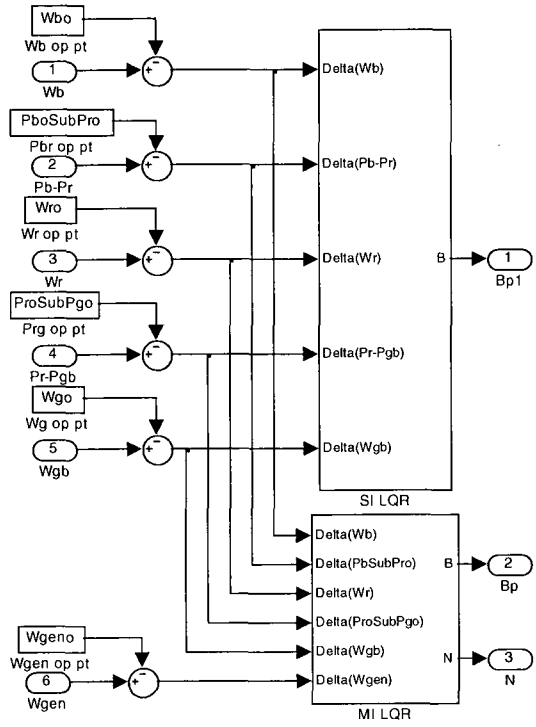

SI LQR

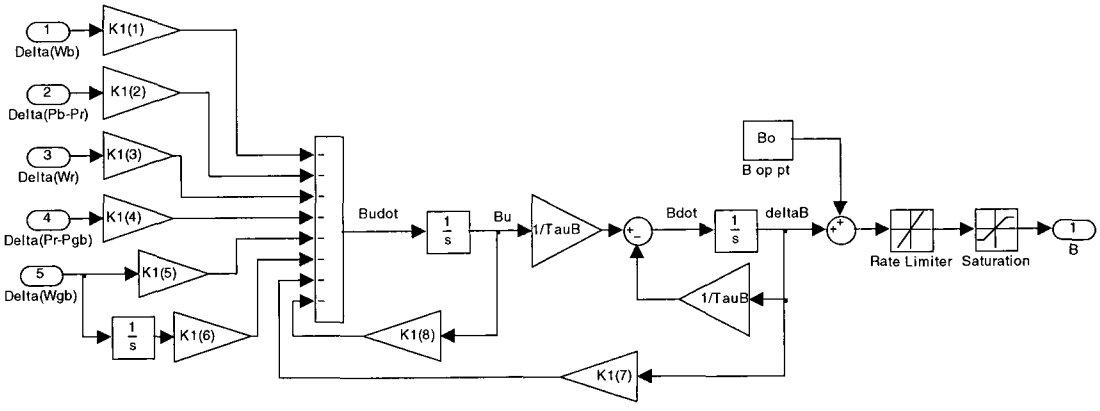

MI LQR

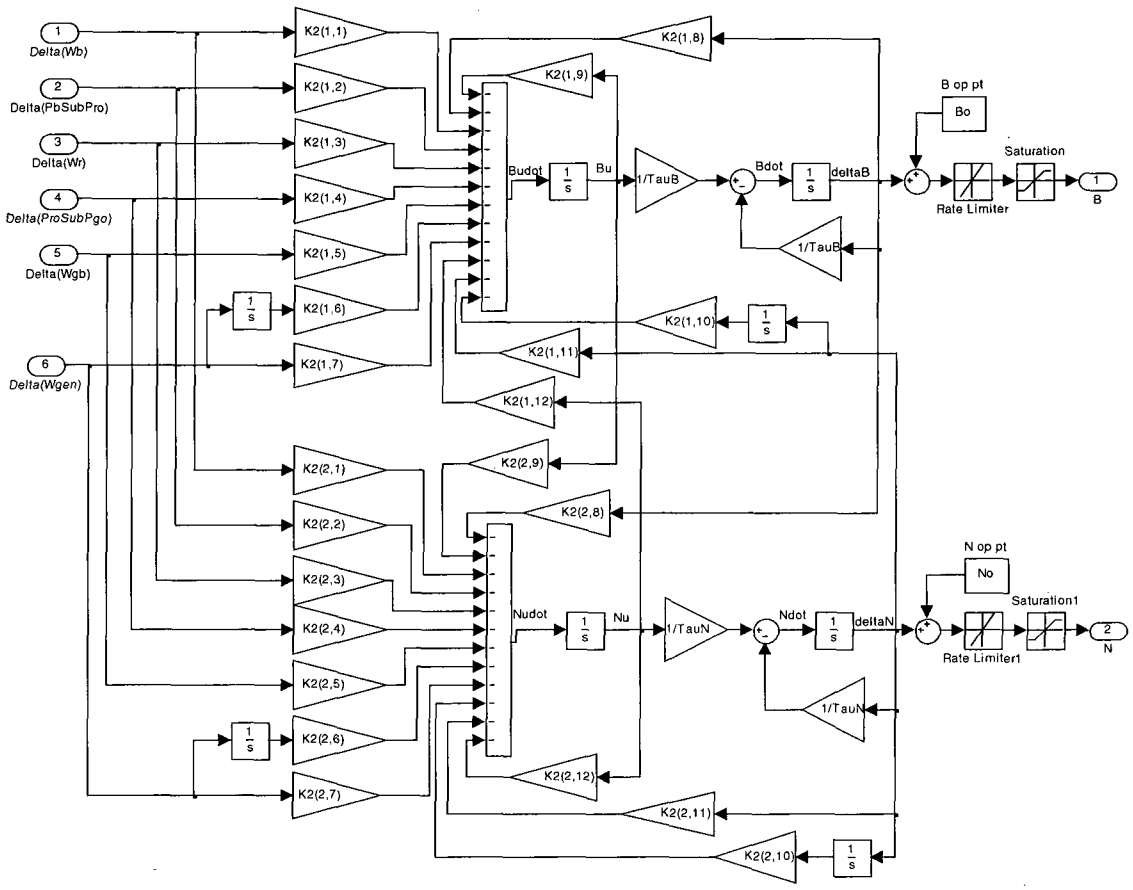

FAST Simulink File

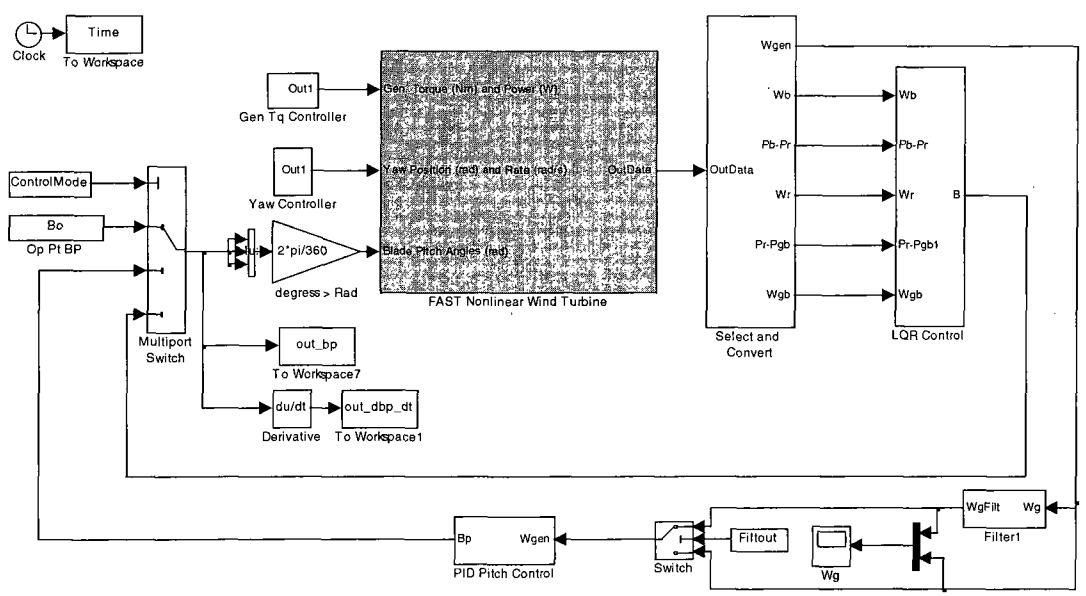

Select and Convert